

bradscholars

Modelling and Simulation of Carbon Dioxide Transportation in Pipelines: Effects of Impurities

Item Type	Thesis
Authors	Peletiri, Suoton P.
Rights	<p>
The University of Bradford theses are licenced under a Creative Commons Licence.</p>
Download date	2025-10-10 19:33:40
Link to Item	http://hdl.handle.net/10454/19190

**MODELLNG AND SIMULATION OF CARBON DIOXIDE TRANSPORTATION
IN PIPELINES: EFFECTS OF IMPURITIES**

S. P. PELETIRI

PHD

2020

Modelling and Simulation of Carbon Dioxide Transportation in Pipelines: Effects
of Impurities

Suoton Philip PELETIRI

Submitted for the Degree of
Doctor of Philosophy

Faculty of Engineering and Informatics
University of Bradford

2020

Suoton Philip Peletiri

**Modelling and Simulation of Carbon Dioxide Transportation in Pipelines:
Effects of Impurities**

Abstract

Keywords: CO₂ pipelines, Carbon capture transportation and storage (CCTS), CO₂ pipeline pressure drop, CO₂ pipeline heat transfer, CO₂ fluid impurities, CO₂ phase envelope, effect of impurities, supercritical CO₂, subcritical CO₂.

Carbon dioxide capture, transportation, and storage has been identified as the most promising way to reduce anthropogenic carbon dioxide (CO₂) released into the atmosphere. Efforts made to achieve this purpose include the Paris (Climate) Accord. This agreement seeks to encourage countries to take the issue of rising global temperatures seriously. With nearly all countries signing this agreement, many CCTS projects are expected. Pipelines are employed in the transportation of CO₂. CO₂ fluids contain impurities that affect the fluid properties and flow dynamics, but pipelines are mostly designed assuming that the CO₂ fluid is pure. CO₂ pipeline fluids contain at least 90 % CO₂ with the balance made up of impurities. The impurities include nitrogen, methane, oxygen, hydrogen, sulphur dioxide, hydrogen sulphide, carbon monoxide, ammonia, argon, etc.

The effects of the impurities are studied using simulation software; Aspen HYSYS, gPROMS and HydraFlash. The results show that all impurities impacted negatively on transportation. At equal concentrations, hydrogen had the greatest effect on fluid properties and hydrogen sulphide the least impact. At the specified allowable concentration, nitrogen had the worst effect on pressure loss (32.1 %)

in horizontal pipeline, density, and critical pressure. Carbon monoxide (with only 0.2-mol %) had the smallest effect in pressure drop (0.3 %).

Analysis of supercritical and subcritical (or liquid) CO₂ fluid transportation shows that subcritical fluids have higher densities (more volume transported) and lower pressure losses than supercritical fluids. Subcritical fluid transportation would therefore have lower pipeline transportation costs than supercritical fluids. Also, soil heat conductivity has greater effect than ambient temperature in buried pipelines. Simple equations that approximate binary CO₂ fluid properties from pure CO₂ properties were developed and presented.

Dedication

I dedicate this thesis to my children; Tariprido Joseph Peletiri, Imomotimi Emmanuel Peletiri, Duduna Claire Peletiri, Bekeowei Ptah Ea Peletiri, and Kurokimi Thoth Peletiri who endured my long absence during my PhD programme.

Acknowledgement

I would like to express my appreciation to my supervisors, Dr Nejat Rahmanian and Prof Iqbal Mujtaba, for accepting me as a student to study under their supervision and for their constructive comments and guide. It would have been impossible for me to complete this work if not for their input.

I would like to say a big thank you to Dr Yakubu Mandafiya John for his help with gPROMS and emotional support during my down times. Many thanks to Prof. Raj Patel for looking out for me. My appreciation also goes to Dr Mudha Al-Obaidi for his help with gPROMS while he was at the University of Bradford.

May I also express my gratitude to the UK Carbon Capture and Storage Research Council (UKCCSRC) for providing funding for me to attend several of their conferences, workshops, trainings, and meetings. I am very grateful.

I say a big thank you to The Worshipful Company of Armourers and Brasiers, Armourers' Hall, 81 Coleman Street, London EC2R 5BJ for providing travel grants for me to attend international conferences in Italy and the Czech Republic.

I am also grateful to the management of Niger Delta University, Wilberforce Island, Bayelsa State, Nigeria for nominating me for a foreign PhD programme. Also grateful to the Tertiary Education Trust Fund (TETFund), Abuja Nigeria for providing funding.

Table of contents

Abstract	i
Dedication.....	iii
Acknowledgement	iv
Table of contents	v
List of Figures	ix
List of Tables	xi
Nomenclature	xiv
List of Publications in Course of this Research.....	1
Chapter 1: Introduction	1
1.1 Properties of pure CO ₂	5
1.2 The CO ₂ capture, transportation, and storage (CCTS) process.....	7
1.2.1 CO ₂ capture processes	8
1.2.2 CO ₂ transportation.....	11
1.2.3 CO ₂ storage.....	14
1.3 World CO ₂ pipelines.....	16
1.4 Simulation software	18
1.5 Scope of research.....	18
1.6 Aim and objectives.....	19
1.7 Thesis structure	20
Chapter 2: Literature Review	23
2.1 Introduction.....	23
2.2 Modelling CO ₂ flow in a Pipeline.....	23
2.3 CO ₂ Fluid Impurities and parameters.....	27
2.3.1 CO ₂ fluid impurities.....	29
2.3.2 CO ₂ fluid vapour - liquid phase envelope.....	33
2.3.3 Density of CO ₂ fluid.....	35
2.3.4 Formation of gas hydrates in CO ₂ fluids.....	39
2.3.5 Viscosity of CO ₂ fluids	40
2.4 CO ₂ pipeline design	46
2.4.1 Pipeline route and length.....	47
2.4.2 CO ₂ pipeline right of way (ROW).....	49
2.4.3 CO ₂ pipeline flow rates and velocity	49

2.4.4	Point-To-Point or Trunk/oversized pipelines.....	53
2.4.5	CO ₂ pipeline wall thickness	55
2.4.6	CO ₂ pipeline pressures, temperatures, and diameter.....	56
2.5	Chapter conclusion	64
Chapter 3: Research Methodology.....		66
3.1	Introduction	66
3.2	Aspen HYSYS	71
3.3	Process System Enterprise (gPROMS)	72
3.4	Equations of state and gas compressibility factor	73
3.4.1	van der Waals (vdW) EoS	75
3.4.2	Ridlich Kwong (RK) EoS	76
3.4.3	Soave Ridlich Kwong (SRK) EoS.....	77
3.4.4	Peng Robinson (PR) EoS.....	77
3.4.5	Peng Robinson Stryjek Vera (PRSV) EoS	78
3.4.6	Patel Tega (PT) EoS.....	79
3.5	Mixing rules.....	80
3.6	Density of CO ₂ fluids.....	81
3.7	Viscosity of CO ₂ fluids.....	82
3.8	Pipeline heat transfer	85
3.9	Other parameters.....	86
3.10	CO ₂ Pipeline pressures	88
3.11	Chapter conclusion.....	89
Chapter 4: Simulation of the effects of single impurities in CO₂ pipelines		90
4.1	Introduction	90
4.2	Effects of single impurities at 10 mol %	90
4.2.1	Methodology.....	91
4.2.2	Effects impurities on critical point	92
4.2.3	Effects of impurities on phase envelope.....	94
4.2.4	Effects of impurities on density.....	99
4.2.5	Effects of impurities on temperature.....	102
4.2.6	Effects of impurities on pressure drop	104
4.2.7	Effects of impurities on pressure in non-horizontal pipelines.....	106
4.2.8	Results and discussion.....	107

4.3	Impact of single impurity at maximum allowed concentrations	110
4.3.1	Methodology.....	110
4.3.2	Impact of impurities on density variation	111
4.3.3	Impact of impurities on critical pressure and temperature	112
4.3.4	Impact of impurities on viscosity.....	113
4.3.5	Impact of impurities on fluid pressure.....	114
4.3.6	Impact of impurities on fluid temperature	117
4.3.7	Impact of impurities on phase envelope	119
4.3.8	Grading of impurities	121
4.4	Chapter conclusion	122
Chapter 5:	CO₂ Pipeline Transportation: Supercritical or Subcritical Flow	124
5.1	Introduction	124
5.2	Methodology and modelling	124
5.3	Results and discussion	127
5.3.1	CO ₂ critical pressure	127
5.3.2	CO ₂ fluid density.....	128
5.3.3	CO ₂ pipeline flowing pressures	128
5.3.4	Viscosity and temperature.....	130
5.3.5	Volume and velocity	131
5.4	Chapter conclusion	133
Chapter 6:	Modelling of effects of impurities	134
6.1	Introduction	134
6.2	Z factor of CO ₂ pipeline fluids	135
6.3	Density of CO ₂ pipeline fluids	138
6.4	Viscosity of CO ₂ pipeline fluids	141
6.5	Temperature of CO ₂ pipelines	144
6.6	Pressure of CO ₂ pipelines.....	148
6.7	Chapter conclusion	150
Chapter 7:	Conclusion, recommendation, and future work	152
7.1	Conclusion	152
7.2	Recommendations.....	155
7.3	Further work.....	155

References	157
Appendix A	169
Table A 1: Regression values for density equation (McCollum and Ogden 2006)	169
Table A 2: Regression coefficients for μ Equation 2.15 (McCollum and Ogden 2006)	170
Table A 3: PVT values for CO ₂ + CH ₄ binary mixtures (Hwang et al. 1997)	171
Appendix B	172
Point-to-point, tree - branch and hub - spoke scenarios. (IEA GHG 2010)	172
Appendix C	173
Table C 1: Dependence of density regression equation coefficient on temperature (McCollum and Ogden 2006)	173
Table C 2: Dependence of viscosity regression equation coefficient on temperature (McCollum and Ogden 2006)	174

List of Figures

Figure 1.1: Schematic of the CCS components.	5
Figure 1.2: Phase envelope of pure CO ₂ (Coquelet et al. 2017).....	6
Figure 1.3: Phase envelopes of the selected pipeline fluids.	7
Figure 2.1: Pictorial of elemental volume of a fluid in pipeline	24
Figure 2.2 CO ₂ viscosity from density (Tarafer and Guiochon 2011).....	46
Figure 2.3: Relationship between flow rate ratio and diameter ratio (Wang et al. 2014).....	52
Figure 2.4: Maximum safe CO ₂ pipeline length against ambient temperature (Witkowski et al. 2014b).....	59
Figure 3.1: CO ₂ pipeline flow sheet created in Aspen HYSYS.....	71
Figure 3.2: Inclined CO ₂ pipeline	71
Figure 3.3: Downhill CO ₂ pipeline profile	72
Figure 3.4: : Location of Selected CO ₂ Pipelines (PowerPlantCCS 2010).....	73
Figure 4.1: P – T phase diagram of binary fluids at 10 mol % impurity concentration.	95
Figure 4.2: P – T phase diagram of selected pipelines fluids.....	97
Figure 4.3: Density of binary fluids at 10 mol % impurity concentration.	100
Figure 4.4: Temperature effect on density at different pressure values of a post combustion fluid.....	101
Figure 4.5: Density change along pipeline.....	102
Figure 4.6: Temperature drop of CO ₂ binary fluids (at 10 % impurity concentration) from inlet to outlet of pipeline.	103
Figure 4.7: Temperature drop of actual pipeline and pure CO ₂ fluids.....	103
Figure 4.8: Pressure drop of CO ₂ binary fluids from inlet to outlet of pipeline.	105
Figure 4.9: Comparison of pressure drop of actual pipeline fluids and pure CO ₂	105

Figure 4.10: Pressure drop of non – horizontal pipelines.....	106
Figure 4.11: Densities of CO ₂ binary mixtures.	112
Figure 4.12: Viscosity of binary CO ₂ fluids at 15MPa and 33 °C.....	114
Figure 4.13: Pressure change of CO ₂ binary fluids in horizontal, uphill and downhill pipeline.....	117
Figure 4.14: Temperature drop of binary mixtures.	119
Figure 4.15: Phase envelope of binary CO ₂ fluids.	120
Figure 5.1: Phase envelopes of CO ₂ capture fluids.	126
Figure 5.2: Critical points of typical CO ₂ capture fluids.	127
Figure 5.3: Oxy-fuel pipeline pressure profiles at indicated temperature.	129
Figure 5.4: Plot of pressure - drop versus velocity.	132
Figure 6.1: Gas deviation factors at 15 MPa and 33 °C (PR EoS).	136
Figure 6.2 Density of binary mixtures.....	139
Figure 6.3: Pure CO ₂ viscosity at different pressures and temperatures.	144
Figure 6.4: Pipeline temperature profile after first elemental flow.	146
Figure 6.5: Steady temperature profile of pipeline.	147

List of Tables

Table 1.1: Percentages of emission sources (Loáiciga 2013).....	9
Table 1.2: Impurities (in volume) from different capture methods (Antonie Oosterkamp 2008).	10
Table 1.3: Specification for enhanced oil recovery fluids (Global_CCS_Institute 2012).....	10
Table 1.4: Planned and operational CCS projects (Forbes et al. 2008).....	11
Table 1.5: CO ₂ Pipeline and CCTS fluid compositions (vol %) (Antonie Oosterkamp 2008; Patchigolla and Oakey 2013).....	12
Table 1.6: Existing and Proposed CO ₂ Storage Demonstration Projects (Forbes et al. 2008).....	15
Table 1.7a: Some existing and planned CO ₂ pipeline projects (IEA GHG 2014).	17
Table 2.1: CO ₂ pipeline stream concentration in mol % (Patchigolla and Oakey 2013).....	31
Table 2.2: Minimum and maximum mole fractions of typical impurities in CO ₂ streams (Munkejord et al. 2016).	32
Table 2.3: The minimum and maximum volume % of CO ₂ streams from capture processes (Antonie Oosterkamp 2008).....	32
Table 2.4: Density of CO ₂ /N ₂ mixtures (Goos et al. 2011)	36
Table 2.5: Coefficients for Equation 2.14 (Heidaryan et al. 2011).....	43
Table 3.1: k_1 and ω values for CO ₂ and impurities.....	79
Table 3.2: Tuned coefficients for Equation 3.8 (Heidaryan et al. 2011).	83
Table 4.1: Hypothetical pipeline specification.	91
Table 4.2: Actual fluid composition of CO ₂ pipelines (Patchigolla and Oakey 2013).....	92
Table 4.3: Critical temperature and pressure of binary CO ₂ fluids.	93
Table 4.4: Critical temperature and pressure of selected pipelines.....	94

Table 4.5: Comparative width of bubble and dew point lines at 20 °C.	98
Table 4.6: Percentage of impurity induced pressure change in pipeline profiles.	107
Table 4.7: Percentage change in horizontal pipelines due to 10 mol % impurities.	109
Table 4.8: Percentage of pressure and temperature change due to impurities	110
Table 4.9: CO ₂ Pipeline specification for impurities at maximum concentration.	111
Table 4.10: Critical pressure and temperature of CO ₂ fluids.....	113
Table 4.11: Dimensionless area of two-phase region of binary fluids at their maximum concentrations from 0 °C to critical temperature.....	119
Table 4.12: Percentage increase of fluid properties due to each impurity.....	121
Table 5.1: Pipeline specification.....	125
Table 5.2: Concentration of Impurities for the capture methods (Antonie Oosterkamp 2008; Seevam et al. 2008).	126
Table 5.3: Percentage increase of mass flow for lower temperatures.....	128
Table 5.4: Pipeline pressure drop.	129
Table 5.5: Percentage increase in fluid transport length for lower temperatures.	130
Table 5.6: Viscosity of fluids at the inlet.	130
Table 5.7: Temperature drop along the pipeline	131
Table 5.8 Pipeline inlet velocity at different inlet temperatures	132
Table 6.1: Binary fluid composition.	134
Table 6.2: z - factors for different EoS.	135
Table 6.3: z – factors with Aspen HYSYS and gPROMS.....	137
Table 6.4: Density values from different EoS.....	139
Table 6.5: Density values from Aspen HYSYS and Equation 6.21.	141

Table 6.6: Percentage deviation of viscosity values calculated with various equations.	143
Table 6.7: Viscosity of binary fluids at 15 MPa and 33 °C.....	144
Table 6.8: Thermal resistance values for fluid, pipeline and soil.	145
Table 6.9: Pipeline final temperature of binary fluids.	147
Table 6.10: Pressure drop of binary mixtures due to acceleration, friction and elevation.	149
Table 6.11: Percentage of pressure drop components.	149
Table 6.12: Grading of impurity impact on each parameter.	151

Nomenclature

°C	Degrees Celsius
CCS	Carbon capture and storage
CCTS	Carbon dioxide capture, transportation and storage
CH ₄	Methane
CHN	China
C _p	specific heat capacity
cP	Centipoise
D	Pipeline internal diameter
Do	Pipeline external diameter
DZA	Algeria
E	Energy OR Pipe efficiency factor
EOR	Enhanced oil recovery
EoS	Equation of state
f	moody friction factor
g	Gravity constant
h	enthalpy
k	Pipe roughness
K	kelvin
MMt	Million metric tonnes
MPa	Million pascals
NLD	The Netherlands
NOR	Norway
Opt.	Operational
P	Pressure
P _c	Critical pressure

PR	Peng - Robinson
PRSV	Peng – Robinson Stryjek Vera
PSE	Process System Enterprise
ROW	Right of way
R_e	Reynold's number
RK	Ridlich-Kwong
SRK	Soave-Ridlich-Kwong
t	Pipeline wall thickness OR time
T	Temperature
u	Velocity
V	Volume
VLE	Vapour liquid equilibrium
wt.	weight
Wy	Wyoming
x	Distance in x – direction
y	year
z	Gas deviation factor

Abbreviations

AUS	Australia
Comb.	Combustion
Comp.	Component(s)
FRA.	France
Hor.	Horizontal
Param.	Parameter
Pract.	Practical

Vol. Volume

Greek letters

α Pipeline elevation angle (degrees)

θ Angle of pipeline inclination

μ Viscosity

ρ density (kg/m³)

Δ Change

ω Acentric factor

Subscripts

ac acceleration

fr friction

gr gravity

hor horizontal

imp impurity

List of Publications in Course of this Research

Peer Reviewed Journal and Conference Articles.

1. Peletiri, S. P., Mujtaba, I. M. and Rahmanian, N. (2019) Process Simulation of Impurity Impacts on CO₂ Fluids Flowing in Pipelines. *Journal of Cleaner Production*, 118145.
2. Peletiri, S., Rahmanian, N. and Mujtaba, I. (2018) CO₂ Pipeline Design: A Review. *Energies* 11 (9), 2184.
3. Peletiri, S. P., Rahmanian, N. and Mujtaba, I. M. (2018) Grading the Impact of Impurities in Rich CO₂ Pipeline Fluids. *Chemical Engineering Transactions* 70, 175-180.
4. Peletiri, S. P., Rahmanian, N. and Mujtaba, I. M. (2017) Effects of Impurities on CO₂ Pipeline Performance. *Chemical Engineering Transactions* 57, 355 - 360.
5. Rehan, M., Rahmanian, N., Hyatt, X., Peletiri, S. P. and Nizami, A.-S. (2017) Energy Savings in CO₂ Capture System through Intercooling Mechanism. *Energy Procedia* 142, 3683-3688.

Chapter 1: Introduction

Humans depend on fossil fuel in their ever-expanding industrialisation. Fossil fuel combustion in the industries releases carbon dioxide (CO₂) into the atmosphere. It is believed that the release of CO₂ and other greenhouse gases causes an increase in the global average temperature. By 2017, human activities were believed to have caused the temperature of the earth to rise by approximately 1 °C above pre-industrial levels and now rising about 0.2 °C per decade or 0.3 – 0.7 °C over a 30 - year period ([Masson-Delmotte et al. 2018](#)). Land regions experience higher warming than the global mean while oceans are warming slower ([Allen et al. 2018](#)). Human activities have impacted so much on the earth that a new epoch, the Anthropocene epoch, has been proposed ([Waters et al. 2016](#)). The observed increase in global temperature is blamed on increases in greenhouse gases, chief of which is CO₂ in the atmosphere. Many industrial processes generate CO₂, including power generation, oil and gas production, steel manufacturing, gas flaring, etc. There is strong evidence that in the past fifty years the burning of fossil fuel has contributed to global warming ([Mollersten et al. 2004](#); [IPCC 2011](#)) and CO₂ alone contributes over 60 % to global warming ([Joel et al. 2015](#)). About 75 % of atmospheric CO₂ increase is due to the use of fossil fuel for combustion ([Olajire 2010](#)) with an attendant increase in global temperatures which may increase Earth's temperature by about 6.4 °C by the year 2100 ([Kianpour et al. 2012](#)). Fossil fuel combusting plants release the largest quantities of CO₂ among stationary anthropogenic CO₂ sources ([Lazic et al. 2014](#)). Global temperature may increase by more than 1.6 °C by 2100 with a 10 - year average increase of 0.2 °C. CO₂ concentrations in the atmosphere have been recorded to exceed 0.04 % in Mauna Loa Observatory in Hawaii ([Keeling](#)

[2013](#)). The impacts of global warming include land and sea surfaces become hotter, increase in the frequency of heatwaves in land regions, prolonged heat waves in marine environments, increase in frequency of heavy precipitation, increase in drought in the Mediterranean region, etc. ([Hoegh-Guldberg et al. 2018](#)).

The [IPCC \(2007\)](#) report, listed some of the future impacts of global temperature rise:

- 10 – 40 % increase in annual mean river runoff and water availability and 10 – 30 % decrease in dry regions at the tropics and mid - latitudes.
- Flood risks will increase with heavy precipitation with widespread draught.
- Decrease in water availability to regions supplied by glaciers and snow-covered mountains.
- About 20 – 30 % of plant and animal species dying out if the earth's temperature exceeds 2.5 °C increase.
- Ecosystems at a high risk from the combined effects of flooding, drought, wildfire, insects, ocean acidification, pollution, over-exploitation of natural resources and land-use.
- The acidification of the oceans from increased CO₂ concentrations will adversely affect marine organisms with shells.
- Warmer temperatures favour increased timber production in the short to medium term but have adverse effects on fisheries.

- Increased heatwaves, fires and drought will cause increases in disease, death, and injury.
- Crop productivity may increase at high altitudes but decrease at low altitudes. Global food production is expected to increase within 1 - 3 °C rise in temperature but decrease above this value.

This frightening prediction makes it imperative to mitigate the adverse effect of releasing CO₂ into the atmosphere. CO₂ must not be released into the atmosphere if the adverse effects are to be avoided. Carbon dioxide capture and storage (CCS) is one of the few viable carbon mitigation technologies ([Ke et al. 2017](#)). CO₂ must be captured, transported, and safely stored underground, used for enhanced oil recovery (EOR) or used in other ways.

The world is still slow in realizing the urgency for capturing anthropogenic CO₂ emissions to combat rising global temperatures. This can be drawn from the number of operational CCS projects around the world. In 2016, only the Boundary Dam Project was a large scale CCS project in the world while others were still being designed ([Lake et al. 2016](#)). Though the portfolio for large – scale CCS projects increased from 8 in 2010 to 15 in 2017, about 22 is expected to be commissioned on or before 2020 ([Lipponen et al. 2017](#)). The most promising way to reduce greenhouse gases is through CCS ([Ilinova et al. 2018](#)). Capturing CO₂ and preventing it from entering the atmosphere is capable of reducing global CO₂ emissions by about 19 % ([Selma et al. 2014](#)).

Pipeline transportation is the preferred means of transporting CO₂ on land. For this reason, more pipelines shall be constructed as the Paris Agreement is implemented by many countries. The world had about 7,000 km of various

diameter CO₂ pipelines, but requires about 360,000 km of new CO₂ pipelines worldwide ([IEA GHG 2014](#)). This means that about 353,000 km of new CO₂ pipelines are to be constructed up to the year 2050. It is projected that the USA alone will build up to 37,000 km of new CO₂ pipelines before the year 2050 ([Dooley et al. 2009](#)), which is over 10 % of the projection for new CO₂ pipelines worldwide.

The CO₂ released from industrial processes is captured and transported to sites where it is stored underground. The captured CO₂ is impure and contains several impurities including CH₄, N₂, SO₂, H₂S, CO, O₂, NH₃, H₂, Ar, H₂O, etc. ([Rehan et al. 2017](#)). Pressure, temperature, density, viscosity, critical pressure and temperature, phase envelope, etc. are all affected by the type of impurities in the CO₂ fluid and the concentration of the impurities. Understanding the impact of impurities on CO₂ pipeline transportation is required to optimise the design of these pipelines. This chapter presents the effects of the impurities assuming the same constant concentration for all impurities and at concentrations at the specified maximum for each impurity.

CO₂, the most common anthropogenic pollutant ([Caravaggio et al. 2019](#)) is purified after capture and transported in pipelines to storage sites and stored in underground sinks ([Piippo et al. 2018](#)). Though it is understood that pipelines are the preferred means of transportation on land, they were found to be cost-inefficient when transporting small volumes over long distances ([Jakobsen et al. 2017](#)).

There are three major components of CO₂ Capture and Storage (CCS) process or CO₂ capture, transportation and storage (CCTS) ([Wang and Lawal 2013](#))

process: capture, transportation and storage/sequestration. Figure 1 is a pictorial of the CCTS process. After capture, CO₂ is compressed before it is fed into the transporting pipeline. Along the pipeline, CO₂ is compressed to provide pressure for transportation and to keep it above supercritical pressure. At the storage location, CO₂ is compressed to overcome the in-situ pressures in the storage reservoir while pumping it down. Pipelines are the most common means of transporting CO₂ on land and competitive with ships offshore ([Joana et al. 2011](#)). It has been shown that pipelines have about 10 % lower CO₂ transportation costs than ships ([Luo et al. 2014a](#)). CO₂ is in a gaseous phase at standard pressure and temperature (STP), i.e. at 0.101325 MPa and 15.6 °C, but for efficient transportation, it is conditioned to a dense phase: supercritical or liquid state.

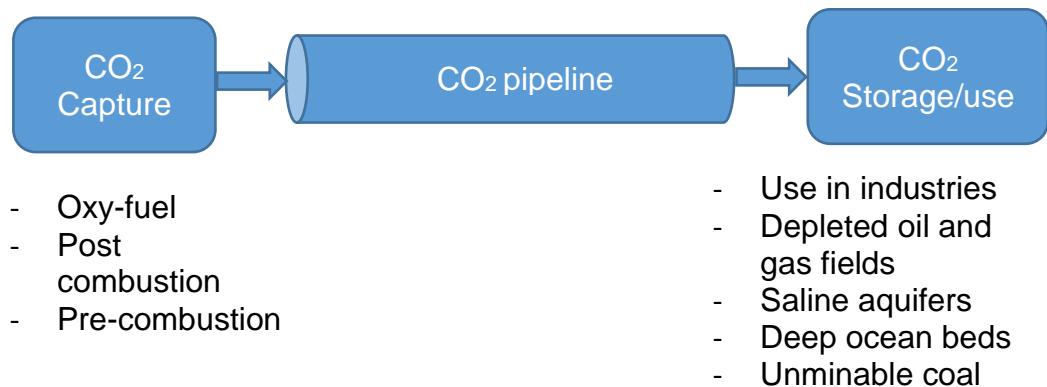


Figure 1.1: Schematic of the CCS components.

1.1 Properties of pure CO₂

CO₂ is a non-polar, colourless, and odourless gas at atmospheric pressure and temperature. It has a triple point at -56.6 °C and 0.52 MPa, critical pressure of 7.38 MPa and critical temperature of 30.9782 °C ([Antonie Oosterkamp 2008](#)). Figure 1.2 shows the pressure – temperature (P – T or phase) diagram of pure CO₂. It is about 1.67 times denser than air with a density of about 1.9 kg/m³.

Above the critical pressure and temperature, CO₂ exist as a supercritical fluid having the density of a liquid and the viscosity of a gas.

The phase diagram of CO₂ with impurities has a two-phase region. See Figure 1.3 for the phase diagram of four CO₂ pipeline fluids. The bubble point curve and the dew point curve meet at the critical point. The fluid exists as a single supercritical fluid at pressures and temperatures above the critical point. Within the bubble point and dew point curves, the fluid exists in two-phases (gaseous and liquid phases). The fluid exists as a liquid above the bubble point curve and as a gas below the dew point curve.

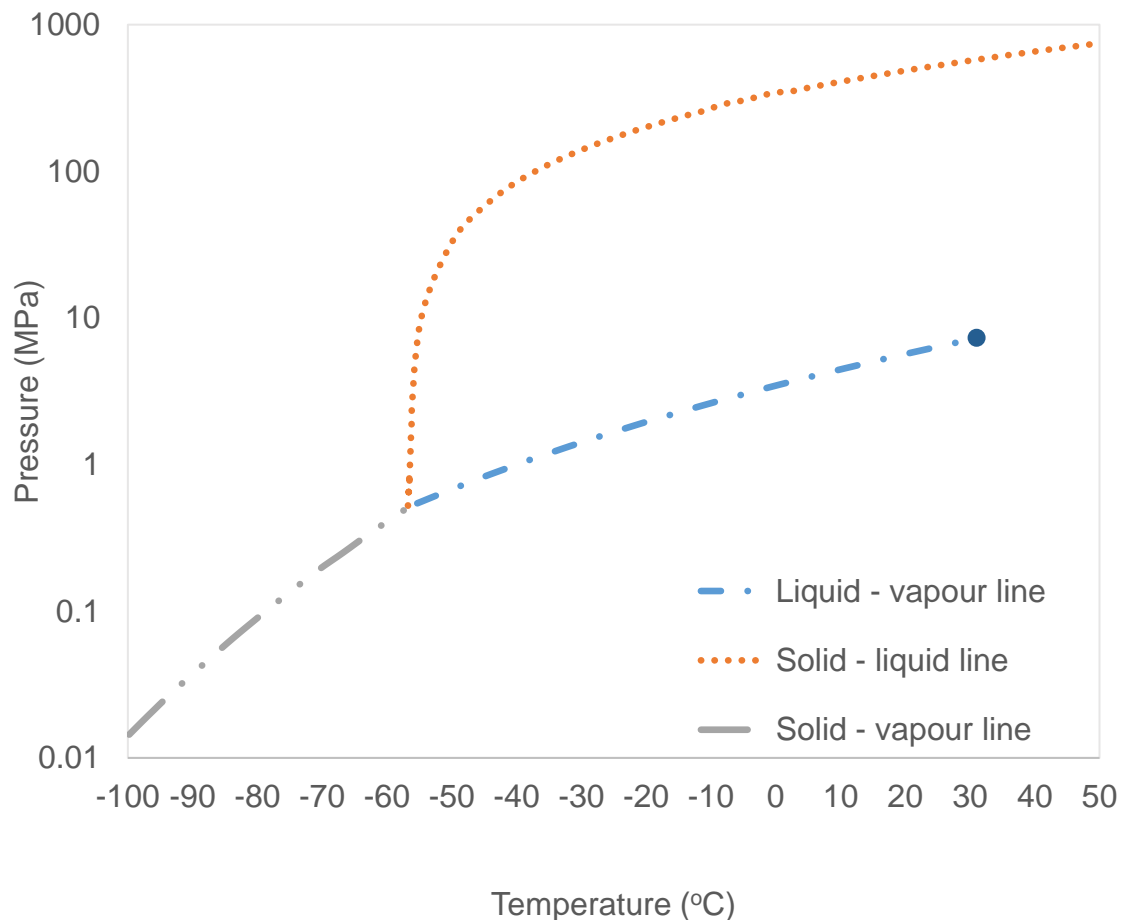


Figure 1.2: Phase envelope of pure CO₂ (Coquelet et al. 2017).

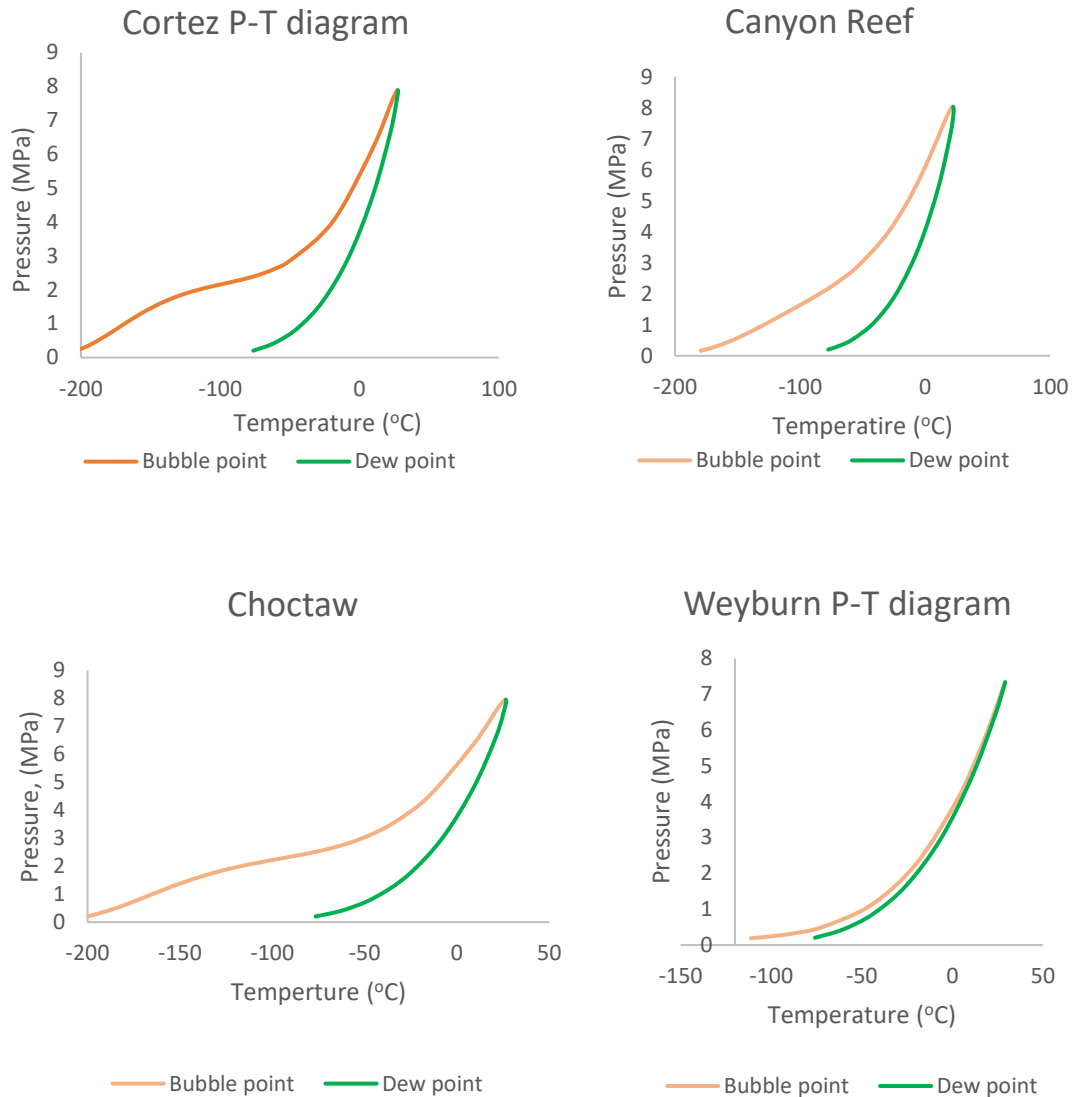


Figure 1.3: Phase envelopes of the selected pipeline fluids.

1.2 The CO₂ capture, transportation, and storage (CCTS) process

CCTS is a three-stage process; capture, transportation, and storage (see Figure 1.1). The CO₂ is captured from the flue gas released from industrial processes. This captured fluid is compressed before it is fed into the pipeline for transportation, with possibly further compression during transportation. The CO₂ is compressed to overcome the in-situ pressures in the reservoir during injection for storage.

1.2.1 CO₂ capture processes

The capture of CO₂ from power plant or industry fuel stream or flue gas or natural gas streams is by chemical solvent absorption or physical adsorption. Chemical solvents used in the capture of CO₂, preferentially absorb CO₂ but are disadvantaged by the thermal regeneration and degradation while physical adsorbents have good pressure swing regeneration and better thermal degradation but limited selectivity for CO₂ ([Rainbolt et al. 2011](#)). CO₂ capture from large point sources such as combustion power plants, cement factories, and other large emitting sources is an advanced technology and in operation in some countries. However, capturing CO₂ emissions from the transportation sector, residential and other smaller commercial sectors may be difficult ([Loáiciga 2013](#)) and is not practiced in any country. The emissions from these sources could be significant as shown by the emission percentages in the United States (see Table 1.1). Of these, the emissions from large volume concentrations or industrial sources are the targets for capturing.

Pre-combustion, oxy-fuel and post-combustion are the three methods of capturing CO₂ from industrial sources. Pre-combustion capture is done before the thermal process and entails coal gasification or natural gas reformation with O₂, producing mostly CO₂, CO and H₂ and finally CO₂ and H₂ after the conversion of CO with steam (see Equation 1.1) ([Kanniche et al. 2010](#)). An absorbent or adsorbent separates the CO₂ from the H₂, which is used as fuel for the generation of electricity or heat.

In the oxy-fuel combustion method, O₂ of about 97% purity used in the combustion process results to exhaust gases with a high percentage and partial

pressure of CO₂. The CO₂ from oxy-fuel can easily be made up to 99% purity by condensing the water out ([Kanniche et al. 2010](#)).

Table 1.1: Percentages of emission sources ([Loáiciga 2013](#)).

Sector	% of emissions
Commercial	18.5
Industrial	27.5
Residential	20.7
Transportation	33.3

For post-combustion capture, the CO₂ is separated from the exhaust gases after combustion of the fuel (coal, crude oil, natural gas, etc.) with air. Chemical absorption is mostly employed in post-combustion capture due to the low partial pressure of the CO₂ in the exhaust (flue) gas. Different capture processes result to different impurities and varying concentrations of impurities (see Table 1.2). Post combustion capture has the highest purity level with up to 99 vol. %.

The most expensive component of the CCS process is capture, making up about 50% ([Kang et al. 2014](#)), or up to 90% including the cost of compression ([Middleton and Bielicki 2009](#)) of the total cost of CCS. Captured CO₂ meant for transportation must meet standards before it is fed into the pipeline. This captured CO₂ contains impurities that are not desirable for transportation and/or storage/usage. Impurities like SO_x, H₂S and NO_x have destructive effects on transportation and storage components of the CCS process and H₂O has the tendency to corrode pipes and form hydrate.

To attain supercritical state, the captured CO₂ is compressed to pressures and temperatures above the critical values before it is pumped into the pipeline for transportation ([Witkowski et al. 2014b](#)). Table 1.3 lists the limits specified for CO₂

pipeline fluids in enhanced oil recovery (EOR) operations. Table 1.4 shows some planned and operational CCS projects ([Forbes et al. 2008](#)). Some of these projects, e.g. the Total Lacq CCS project, are fully integrated projects with capture, transportation and storage components ([Cieutat et al. 2009](#)).

Table 1.2: Impurities (in volume) from different capture methods ([Antonie Oosterkamp 2008](#)).

Component	Post Combustion	Pre - Combustion	Oxyfuel
CO ₂	> 99 %	> 95.6 %	> 90 %
CH ₄	<100 ppm	< 350 ppm	--
N ₂	<0.17 %	< 0.6 %	< 7 %
H ₂ S	Trace	< 3.4 %	trace
C ₂₊	<100 ppm	< 0.01 %	--
CO	<10 ppm	< 0.4 %	Trace
O ₂	< 0.01 %	Trace	< 3 %
NO _x	< 50 ppm	--	< 0.25 %
SO _x	<10 ppm	--	< 2.5 %
H ₂	Trace	< 3 %	Trace
Ar	Trace	< 0.05 %	< 5 %

Table 1.3: Specification for enhanced oil recovery fluids ([Global CCS Institute 2012](#))

Constituent	Specification	Reason
CO ₂	95% minimum	MMP
Nitrogen	4% maximum	MMP
Hydrocarbons	5% maximum	MMP
Water	480 mg/cubic meter max	Corrosion
Oxygen	10 ppm max	Corrosion
H ₂ S	10-200 ppm max	Safety
Glycol	0.04 ml/cubic meter max	Operations
Temperature	65° C max	Material Integrity

Table 1.4: Planned and operational CCS projects ([Forbes et al. 2008](#))

Project Name	Location	Feed	Size (MW)	Capture Process	Start-up Date
Total Lacq	France	Oil	35	Oxy-fuel	2008
AEP Alstom Mountaineer	USA	Coal	30	Post-C	2008
Callide-A Oxy Fuel	Australia	Coal	30	Oxy-fuel	2009
GreenGen	China	Coal	250/800	Pre-C	2009
Williston	USA	Coal	450	Post-C	2009–15
NZEC	China	Coal	Undecided	Undecided	2010
AEP Alstom	USA	Coal	200	Post-C	2011
Sargas Husnes	Norway	Coal	400	Post-C	2011
Scottish & Southern	UK	Coal	500	Post-C	2011–12
Naturkraft Kårstø	Norway	Gas	420	Post-C	2011–12
Fort Nelson	Canada	Gas	Gas	Pre-C	2011
ZeroGen	Australia	Coal	100	Pre-C	2012
WA Parish	USA	Coal	125	Post-C	2012
UAE Project	UAE	Gas	420	Pre-C	2012
Appalachian Power	USA	Coal	629	Pre-C	2012
RWE npower Tilbury	UK	Coal	1600	Post-C	2013
Tenaska	USA	Coal	600	Post-C	2014
UK CCS Project	UK	Coal	300–400	Post-C	2014
Statoil Mongstad	Norway	Gas	630 CHP	Post-C	2014
RWE Zero CO ₂	Germany	Coal	450	Pre-C	2015
Monash Energy	Australia	Coal	60,000 bpd	Pre-C	2016
Powerfuel Hatfield	UK	Coal	900	Pre-C	Undecided
ZENG Worsham-Steed	USA	Gas	70	Oxy-fuel	Undecided
Polygen Project	Canada	Coal	300	Pre-C	Undecided
E.ON Karlshamn	Sweden	Oil	5	Post-C	Undecided

1.2.2 CO₂ transportation

The link between CO₂ capture and storage is transportation. Usually, CO₂ sources and storage locations do not occur close together. Therefore, a means of transportation is required to move the CO₂ fluid from the source to the storage location.

Although transportation may be the least expensive component of the CCS process, when it comes to guidance and planning, it may be the most demanding ([Neele et al. 2011](#)). On land, pipelines, truck tankers, and railcars are employed in the transport of CO₂ while offshore transportation requires the use of ships and

pipelines. Large volume transportation of CO₂ on land is most economical by pipeline and in offshore transportation, pipelines are competitive with ships ([Parfomak and Folger 2007](#)). Pipeline CO₂ is specified by the US Department of Transportation as a compressed supercritical fluid consisting of more than 90 % CO₂ molecules ([Forbes et al. 2008](#)). CO₂ transportation in the US is mostly for enhanced oil recovery (EOR) and it is from natural CO₂ sources. Table 1.5 shows some typical compositions of existing pipelines and impurity ranges for the three types of CO₂ capture processes.

Table 1.5: CO₂ Pipeline and CCTS fluid compositions (vol %) ([Antonie Oosterkamp 2008](#); [Patchigolla and Oakey 2013](#)).

Gas	Weyburn CO ₂ pipeline	Denbury CO ₂ pipeline	Canyon Reef Carriers	Post comb.	Oxy-fuel comb.	Pre – comb.
CO ₂	96	≥ 95	≥ 85	> 99	> 90	> 95.6
N ₂	< 0.03	≤ 4	≤ 0.5	< 0.17	< 7	< 0.6
CH ₄	0.7	≤ 5	≤ 15	< 0.01	-	< 0.035
H ₂ S	0.9	0.0015	< 0.002	trace	trace	< 3.4
O ₂	0.005	-	-	<0.01	<3	trace
CO	-	-	-	<0.001	<trace	< 0.4
NO _x	-	-	-	<0.005	<0.25	-
SO _x	-	-	-	<0.001	<2.5	-
H ₂	trace	-	-	trace	<trace	<3
Ar	-	-	-	trace	<5%	<0.05
H ₂ O	0.002	0.047	0.005wt.	0.14	0.14	0.14

Storage sites for CO₂ are usually offshore or far away from CO₂ sources, so the demand for pipelines for transportation may increase in the near future ([Zargarzadeh et al. 2013](#)). [Knoope \(2015\)](#) stated that between 6,000 to 7000 km

of CO₂ pipelines exist worldwide with most of them in the United States transporting CO₂ fluids for EOR. The projection is that world total pipeline length will increase to about 100,000 km in 2030 for the expected volume of 1.4 Gt and to about 200,000 km for about 2.2 Gt in 2050 ([IEA GHG 2010](#)). [Knoope et al. \(2015\)](#) put the projected length of pipelines by 2050 at between 200,000 km and 550,000 km. The figure for Europe is between 5,000 km and 15,000 km in 2030 and 11,000 km and 17,000/20,000 km in 2050 ([Morbee et al. 2012](#); [Knoope 2015](#)). There is therefore need to understand all aspects of CO₂ pipelines and effectively design and build them to transport CO₂ from the source(s) to the sink(s) ([Mazzoldi et al. 2008](#)).

In the development of a suitable CO₂ pipeline, it is necessary to consider pipeline integrity, operation, flow assurance, and health and safety ([Lazic et al. 2014](#)). The physical properties of the flowing fluid determine the CO₂ pipeline parameters. There have been several studies on the behaviour of rich CO₂ fluids in various phases but the operational pressure and temperature of CO₂ pipelines make the behaviour unusual ([Lazic et al. 2014](#); [Zahid et al. 2014](#)). Therefore, there is need for CO₂ pipelines to be specifically designed for good performance, safe operation and low cost ([Zahid et al. 2014](#)).

The [IEA GHG \(2002\)](#) report identified the stages of CO₂ pipeline operations to include; design, construction and operation. Parameters that affect CO₂ pipeline design include, corrosion protection, over-pressure protection systems, protection from damage, pipe wall thickness, access route, monitoring and safety facilities, etc. A complete CO₂ pipeline design will involve determining the physical properties of the process stream, selecting an optimal pipeline size,

pipeline pressure requirement, knowledge of pipeline route topography, geotechnical considerations and the local environment ([Lazic et al. 2014](#)).

1.2.3 CO₂ storage

Geologic formations having sufficient porosity and permeability can store CO₂. These formations (saline aquifers and depleted oil and gas reservoirs) must be of sufficient depth at pressures high enough to keep the injected CO₂ in dense phase (supercritical or liquid state) and be competent enough to hold the injected CO₂ preventing leakage back to the surface. [IEA GHG \(2005\)](#) studied the following storage options:

- Deep saline aquifers.
- Abandoned hydrocarbon fields.
- Oil field with incremental oil production (EOR).
- Deep unminable coal seams with CH₄ production.

The technical storage capacity of these reservoirs was determined after compiling geological storage data for CO₂ storage and developing cost curves for each option. Aquistore, an independent and monitoring project, seeks to show that it is safe to store liquid CO₂ in deep underground (brine and sandstone water formations) ([Worth et al. 2014](#)). The geologic parameters considered in the Aquistore project include depths more than 800m, groundwater, mineral and energy sources protection, adequate capacity, injectivity, and competent seals restricting upward migration and risk of CO₂ leakage back to the surface to endanger the public.

Besides geologic characteristics, proximity to the source, ease of pipeline route, and availability of rights to the surface were also considered in the Aquistore project ([Whittaker and Worth 2011](#)). A good candidate for CO₂ storage would then be a reservoir with adequate capacity, good pressures, and competent seals/cap rock to prevent CO₂ migration to the surface. Table 1.6 presents some existing and proposed CO₂ storage projects as at 2008. The projects that have been commissioned was not confirmed.

Table 1.6: Existing and Proposed CO₂ Storage Demonstration Projects ([Forbes et al. 2008](#))

Project	Location	CO ₂ Source	Size MMt/y	Start Year
Sleipner	Norway	Gas Proc.	1	1996
In Salah	Algeria	Gas Processing	1.2	2004
Zama	Canada	Gas Processing	0.067	2006
Snohvit	Norway	LNG Processing	0.7	2008
Ketzin	Germany	H ₂ Production	0.03	2008
Decatur	Illinois, U.S.	Ethanol Prod.	0.3	2009
Cranfield	U.S.	Gas Processing	1	2008-9
TAME	Ohio, U.S.	Ethanol Prod.	0.28	2011
Lindach	Australia	Industrial	0.3	TBD
Casablanca	Spain	Refinery	0.5	TBD
Weyburn	Canada	Coal Gasification	1	2000
K12-B	Netherlands	Gas Processing	0.2	2004
Gorgon	Australia	Gas Processing	3.3	2009
Entrada	Colorado US	Gas Processing	1.1	2008-12

There have been several estimates of the storage capacity in the UK with widely varying figures. A major reason for the different values is due to the assumptions made, e.g. the pore volume. The UK saline aquifer storage capacity was

estimated to be about 78 Gt by [Bentham et al. \(2014\)](#). An earlier estimate puts the capacity of the Southern North Sea at about 14 Gt which can hold 89 years of CO₂ emissions and oil and gas fields' storage capacity of about 6.2 Gt which is enough to hold 35 years CO₂ emissions from the power sector at 2006 emission levels ([Gough et al. 2006](#)).

1.3 World CO₂ pipelines

There are just over 6500 km of CO₂ pipelines in the world ([IEA GHG 2014](#)), an increase from 2400 km in 2007 ([Towler et al. 2007](#)). Of these pipelines, the US alone has over 6000 km of CO₂ pipelines ([Dooley et al. 2009](#); [Noothout et al. 2014](#)). As stated by [Chandel et al. \(2010\)](#), the US had over 2500 km of pipeline in 2010 transporting 50 million tonnes of CO₂ annually, while as at 2013, Europe only had about 500 km of CO₂ pipelines ([Forgács and Horánszky 2013](#)). Table 1.7 lists some existing and planned CO₂ pipelines ([IEA GHG 2014](#)). Of the pipelines listed in Table 1.7, there is only one project each located in Africa, China, Germany, Australia and France. It is expected that after the signing of the Paris Agreement, many more countries will implement CCS and more CO₂ pipelines would be built around the world.

In Table 1.7, the Peterhead and White Rose projects were reported as planned but both projects were cancelled. The UK government cancelled the £1 billion CCS Competition on the 25th November 2015 essentially stopping contracts for both the Peterhead and the White Rose CCS projects. The former UK prime minister, David Cameron, was quoted as saying that Carbon capture and storage is £1 billion of capital expenditure - £1 billion that we could spend on flood defenses, schools or the health service – but even after we've spent that £1

billion, the economics of carbon capture and storage really aren't working at the moment ([Duckett 2016](#)).

Table 1.7: Some existing and planned CO₂ pipeline projects ([IEA GHG 2014](#)).

	Project name	Length (km)	(Mtpa)	D (mm)	Status	Country
1	Quest	84	1.2	324	Plan	CAN
2	Alberta Trunk line	240	15	406	Plan	CAN
3	Weyburn	330	2.0	305-356	Opt	CAN
4	S B Dam	66	1.2		Plan	CAN
5	Beaver Creek	76	-	457	Opt	USA
6	Monell	52.6	1.6	203	Opt	USA
7	Bairoil	258	23		Opt	USA
8	Salt Creek	201	4.3		Opt	USA
9	Sheep Mountain	656	11	610	Opt	USA
10	Slaughter	56	2.6	305	Opt	USA
11	Cortez	808	24	762	Opt	USA
12	Central Basin	231.75	27	406	Opt	USA
13	CanyonReef Carriers	225	-	324-420	Opt	USA
14	Chowtaw (NEJD)	294	7	508	Opt	USA
15	Decatur	1.9	1.1		Opt	USA
16	Snohvit	153	0.7		Opt	NOR
17	Peterhead	116	10		Canc.	UK
18	White Rose	165	20		Canc.	UK
19	ROAD	25	5	450	Plan	NLD
20	OCAP	97	0.4		Opt.	NLD
21	Lacq	27	0.06	203-305	Opt.	FRA
22	R N Q	30	0.5		Plan	DZA
23	Qinshui	116	0.5	152	Plan	CHN
24	Gorgon	8,4	4	269-319	Plan	AUS

1.4 Simulation software

Three different simulation software Aspen HYSYS, gPROMS, and HydraFlash were used in this research. Aspen HYSYS is an industry leading simulation package used for oil and gas, refining, and general engineering process. gPROMS is a general Process Modelling System with the ability to simulate, optimise and estimate parameters in both steady-state and dynamic simulations. HydraFLASH is a gas hydrate and thermodynamic prediction software which calculates the physical properties and phase equilibria of petroleum reservoir fluids.

1.5 Scope of research

With nearly all countries signing the Paris (Climate) Agreement, billions of dollars are expected to be spent for the design and construction of CO₂ pipelines around the world. Therefore, there is need to fully understand the flow dynamics of CO₂ fluids in pipelines in both steady and dynamic states and design them for optimal operation. Most available models use pure CO₂ ignoring the effects of impurities in the determination of pressure drop and/or diameter calculations. The scope of this research is stated below.

- There are several impurities found in CO₂ fluids flowing in pipelines but only the impurities that have significant impact on the parameters (N₂, CH₄, H₂S, SO₂, NH₃, Ar, CO, O₂, H₂, H₂O) are considered. Impurities with negligible concentrations were ignored.
- The effect of the common impurities on the density, viscosity, critical pressure, critical temperature, phase envelope, pressure and temperature changes are investigated.

- Only steady state flow is considered in this study. Dynamic flow during start-up and shutdown or ramp up and ramp down is not considered.
- Thermodynamic analysis of subcritical and supercritical flow is also investigated to see which state of fluid transportation is preferable.

1.6 Aim and objectives

The aim of this research is to investigate the effect of impurities on the transportation of CO₂ fluids in pipelines. All impurities impact on the thermodynamics of rich CO₂ fluids. Lacking in the available literature is the effects of each CO₂ impurity on the flowing fluid in the pipeline. This research will study the effect of all common impurities in CO₂ pipelines (N₂, CH₄, H₂S, SO₂, CO, H₂, Ar, NH₃, and O₂) and supplement the existing knowledge. The observed effects of the impurities are used to convert pure CO₂ properties to binary fluid properties for the design of CO₂ pipeline transportation.

The objectives include:

- Study the effects of impurities on the pressure losses, temperature changes, critical pressure, critical temperature, and phase envelope using process simulation software e.g. gPROMS and Aspen HYSYS.
- Indicate the impurities with adverse effect on each property/parameter for effective design of CO₂ pipelines.
- It is unclear which fluid state is preferable for pipeline transportation. This research thermodynamically analyses supercritical and subcritical CO₂ fluids flowing in pipelines and show the preferable fluid state for pipeline transportation.

- To analyse the impact of the impurities at equal concentrations and at the maximum allowed concentrations and rank the impurities according to the degree of their impacts.

1.7 Thesis structure

This thesis is arranged in seven chapters and the chapters are presented as follows:

Chapter 1: Introduction

The general overview of the carbon dioxide capture, transportation, and storage process. The three common capture processes, oxy–fuel, pre – combustion, and post – combustion, and their impurity concentrations were briefly discussed. Actual CO₂ pipelines and their impurities were also mentioned.

Chapter 2: Literature Review

A critical review of the current state-of-the art that is accessible in the available literature was conducted. These include CO₂ fluid impurities, flow parameters, density, viscosity, gas hydrates, pressure and temperature behaviour, etc. A comprehensive review of CO₂ pipeline design including pipeline route, right of way, flow rates, pipeline wall thickness, temperatures, and pressures was done.

Chapter 3: Research methodology

The equations used in the two software were presented. Several equations used in the computation of the various parameters were considered. Where possible the same equations were used in both Aspen HYSYS and gPROMS to see how both software performed relative to each other and available data.

Chapter 4: Simulation of the effects of single impurities in CO₂ pipelines

The impact of the impurities at equal concentration and at the maximum allowed concentration in CCS was analysed. This Chapter shows the effect of each impurity on the thermodynamic properties of CO₂ fluids flowing in pipelines. The knowledge presented in this chapter has provided necessary data bridging the gap in the available literature. At equal concentration, H₂, was found to have the greatest impact on pressure loss, critical pressure, temperature change, and density. SO₂ has the greatest effect on critical temperature. At the specified maximum concentrations, N₂ having the highest concentration, has the worst impact on pressure loss, density, critical pressure, critical temperature, phase envelope, and temperature. At 6.5 mol % concentration, H₂O has the maximum increase in viscosity. The impact of impurities at equal concentrations and at permitted concentrations is a useful guide during design to analyse the necessary parameters for optimisation. Generally, gases with lower molecular weight will result in lower pressure losses in inclined pipelines. These same gases will result in lower pressure gains or higher pressure losses in declined pipelines. Molecular weight of gases is directly proportional to pressure loss in inclined pipelines but inversely proportional to pressure loss in declined pipelines.

Chapter 5: CO₂ Pipeline Transportation: Supercritical or Subcritical Flow

The question of the better fluid state, supercritical or liquid/subcritical, in which to transport CO₂ in pipelines was answered in this chapter. It clearly shows that transporting CO₂ in subcritical state is more economical than transporting it in supercritical. More volume of fluid is transported for longer distances under subcritical flow than supercritical flow. Transporting fluid for longer distances may require fewer boosting stations in long distance pipelines saving both capital and operational costs. The evidence presented in this chapter can be used to review

the requirement or specification for supercritical fluid state in CO₂ pipeline transportation. By holding the inlet pressure constant, at above the critical value, and varying the temperature, it was shown that lower fluid temperature results to overall lower pressure losses. Subcritical fluids performed better in all parameters studied. Therefore, transporting CO₂ fluid as a subcritical fluid is better than transporting it as a supercritical fluid.

Chapter 6: Modelling of the effects of impurities

Equations to convert pure CO₂ parameters to impure CO₂ fluid parameters in CCTS operations were developed and presented in this chapter. CO₂ pipeline design parameters obtained assuming pure CO₂ fluids can easily be converted to impure CO₂ parameters using these equations. The temperature change of buried pipelines was also investigated in this chapter.

Chapter 2: Literature Review

2.1 Introduction.

In this section, a review of CO₂ pipeline design and the impact of impurities found in CO₂ fluids, the fluid parameters affected by these impurities is presented. The parameters include thermodynamic properties (temperature, pressure, and density), miscellaneous properties (viscosity, and vapour pressure) and kinematic properties (velocity). The current CO₂ pipeline design equations and parameters are discussed. To study the effects of impurities on CO₂ pipeline transportation, flow parameters affected by the impurities are studied. The results are used to quantify the effect of each impurity.

2.2 Modelling CO₂ flow in a Pipeline.

The traditional model of fluid flow is based on the Navier-Stokes equations which were derived in the 1840s on the basis of conservation laws and first-order approximations ([Wolfram 2002](#)). The modelling of fluid flow requires the solution of a system of partial differential equations. These equations are based on the conservation of mass, momentum, and energy at each point along the pipeline.

The motion of a fluid is governed by mass, momentum, and energy conservation laws. Inaccurate predictions of fluid properties could result in differences from experimental values. For example, a wrong value of density would result in a wrong pressure drop value. Fluid/fluid or fluid/wall interactions create frictional pressure loss, which is always present in fluid flow. In inclined pipelines, the effect of gravitation may supersede the frictional pressure loss and govern the flow behaviour. The Navier-Stokes equations are used to formulate a complete model of fluid flow. The equations consider the changes in fluid properties with time and

in the three spatial directions. The solution of the three-dimensional problem is complex and not necessary because a one-dimensional flow model is sufficient for CO₂ fluid flow in pipelines. The following assumptions are made to simplify the solution but still maintain the accuracy.

- Flow in the pipeline is one-dimensional
- Homogeneous equilibrium fluid flow (HEM).
- Constant cross-sectional area of pipeline.

2.2.1.1 Conservation of mass

The mass conservation equation can be derived by applying the mass balance for a finite element (Δx) of fluid. Figure 2.1 show a finite element of a fluid flowing in a pipeline.

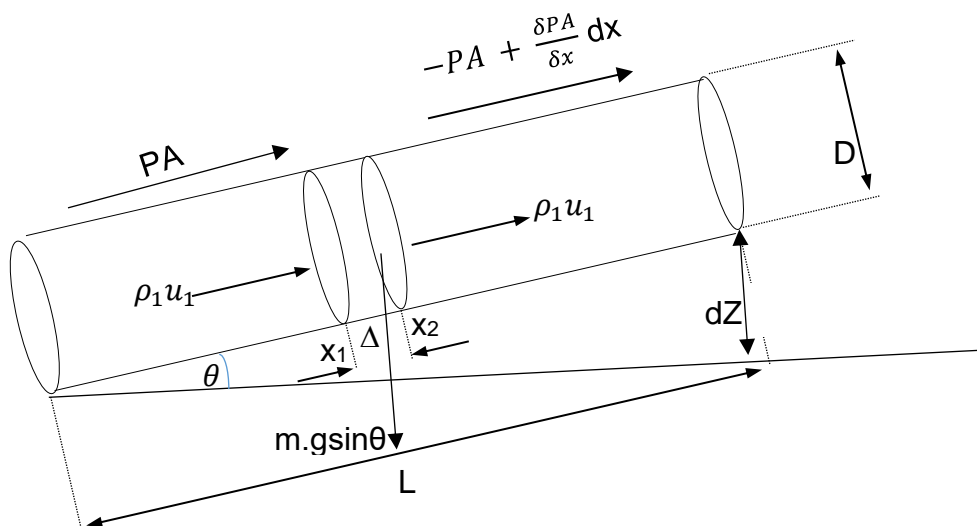


Figure 2.1: Pictorial of elemental volume of a fluid in pipeline

In a flowing fluid the mass accumulation is equal to the mass into the element minus the mass out of the element. Mathematically,

$$\frac{\delta \rho}{\delta t} + \nabla \cdot [\rho U] = 0 \quad (2.1)$$

$$\rho_1 u_1 A = \rho_2 u_2 A \quad (2.2)$$

Writing Equation 2.2 in differential form.

$$\frac{\delta}{\delta t} \int_1^2 \rho(x, t) A dx = (\rho_1 u_1 A)_t - (\rho_2 u_2 A)_t \quad (2.3)$$

The continuity equation for one-dimensional fluid flow in circular pipes can be written in terms of the density as:

$$\frac{d\rho}{dt} + \rho \frac{\delta u}{\delta x} = 0 \quad (2.4)$$

Where ρ is the density, u is the velocity in the x direction, t is the time, and x is the fluid density. By expanding and applying thermodynamic transformations, Equation 2.4 can be written as:

$$dP = \left(\frac{\delta P}{\delta \rho}\right)_s d\rho + \left(\frac{\delta P}{\delta s}\right)_\rho ds \quad (2.5)$$

The density of the fluid changes with time as it flows in the pipeline according to [Oke et al. \(2003\)](#)

$$\frac{d\rho}{dt} \frac{1}{a^2} \left[\frac{dP}{dt} \left(1 + \frac{\varphi}{\rho T} \right) - \frac{\varphi}{T} \frac{dh}{dt} \right] \quad (2.6)$$

Where, a is the speed of sound, h is the enthalpy, P is the pressure and T is the temperature. Also,

$$a^2 = \left(\frac{\delta P}{\delta \rho}\right)_s \quad (2.7)$$

$$\varphi = \left(\frac{\delta P}{\delta s}\right)_\rho = \frac{a^2 \rho \xi T}{c_p \gamma - T a^2 \xi^2} \quad (2.8)$$

Where, k is the isothermal coefficient, ξ is the isobaric coefficient, C_p is the specific heat at constant pressure and γ is the ratio of specific heats. The continuity equation can be expressed as in Equation 2.9 by substituting Equation 2.6 into 2.4.

$$(\rho T + \varphi) \frac{dP}{dt} - \rho \varphi \frac{dh}{dt} + \rho^2 a^2 T \frac{\delta u}{\delta x} = 0 \quad (2.9)$$

2.2.1.2 Conservation of momentum

The sum of the forces acting on a fluid particle in motion is equal to change in momentum of the particle. The momentum conservation equation can be derived from Newton's second law. Considering the gravitational, frictional and pressure forces acting on a fluid particle, the momentum balance equation may be derived in the x-direction. ([Martynov et al. 2013](#)).

$$\rho \frac{\delta u}{\delta t} + \rho u \frac{\delta u}{\delta x} + \frac{\delta P}{\delta x} = \alpha \quad (2.10)$$

$$\alpha = - \left(\frac{f \rho u |u|}{2D} \right) + \rho g \sin \theta \quad (2.11)$$

Where, f is Darcy Weisberg friction Factor, θ is angle of pipeline inclination to horizontal, D is pipeline internal diameter, and g is gravity acceleration constant.

2.2.1.3 Conservation of energy

Considering the first law of thermodynamic, the energy balance for a fluid element in motion can be presented as ([Mahgerfteh et al. 2016](#)).

$$\rho \frac{dE}{dt} = W_{shear} + W_{ext} + W_n + q_{conv.} + q_{cond.} \quad (2.12)$$

Where, E is the total energy per unit mass of the fluid, W_{shear} is work done by the viscous forces inside the fluid, W_{ext} is the work done on the fluid by other

external forces, W_n is the work done by the pressure forces on the fluid, $q_{conv.}$ is the heat transferred by fluid convection, and $q_{cond.}$ is the heat transfer by conduction. If no work is done on or by the fluid and neglecting the heat conduction, the complexity of the energy equations, Equation 2.12 reduces to:

$$\rho \frac{dE}{dt} = W_n + q_{conv.} \quad (2.13)$$

The total energy E of the fluid is given by:

$$E = i + \frac{1}{2}u^2 + gz \quad (2.14)$$

Where, i is the internal energy of the fluid, z is the vertical elevation of the fluid element, and u is the velocity in x direction. The second and third terms represent the kinematic energy and potential energies of the fluid.

2.3 CO₂ Fluid Impurities and parameters

The CO₂ transported in pipelines from the source to the storage location is impure. Anthropogenic activities churn out millions of tonnes of CO₂ every year. Carbon capture and storage (CCS) plays a vital part in mitigating the release of CO₂ into the atmosphere. The world is only gradually implementing CCS, even after the Paris Climate Agreement came into effect in November 2016. In Europe, there are two large scale CCS projects in operation; seven large CCS projects under construction and plans for additional eighteen that will bring the total to over forty by the year 2025 ([Jakobsen et al. 2017](#)). In Scotland where a reporting threshold of 10,000 tonnes is specified, eighty- eight CO₂ emission sites reported a total of 19.1 Mt in 2014 ([Brownsort et al. 2016](#)). The released CO₂ is usually with other gases. These other gases (or impurities), where it is transported in pipelines, affect the flow properties of the fluid. There has not been much

academic research on the effects of impurities on rich CO₂ streams in pipelines. Therefore, the current available models for CO₂ pipeline design have generally assumed pure CO₂. Any impurity present in the fluid may change the phase behaviour and physical and thermodynamic properties of the mixture such as pressure and temperature behaviour, critical pressure and temperature, or create a two-phase region where liquid and vapour co-exist thereby making pure CO₂ models inadequate. Although, some models exist in literature for binary and ternary mixtures of CO₂ fluids, there is none to address all impurities found in the stream. This project is aimed at bridging that gap by considering all common impurities found in CO₂ pipeline fluids.

The impurities generally affect the fluid flow properties and affect the cost of transporting CO₂ ([Coquelet et al. 2014](#)). The effect of impurities on the cost of transportation is outside the scope of this study. A wide range of pressures and temperatures are encountered in CO₂ pipeline transportation. [Li et al. \(2011a\)](#) and [Coquelet et al. \(2014\)](#) gave the range of pressure and temperature encountered in the transportation of CO₂ fluids to be between 0.5 and 20.0 MPa and -55 and 30 °C respectively, though some other authors have put the maximum temperature as high as 50 °C ([Farris 1983](#); [Wetenhall et al. 2014b](#)). In CO₂ pipeline transportation, the pressure is always maintained above critical value to avoid gaseous or two-phase flow, but the temperature may be allowed to drop below critical value. The determination of thermodynamic properties of CO₂ mixtures in several combinations of pressure and temperature is crucial to the accurate design of pipelines transporting rich CO₂ fluids.

2.3.1 CO₂ fluid impurities

Captured CO₂ is never 100% pure and there are several impurities in impure CO₂ fluids. The common impurities in CO₂ pipeline streams include; nitrogen (N₂), hydrogen (H₂), methane (CH₄), hydrogen sulphide (H₂S), sulphur dioxide (SO₂), carbon monoxide (CO), oxygen (O₂), ammonia (NH₃), Argon (Ar) and water (H₂O) ([Ke et al. 2017](#)). In this project, all these impurities are studied at their maximum allowable concentrations. CO₂ stream impurities could be classified into three categories; fuel oxidation, excess oxidation, and process fluids ([Porter et al. 2016](#)). There are sources from which the impurities enter the CO₂ fluid. The air used for combustion contains CO₂, N₂, O₂ and Ar. The combustion of carbon – based compounds produces CO₂. If there is incomplete combustion, CO may be produced. Water vapour and oxides of N₂ are products of H₂ combustion and the combustion of N₂, respectively. Oxides of N₂ constitute only minimal concentrations in CCS and are ignored. An elaborate source of impurities, the reasons for their limitations and classifications are given in ([Porter et al. 2016](#)).

The flue gas from the power plant is termed lean CO₂ and may have a typical CO₂ concentration of about 15 % ([Aaron and Tsouris 2005](#)) or below 17 % ([Kikkinides et al. 1993](#)). The percentage of gases in the flue gas depends on the composition of the feed (natural gas, coal, oil, biomass or a composition of them), and type and efficiency of the combustion process. CO₂ gases from natural sources typically have higher percentages of CO₂. After capture, the percentage of CO₂ in the gas stream may increase to over 90 %. The balance consists of impurities, which are undesired because they adversely affect the flow and behaviour of the fluid. The capture process purifies the CO₂ before it is transportation, but it is expensive to remove all impurities in the CO₂ fluid. It may

be more economical to leave some small percentage of impurities in the stream than removing them completely.

Thermodynamic properties, phase behaviour, and viscosity are all affected by the impurities in the stream ([Antonie Oosterkamp 2008](#)). Impurities in the CO₂ stream also affect the number and the design of the pressure boosting stations. With impurities, the critical pressure is higher leading to higher pressures required to maintain the fluid in dense phase ([Antonie Oosterkamp 2008](#)). Ice and/or gas hydrate may form and block or restrict flow if H₂O is present ([Chapoy et al. 2014](#)). To avoid hydrate formation, H₂O in the CO₂ pipeline fluid is reduced below 30 lbs/MMscf or 0.00048 kg/m³ ([Race et al. 2012](#)). Hydrates were not observed to form under the pressure and temperature range considered in this study and was ignored. Interested readers may see [Chapoy et al. \(2014\)](#) for modelling of hydrate formation in CO₂ binary mixtures.

Different impurities and/or concentration of impurities left in the CO₂ fluid is also determined by the capture process. The major impurities from an oxy-fuel capture process will be Ar, N₂, O₂ and H₂O ([Chapoy et al. 2013](#)). For a pre-combustion, which result to a purer CO₂ fluid, it is H₂, H₂S and H₂O. While for a post-combustion capture, even purer than pre-combustion, it is mainly N₂ and H₂O. CO₂ from natural sources may also contain CH₄ at a high percentage as seen in CO₂ pipelines in the US. Table 2.1 shows some pipelines with the actual compositions.

Table 2.1: CO₂ pipeline stream concentration in mol % ([Patchigolla and Oahey 2013](#)).

	Canyon Reef	Central Basin	Sheep Mountain	Cortez Pipeline	Weyburn	Jackson Dome
CO ₂	85 – 98	98.5	96.8 – 97.4	95	96	98.7 – 99.4
CH ₄	2 -15	0.2	1.7	1 – 5	0.7	Trace
N ₂	< 0.5	< 0.5	0.6 – 0.9	4	< 0.03	Trace
H ₂ S	< 0.02	< 0.02wt		0.002	0.9	Trace
C ₂₊			0.3 – 0.6	Trace	2.3	
CO					0.1	
O ₂		<0.001wt			< 0.005wt	
H ₂					Trace	
H ₂ O	0.005wt	0.0257wt	0.0129wt	0.026wt	0.002 v	

Two or more CO₂ streams may mix in a trunk line and change the initial composition from any single pipeline. When this happens, the new composition has to be determined to model the flow in the trunk line. The modelling of the composition even from a single source from time to time may be necessary as it can change over time ([Brown et al. 2015](#)). The composition of the fluid stream affects the phase envelope, density, gas hydrate formation, viscosity, and pressure and temperature changes as the fluid flows in the pipeline. Depending on the type of feed fuel, purity of the feed fuel and the capture process, the concentration and number of impurities may be large, see Table 2.2 and Table 2.3.

Table 2.2: Minimum and maximum mole fractions of typical impurities in CO₂ streams ([Munkejord et al. 2016](#)).

Component	Min. %	Max. %
CO ₂	75	99
N ₂	0.02	10
O ₂	0.04	5
Ar	0.005	3.5
SO ₂	< 0.001	1.5
H ₂ S	0.01	1.5
NO _x	< 0.002	0.3
CO	< 0.001	0.2
H ₂	0.06	4
CH ₄	0.7	4
H ₂ O	0.005	6.5
Amines	< 0.001	0.01
NH ₃	< 0.001	3.0
COS	0.01	1.5

Table 2.3: The minimum and maximum volume % of CO₂ streams from capture processes ([Antonie Oosterkamp 2008](#))

Comp.	Pre - combustion		Post combustion		Oxy-fuel	
	Min	Max	Min	Max	Min	Max
CO ₂	95.6	99.7	99.8	99.97	85	99.94
N ₂	0.03	1.3	0.021	0.17	0.01	7
CH ₄	0.035	2	-	0.01	-	-
H ₂ S	0.01	3.4	-	-	-	-
SO _x	-	-	0.001	0.01	0.007	2.5
NO _x	-	-	0.002	0.01	0.01	0.25
CO	0.03	0.4	0.001	0.002	-	-
Ar	0.03	1.3	0.003	0.045	0.01	5.7
O ₂	0.03	1.3	0.003	0.03	0.01	7
H ₂	0.002	1.7	-	-	-	-

2.3.2 CO₂ fluid vapour - liquid phase envelope.

CO₂ may be transported a gas, subcooled liquid, subcritical or supercritical fluid in pipelines. These different phases show different thermodynamic properties and these properties are determined for the proper design of pipelines transporting CO₂ fluids. The gaseous transportation of CO₂ is uneconomical except for short distances due to the low volume and high-pressure losses. Subcooled liquid, subcritical and supercritical fluid transportations are comparable in terms of costs but pipeline CO₂ transportation is mostly in the supercritical state ([Forbes et al. 2008](#)). The reason for this preference is unclear as liquid (or subcritical) fluid transportation has clear advantages over supercritical fluid transportation, including lower pressure losses and higher volumes transported ([Zhang et al. 2006](#)).

Phase envelope or Pressure-Temperature (P-T) diagram shows the physical state of the fluid with various combinations of pressure and temperature. The P-T diagrams are different for pure and impure CO₂ fluids. An undesirable two-phase region appears with impurities and different impurities have different degrees of effect on the phase envelope. [Ahmad et al. \(2014\)](#) showed that with higher concentration of impurities, phase envelope had a wider expansion between the dew point and bubble point curves. The two-phase envelope is a zone where both liquid and gaseous phases coexist in equilibrium. The phase transition zone (critical point) occurs at lower pressures for pure CO₂ than for CO₂ with impurities. Therefore, supercritical phases occur at higher pressures and lower temperatures than pure CO₂. These higher critical pressures translate to higher energy costs for CO₂ fluids with impurities. [Ahmad et al. \(2014\)](#) considered 5 % impurity at 5 °C and reported that N₂ had the most effect on vapour – liquid

transition zone with an expansion of 2.74 MPa, followed by O₂ with an expansion of 1.91 MPa, Ar had an expansion of 1.68 MPa and CH₄ with an expansion of 0.96 MPa. Their analysis of 2.5% impurity at 5 °C showed reduced expansion of the phase envelope with N₂ at 0.94 MPa, O₂ at 0.89 MPa, Ar at 0.68 MPa and CH₄ at 0.46 MPa.

[Goos et al. \(2011\)](#) used GERG 2004 equation to predict the critical pressure and temperature of 90 mol % CO₂ and 10 mol % N₂ to be 8.77 MPa and 22.51 °C. Using the PR EoS, the critical pressure and temperature was 7.4 MPa, 31 °C. A difference of 1.37 MPa and 8.5 °C between GERG 2004 and PR EoSs. They further gave the critical pressure and temperature of 95 mol % CO₂ and 5 mol % N₂ to be 8.11 MPa and 27.12 °C and of 80 mol % CO₂ and 20 mol % N₂ to be 10.22 MPa and 12.00 °C. The critical point of CO₂/N₂ mixture changed from 7.38 MPa and 31.06 °C at 0.01 mol % N₂ to 10.55 MPa and 14.55 °C at 20 mol % N₂. These data in [Goos et al. \(2011\)](#) shall be used to compare with results of the simulations at the same conditions. [Chapoy et al. \(2013\)](#) stated that the SRK EoS can accurately predict the P-T profile of CO₂ multicomponent systems, with improved accuracy at higher temperatures, though the temperature range was not specified. The critical pressure and temperature of CO₂ (89.83 mol%), O₂ (5.05 mol%), Ar (2.05 mol%) and N₂ (3.07 mol%) mixture was found to be 8.79 MPa and 23.75 °C.

If the critical pressure is equal to or higher than the cricondenbar, CO₂ pipeline fluids change phase from critical phase to liquid phase if temperature declines below the critical value as long as pressures remain above the critical value. In a situation where the critical pressure is less than the cricondenbar, (not seen in CO₂ fluids but common in oil reservoir gases), the flowing fluid enters the two-

phase region when temperature drops below the critical value even though the pressure remains about critical. Subcritical or uncooled liquid transportation is an interesting scenario of transporting CO₂ fluids without the added cost of cooling the fluid. The two-phase region may occur either above or below the VLE line of pure CO₂. [Wetenhall et al. \(2014b\)](#) pointed out that impurities with higher critical pressure and temperature will create two – phase regions below the VLE line of pure CO₂ and those with lower critical pressure and temperature will create two – phase regions above the VLE line of pure CO₂.

2.3.3 Density of CO₂ fluid

Density is an important parameter in the modelling of CO₂ fluids in pipelines. The accuracy of the available pressure loss models depends on the accurate evaluation of density, friction factor and velocity or flow rate. Each impurity alters the density of the mixture and to ensure accuracy, the correct density must be evaluated before it is used in the pressure drop/diameter equations. Expectedly, impurities lighter than CO₂ will reduce the density of the mixture while heavier impurities will have the opposite effect. [Wetenhall et al. \(2014b\)](#) found that the relationship between density, pressure and temperature for CO₂ fluids was non-linear with a sharp discontinuity in density as the fluid changes from liquid to vapour. Close to the VLE line, large changes in density values were observed for small changes in pressure and temperature. Table 2.4 presents some density values of CO₂/N₂ mixture at 11.0 MPa and 30 °C. From Table 2.4, it can be seen that 5 %, 10 %, and 20 % concentration of N₂ impurity reduced the density of the CO₂ fluid at 11 MPa and 30 °C by 14 %, 32 %, and 56 % respectively. Density data for CO₂ and H₂ mixtures were presented by ([Sanchez-Vicente et al. 2013](#)). Analysing the densities at 2 %, 7.5 %, and 10 % between 1.5 and 23 MPa and

between 15 and 60 °C, it was found that 2 % of H₂ impurity can reduce the density of CO₂ by as much as 25 % in the critical region.

Table 2.4: Density of CO₂/N₂ mixtures (Goos et al. 2011)

Gas mixture	% CO ₂ (balance N ₂)	Temp.(°C)	Press. (MPa)	ρ (kg/m ³) (GERG 2004)
1	100 CO ₂	30	11.0	792
2	95 CO ₂	30	11.0	681
3	90 CO ₂	30	11.0	536
4	80 CO ₂	30	11.0	343

The density of pure CO₂ at temperatures between 7 °C and 100 °C and pressures between 7.4 MPa and 30.0 MPa is between 150.0 kg/m³ and 1000.0 kg/m³ (Tarafer and Guiochon 2011). Within the operational pressures and temperatures of CO₂ pipelines, Liu et al. (2017) experimentally determined the density of 0.8988 CO₂ and 0.01012 CH₄ at 18 MPa to be 742.99 kg/m³ at 30.02 °C and 711.77 kg/m³ at 34.95 °C. Holding the temperature constant and varying the pressure, they recorded 522.74 kg/m³ at 10.01 MPa and 742.99 kg/m³ at 18 MPa. In the analysis of Cole et al. (2012), between the temperature range of 15 °C – 33 °C and pressure range of 5.0 MPa – 15.0 MPa, the density of CO₂ was between 600 kg/m³ – 730 kg/m³ and the kinematic viscosity was about (0.08 – 0.09) x 10⁻⁶ m²/s². To avoid exponential variations in densities around the critical point, CO₂ fluids are transported above critical pressure in pipelines (Arai et al. 2005). Density of CO₂ fluid was measured with a vibrating tube densitometer by Chapoy et al. (2013). Since the density is not absolute, Equation 2.15 was used to analyse the raw data to obtain the accurate density.

$$\rho(T, P) = A(T, P) \tau^2(T, P) - B(T, P) \quad (2.15)$$

$$A(T, P) = \frac{\rho(T, P_1) - \rho(T, P_2)}{\tau^2(T, P_1) - \tau^2(T, P_2)} \quad (2.16)$$

$$B = \frac{\tau^2(T, P_2) \rho(T, P_1) - \tau^2(T, P_1) \rho(T, P_2)}{\tau^2(T, P_1) - \tau^2(T, P_2)} \quad (2.17)$$

where ρ is the sample density at P and T , τ is period of oscillation at P and T , and A , B are apparatus parameters at P and T .

[Chapoy et al. \(2013\)](#) used the SRK-EoS to calculate the density of CO₂ and CO₂ – rich mixtures but corrected the molar volume by using the correct volume of pure CO₂ at the pressure and temperature. Equations 2.18 to 2.20 describe the procedure.

$$V^{new} = V^{EoS} - V^C \quad (2.18)$$

where V^{EoS} is the molar volume from the EoS, V^C is the correction factor, defined as:

$$V^C = \sum_{k=1}^N x_i V_i^C \quad (2.19)$$

where x_i is composition of component i in the phase that the volume is computed.

For CO₂,

$$V_{CO_2}^C = V_{Pure\ CO_2}^{EoS} - V^{MBWR} \quad (2.20)$$

Another equation to calculate the density, the [Ely et al. \(1987\)](#), a form of the MBWR equation is given in Equation 2.21 ([Chapoy et al. 2013](#)).

$$P = \sum_{n=10}^9 a_n(T) \rho^n + \sum_{n=10}^{15} a_n(T) \rho^{2n-17} e^{-\gamma \rho^2} \quad (2.21)$$

[McCollum and Ogden \(2006\)](#) developed a set of equations for density over temperatures and pressures for CO₂ pipeline transportation using data from the Kinder Morgan pipeline company. Equation 2.22 shows the pressure dependent

density equation and the regression values for the equation are given in Appendix A, Table A1. This equation has a regression coefficient (R^2) of 0.986587 at 32.2 °C and 0.999996 at -1.1 °C.

$$\rho = a * P^6 + b * P^5 + c * P^4 + d * P^3 + e * P^2 + f * P + g \quad (2.22)$$

where ρ is density (kg/m³) and P is pressure (MPa).

A satisfactory equation for correlating phase behaviour of binary components is the PR EoS with van der Waals mixing rules ([Chen et al. 2009](#); [Ke et al. 2017](#)). [Chen et al. \(2009\)](#) used the PR EoS to correlate the density of CO₂ and 1-methylimidazole binary component at temperatures of 293.15, 309.75 and 323.15 K and pressures between 28.3 and 13.86 MPa. Some of the densities recorded were 543.5 kg/m³ at 98.98 mol % CO₂, 8.02 MPa and 36.6 °C and 993.5 kg/m³ at 86.02 mol % CO₂, 10.11 MPa and 36.6 °C. CO₂ density is observed to change disproportionately around the critical point. [Patchigolla and Oakey \(2013\)](#) stated that the density of CO₂ varies drastically with a slight change in temperature at the critical point, where a doubling of density is observed for a change of temperature from 47 to 37 °C at a pressure of 9 MPa.

Some density data is available for CO₂ with impurities. [Li et al. \(2011a\)](#) stated that there is density data for CO₂ with N₂, CH₄, H₂S and H₂O as impurities in a wide range of temperatures and pressures. This data will be helpful in validating density correlations for rich CO₂ fluids. Volumetric properties of CO₂/N₂ binary mixtures at pressures between 0.60 and 5.18 MPa and temperature of 20 °C were presented by [Jiang et al. \(1990\)](#). This pressure range is outside the scope of CO₂ pipeline transportation. Within pressures of 0.08 and 48.3 MPa and temperature of -36 and 47 °C, [Esper et al. \(1989\)](#) measured the densities of 0.476 mol % CO₂

and 0.524 mol % CH₄, and 0.447 mol % CO₂ and 0.553 mol % N₂. They obtained a maximum density of 548 kg/m³ for CO₂/CH₄ mixture at -53.81 °C and 6.14 MPa and 625 kg/m³ for CO₂/N₂ mixture at 26 °C and 6.14 MPa. The minimum density of 0.98 kg/m³ occurred at 26.8 °C and 0.83 MPa for CO₂/CH₄ mixture and 1.24 kg/m³ at 27 °C and 0.089 MPa for CO₂/N₂ mixture. These pressures are below the values under consideration for CO₂ pipeline transportation but can be used for testing the robustness of correlations. Density values of CO₂/CH₄ binary mixtures at pressures from 1.82 to 35.20 MPa and temperatures of – 58 to 76 °C were also reported by [Hwang et al. \(1997\)](#) see Appendix A, Table A3. These pressure and temperatures values are within those considered in this study and may be used for validation.

2.3.4 Formation of gas hydrates in CO₂ fluids

Low molecular weight gases may form gas hydrates when they physically react with H₂O ([Adisasmito et al. 1991](#)). Gas hydrates only form in the presence of H₂O molecules, gas components and the right pressure and temperature condition. Gas hydrates are solid structures composed of gas molecules caged in a hydrogen-bonded H₂O molecule ([Dashti et al. 2015](#); [Mahabadian et al. 2016](#)). Typically, clathrate hydrates form when molecules less than 0.9 nm contact H₂O at temperatures typically less than 26.85 °C and pressures typically above 0.6 MPa ([Sloan 2003](#)). When gas hydrates form, it causes flow assurance issues by blocking the pipeline and causing no-flow conditions. Gas hydrates may plug pipelines, prevent free flow of gases and cause casing or tubing collapse and foul the valves of heat exchangers ([Salam et al. 2013](#)).

CO₂ pipelines operate at much higher pressures than 0.6 MPa but the CO₂ fluids are dehydrated to prevent corrosion and hydrate formation. Hydrates (CO₂, CH₄

and H₂S) formed with dissolved water in CCS streams is too small to create operational problems ([De Visser et al. 2008](#)). Since some H₂O content is always present, it is necessary to understand the effect of the H₂O content on the formation of hydrates along the pipeline in case hydrate formation conditions were inadvertently crossed. When conditions are right, CO₂ will form the structure “I” hydrate at appropriate pressure and temperature condition with a hydrate phase, H₂O rich phase, an ice phase and a CO₂ rich phase with two quadruple points ([Chapoy et al. 2014](#)). Within the temperature range studied by [Chapoy et al. \(2014\)](#), it was concluded that the liquid phase region of pure CO₂ is 2 – 5 MPa lower than CO₂ rich mixtures. They also stated that irrespective of the pressure, CO₂ hydrates could not form above 21 °C. This assertion needs further investigation because Aspen HYSYS simulation of hydrate formation temperatures and pressures for CO₂ binary mixtures shows that hydrate formation temperatures for CO₂/SO₂, CO₂/CO, and CO₂/H₂ mixtures were above 20 °C. The simulations with HydraFLASH shows that hydrate dissociation temperatures at 15 MPa was below 12 °C. Hydrates do not form at temperatures above hydrate dissociation temperature ([Bai and Bai 2005](#)). All hydrate stability curves in ([Nair and Rahmanian 2017](#)) were below 20 °C at pressures not exceeding 8 MPa. In the analysis, it was found that N₂, O₂, CH₄, Ar, and H₂S increased the likelihood of hydrate formation while SO₂, COS, NO₂, CO, H₂, and NH₃ reduced the likelihood.

2.3.5 Viscosity of CO₂ fluids

An important fluid flow property is viscosity and the correct estimation of viscosity is essential for the accurate prediction of pressure behaviour of CO₂ fluids in pipelines. At supercritical pressures and temperatures, pure gases have densities

close to the liquid state and gas-like viscosities ([Koga et al. 2005](#)). Impurities in CO₂ fluids impact on the overall viscosities of the fluid. Viscosity varies with density, which changes with pressure and temperature. Density of the fluid affects the temperature dependence of viscosity. Generally, viscosity of a fluid increases with increase in pressure and temperature. However, viscosity decreases with temperature at high densities and increase with temperature at low densities ([Zabaloy et al. 2005](#)). [Al-Syabi et al. \(2001\)](#) stated that the difference of the dense and gaseous phase viscosities does not depend on temperature but is a function of density. However, viscosity depends indirectly on temperature because the density of a fluid is a function of the temperature and pressure. The authors presented ([Jossi et al. 1962](#)) (JST) correlation for reduced residual viscosity for non-polar substances, see Equation 2.23.

$$\left[(\mu - \mu^o) (T_c^{\frac{1}{6}} * M^{-\frac{1}{2}} * P_c^{-\frac{2}{3}}) + 10^{-4} \right]^{1/4} = a_1 + a_2 \rho_r + a_3 \rho_r^2 + a_4 \rho_r^3 + a_5 \rho_r^4 \quad (2.23)$$

where μ is viscosity of the fluid (mPa.s), μ^o is viscosity of diluted (gas) state of the fluid at the same temperature, M is the molecular weight, P_c is the critical pressure, T_c the critical temperature, a_{1-5} are the coefficients of correlation. They found the JST correlation to be accurate to within 20% range of all normal alkanes having carbon numbers below 8 and reduced density below 2.5. They then presented Equation 2.24 for other conditions.

$$(\mu - \mu^o) = \text{Exp}(A + B\rho_r + C\rho_r^2) \quad (2.24)$$

$$\text{where } A = 9.8338 - 0.15568M + 1.8935 E - 4M^2 \quad (2.25)$$

$$B = -12.150 + 0.10345M - 1.3971 E - 4M^2 \quad (2.26)$$

$$C = 2.3990 - 1.6355M + 2.5338 E - 5M^2 \quad (2.27)$$

The viscosity equation by [Al-Syabi et al. \(2001\)](#) is:

$$\begin{aligned} [(\mu - \mu^0)\lambda + 10^{-4}]^{1/4} = & 0.094754 + 0.062016\rho_r - \\ & 0.0010273T_r^{-2.0183}M^{0.4462}\rho_r^2 + 0.00040403T_r^{-2.4706}M^{0.19188}\rho_r^3 \\ & + 0.000086159T_r^{-1.1577}M^{0.58683}\rho_r^4 \end{aligned} \quad (2.28)$$

Note that λ is equal to $(T_c^{\frac{1}{6}} * M^{-\frac{1}{2}} * P_c^{-\frac{2}{3}})$.

One of the most suitable correlations for computing the viscosity of pure CO₂ is that by [Heidaryan et al. \(2011\)](#). They stated that the viscosity of CO₂ at the supercritical region is a strong function of both the temperature and pressure. See Equation 2.29.

$$\mu = \frac{A_1 + A_2P + A_3P^2 + A_4 \ln(T) + A_5(\ln(T))^2 + A_6(\ln(T))^3}{1 + A_7P + A_8 \ln(T) + A_9(\ln(T))^2} \quad (2.29)$$

where μ is viscosity (cP), P is pressure (bara), T is temperature (K), and A_{1-9} are correlating parameters (Table 2.5).

Gas viscosity is a strong function of pressure ([Li et al. 2011b](#)) especially near the critical point. At very high pressures, viscosity decreases with increase in temperature resembling liquid viscosity but at very high temperatures the pressure effect is reduced and viscosity increases with temperature ([Li et al. 2011b](#)). The pressure dependent viscosity correlation developed by ([McCullum and Ogden 2006](#)) can be used to calculate viscosity of CO₂ at pressure and temperature values of interest.

Table 2.5: Coefficients for Equation 2.14 ([Heidaryan et al. 2011](#)).

Coefficients	Tuned coefficients
A1	-1.146067 x 10 ⁻¹
A2	6.978380 x 10 ⁻⁷
A3	3.976765 x 10 ⁻¹⁰
A4	6.336120 x 10 ⁻²
A5	-1.166119 x 10 ⁻²
A6	7.142596 x 10 ⁻⁴
A7	6.519333 x 10 ⁻⁶
A8	-3.567559 x 10 ⁻¹
A9	3.1804730 x 10 ⁻²

The correlation is given in Equations 2.30 (similar to Equation 2.22). They noted that at temperatures above the critical value, the R² regression coefficient is less than 1.0 though greater than 0.983. R² is a statistical measure of how well the regression line fits the actual data. 0 indicates a no-fit while 100 indicates a perfect fit. Accurate viscosity values can be calculated with these regression equations within the specified pressure and temperature ranges. Appendix A, Table A3 shows the regression coefficients for viscosity respectively between 10 °C and 43.3 °C. To calculate the viscosity at any temperature not included in the table, an upper and lower temperature value is chosen, and viscosity values calculated at both temperatures. These two values are then interpolated to determine the viscosity at the temperature of interest. Equation 2.31 shows the interpolation Equation.

$$\mu = a * P^6 + b * P^5 + c * P^4 + d * P^3 + e * P^2 + f * P + g \quad (2.30)$$

where ρ is density (kg/m³), μ is viscosity (Pa.s) and P is pressure (MPa)

$$\mu = [(\mu_{high} - \mu_{low}) * (T - T_{low}) / (T_{high} - T)] + \mu_{low} \quad (2.31)$$

where μ_{high} is the viscosity at the higher temperature (T_{high}), μ_{low} is the viscosity at the lower temperature (T_{low}) and T the actual temperature.

There have been several correlations for CO₂ mixtures with varying degrees of absolute average deviations (AAD). [Pensado et al. \(2008\)](#) considered the [Kanti et al. \(1989\)](#) method as having general applicability and used it to determine the viscosity of 98.79 % CO₂ and 1.21 % PEC9 giving low AAD. The maximum AAD of 28% was at 353.15K and 60 MPa. The [Kanti et al. \(1989\)](#) Equation is given in Equation 2.32.

$$\ln \left[\frac{\mu(P,T)}{\mu(P_{ref},T_o)} \right] = (ay^2 + by + c) \ln \left[1 + \frac{(P-P_{ref})}{ay^2+ey+f} \right] + (gy_o^2 + hy_o + i) \left(\frac{1}{T} - \frac{1}{T_o} \right) \quad (2.32)$$

where $y = y_o + (gy_o^2 + hy_o + i)(1/T - 1/T_o)$ and $y_o = \ln[\mu(P_{ref}, T_o)]$, T(K), P(MPa), μ (mPa.s)

[Pensado et al. \(2008\)](#) stated that [Monsalvo et al. \(2005\)](#) adopted a generalized mixing rule after fitting the nine parameters in the [Kanti et al. \(1989\)](#) Equation against each pure compound. The [Kanti et al. \(1989\)](#) Equation referred to as self-referencing requires only one experimental viscosity value at reference pressure and temperature. The mixing rule is given in Equation 2.33.

$$\alpha_{mix} = x_1\alpha_1(1 - x_1)\alpha_2 \quad (2.33)$$

where α is any one parameter, x_1 is mole fraction of CO₂.

[Chapoy et al. \(2013\)](#) used the Poiseuille Equation to relate viscosity and pressure drop along a capillary tube, Equation 2.34. This is an interesting equation because it eliminates the computation of Reynolds number and friction factor.

$$\Delta P = \frac{128 L Q \mu}{C \pi D^4} \quad (2.34)$$

where ΔP is pressure difference across capillary tube (psi), Q is flow rate in cm^3/s , L is length of capillary tube (cm), D is the internal diameter of the capillary tube (cm), μ is the viscosity (cP), C is the unit conversion factor (6894757).

By the corresponding states theory, the reduced viscosity for any two components of gases at the same reduced temperature and pressure are the same ([Chapoy et al. 2013](#)). The use of the reduced viscosity (Equation 2.35) eliminates the units of the computation.

$$\mu_r = \frac{\mu(P,T)T_c^{1/6}}{P_c^{2/3} M^{1/2}} \quad (2.35)$$

where μ_r is reduced viscosity, P_c is critical pressure, T_c is critical temperature and M is molecular weight. At supercritical pressures, impurities with higher critical pressures and temperatures increase the viscosity of CO_2 fluids while impurities with lower critical temperatures and pressures reduce the viscosity ([Wetenhall et al. 2014b](#)). A low viscosity means a reduced resistance to flow and reduced pressure losses. This means that impurities with low critical pressure and temperature would enable CO_2 to flow for longer distances before recompression.

[Tarafer and Guiochon \(2011\)](#) showed the dependence of viscosity on density (see Figure 2.2). The pressures and temperatures of CO_2 pipeline transportation are within the range used in generating the values of Figure 2.2, between 7.4 and 30 MPa and 7 and 101 °C. Irrespective of pressure and temperature combinations, the viscosity of CO_2 is dependent only on the density within this range. As stated before, the viscosity can be shown to be dependent on the pressure and temperature because the density is also dependent on temperature and pressure.

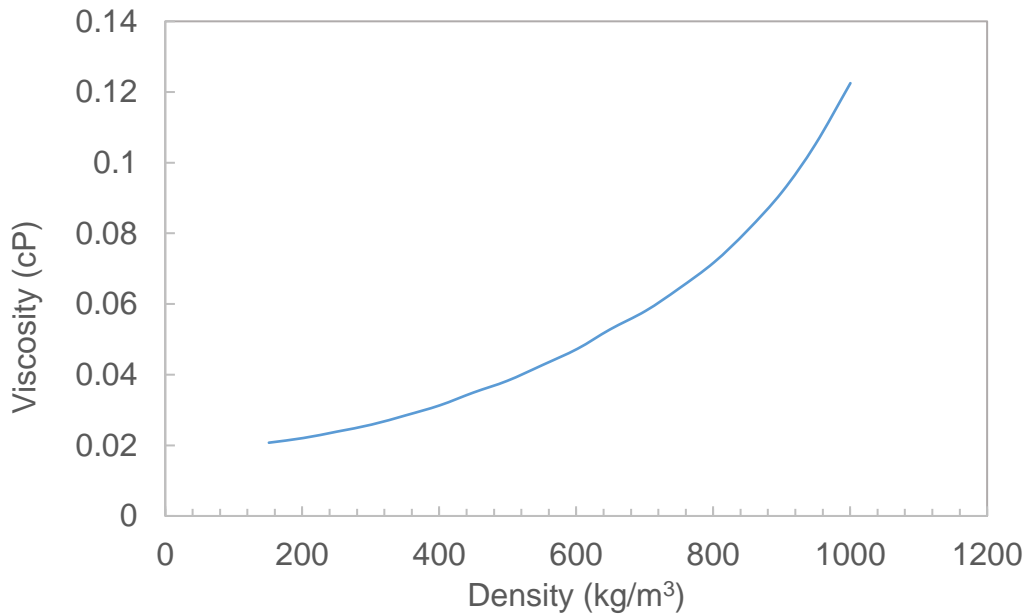


Figure 2.2 CO₂ viscosity from density ([Tarafer and Guiochon 2011](#)).

Viscosity data in the literature for multi-component CO₂ fluids are scarce or non-existing. However, some data exist for binary (CO₂ + CH₄), (CO₂ + C₃H₈) and ternary components (CH₄ + C₃H₈ + CO₂) ([Al Ghafri et al. 2018](#)). Also lacking in the open literature is the viscosity data for impure CO₂ at the allowable concentrations of the common impurities.

2.4 CO₂ pipeline design

The essence of this research is to proffer ways to improve the design of CO₂ pipelines and optimise operations. A design assuming pure CO₂ is bound to give inaccurate results when applied to impure CO₂. CO₂ pipelines may have different impurities with varying concentrations. Each pipeline fluid must, therefore, be separately analysed and designed for CO₂ transportation.

Although CO₂ is not currently classified as a dangerous fluid in the UK Pipelines Safety Regulations Act 1996, CO₂ pipelines are designed to meet the specifications for hazardous fluids ([Cooper and Barnett 2014](#)). Safety and economic reasons are considered while designing CO₂ pipelines. Some of the

parameters to be considered while designing CO₂ pipelines are; pressure and temperature of the fluid, CO₂ mixture composition, Impact of possible pipeline rupture on human health, Corrosion rate of the pipeline, Atmospheric or ambient temperatures, Topography of the pipeline route, Compressor, seal, and auxiliary materials, Dehydration requirement of CO₂ Fluid, Minimising flow transients, etc ([Ozanne 2011](#); [Witkowski et al. 2014b](#)). [IEA GHG \(2002\)](#) and [Lazic et al. \(2014\)](#) included fluid physical properties, optimal size of pipeline, pipeline pressure rating, topographic profile of the pipeline route, soil types and strength and human populations among the parameters to be considered while designing CO₂ pipelines. Some of the specific considerations are discussed below.

2.4.1 Pipeline route and length

The first consideration while designing a CO₂ pipeline is the pipeline route selection. CO₂ sources and CO₂ sinks or usage points are connected by pipelines running along an optimum route. This route may not be the shortest distance between the CO₂ source and sink but it is the most ideal path in terms of economics and safety. To select the optimum path, several options are considered. As many as twenty possible paths were considered during the design stage of the Peterhead project in the UK ([IEA GHG 2014](#)). [Forbes et al. \(2008\)](#) stated that selecting the route of a pipeline involves determining, assessing and evaluating several possible routes and securing the Right of Way (ROW) document. The designing of the shortest pipeline route for a reduced cost of the pipeline material and reduced pressure losses may be hampered by the existence of cities/towns, archaeological sites, roads, natural reserves/resources, national heritage sites, etc. ([IEA GHG 2014](#)). For these reasons, CO₂ pipelines do not usually have a straight path and may run through routes longer than

desired, resulting to higher pressure losses and costs ([Witkowski et al. 2013](#)). Increasing the length inevitably increases pipeline length, the number of booster stations, affect pipeline material, number of bends and the construction and operational costs of the pipeline ([Vandeginste and Piessens 2008](#); [Gao et al. 2011](#)).

Planning a CO₂ pipeline route entails the consideration of many factors. Safety is a major factor considered and pipelines are laid along uninhabited areas ([Witkowski et al. 2014b](#)) to avoid obstacles . [Ozanne \(2011\)](#) listed some objectives of pipeline route selection to include:

- To reduce the cost of materials, construction and number of boosting stations, pipelines are laid along the shortest route.
- To cut costs, existing ROW and infrastructure are used if possible.
- To avoid paying damages or destroy existing infrastructure, places like roads, rails, waterways and crossings are bypassed if possible.
- Impact or destruction of eco-systems are minimised.
- Pipelines are routed through unpopulated areas where possible.
- Ease of access along the entire length of the pipeline for personnel and equipment is considered.
- Obstacles such as hills, wells, houses, lakes, ponds, rivers, orchards, etc. are avoided.

The desire for shortest route is because longer pipelines have higher pressure drop than shorter ones with similar diameter ([Witkowski et al. 2013](#)). ([Gao et al. 2011](#)) concluded that larger pipeline diameters are required in longer pipelines

thereby increasing the pipeline construction and levelised costs. However, pipeline diameter is selected to accommodate the expected flow rate and not result to excessive velocities. Increasing the diameter of long pipelines would reduce the number of booster stations installed along the length of the pipeline but may increase the cost of pipeline and result to very slow velocities. Longer pipelines therefore need not have larger diameters.

2.4.2 CO₂ pipeline right of way (ROW)

After determining the path of the pipeline, the right of way (ROW), a legal document that gives permission to access the route, has to be acquired. The ROW is secured by negotiations with the legal owners or authorities of the land through which the pipeline passes. These authorities may be private owners, county officials, region and federal agencies ([Ozanne 2011](#)). This document which gives legal backing for the laying of the pipeline may be difficult or expensive to acquire and failure to acquire it could result to changing the route of the pipeline. The acquisition of ROW document adds to the cost of construction of a CO₂ pipeline. This cost may be between 4 - 9% ([Oei et al. 2014](#)), 5 % ([Forgács and Horánszky 2013](#)) or over 10% ([Bauer 2011b](#)) of the overall cost of the pipeline. Some of the items for which permit to work on or around include railroads, roadways, canals, overhead power cables, pipelines and underground cables ([Bauer 2011a](#)).

2.4.3 CO₂ pipeline flow rates and velocity

After securing the ROW, the actual design of the pipeline can commence. The quantity of fluid to be transported is the first parameter considered. The expected fluid flow rate determines the size or diameter of the CO₂ pipeline. Flowrates are set to avoid pressures and velocities that are too high by selecting appropriate

pipeline diameter. Very high fluid flow velocities can cause the eroding of the pipeline inner wall and result to high pressure losses. A maximum velocity of 3 m/s is usually specified to avoid erosion of the pipe wall ([API 1991](#)). To design CO₂ pipelines effectively, adequate knowledge of mass/volume flowrate, fluid phases, pressure, temperature, and composition is required ([Brown et al. 2015](#)). [Wang et al. \(2013\)](#) stated that the flow rate if kept constant, determines the most ideal diameter size of the pipeline. However, there are other factors considered in choosing pipeline diameter, including fluid density and pipeline distance. Since flowrate is an indication of the volume of fluid transported in a pipeline, it becomes the single most important factor in the design of the pipeline. [Gao et al. \(2011\)](#) concluded that pipeline diameters are increased to accommodate increased flow rates which in turn increase the cost of the pipeline. If future CO₂ sources are expected, pipelines may be designed to accommodate the future flow rate. These oversized pipelines are underutilized at the start of operations but saves the cost and time to construct a new pipeline in the future. Pipelines with large diameter sizes, though more expensive, result in slower velocities, lower pressure losses and fewer boosting stations ([Witkowski et al. 2014a](#)).

An optimal pipeline diameter must be large enough for the expected volume of flow to be transported yet it must not be too expensive. Picking a very large pipeline diameter is easy but this is constrained by the cost of the pipe material. The decision to pick a pipe size is based on economic analysis of pipeline diameter, pressure boosting stations requirements, fluid velocity, etc. A large diameter may be too expensive while a small diameter may cause high fluid velocity, erosion of the pipe walls and very high pressure losses. A simple relationship between flow rate in mass and volume units is given in Equation 2.36.

$$q = q_v * \rho \quad (2.36)$$

where q = mass flow rate (kg/s), q_v = volume flow rate (m³/s) and ρ = density (kg/m³).

[Wang et al. \(2013\)](#) pointed out that point to point CO₂ pipelines, which connect one CO₂ source to one sink, are relatively easy to model and that most literature on CCS pipeline design employ static models ([Weihs et al. 2011a](#); [Weihs et al. 2011b](#); [Middleton et al. 2012](#)). Employment of static model is justified because CO₂ pipelines are usually pressurised with an inert gas (N₂) before introducing the CO₂ fluid. For oversized pipelines that transport CO₂ from more than one source to a sink, the optimal diameter is between the optimum for the initial and final flow rates depending on the time difference between the times the two sources come onstream. In the analysis of [Wang et al. \(2014\)](#), the ratio (D_t/D_1) over (Q_t/Q_1), was linear with a correlation of 0.935, see Figure 2.3. Where D_t is the oversized pipeline diameter and D_1 is the optimal diameter for the first (initial) flow rate. Q_t is the total flow rate and Q_1 is the initial flow rate. Over-sizing is more economical for smaller (Q_t/Q_1) ratio, shorter pipelines, and smaller time gap between CO₂ sources. Proportionally, larger increases in flow rate (Q_t/Q_1) require larger diameters.

[Gao et al. \(2011\)](#) concluded that a larger pipeline diameter is required for a higher mass flow rate, which will in turn increase the capital cost of the pipeline. Some cost models that use CO₂ flow rate and length of pipeline include ([Dooley et al. 2009](#)) and ([Knoope et al. 2013b](#)) models. [Chandel et al. \(2010\)](#) used only flow rate and fluid velocity as input variables in the determination of the internal diameter of CO₂ pipelines (Equation 2.20).

$$D = \sqrt{\frac{4 Q_v}{\pi u}} \quad (2.34)$$

where D = inner diameter (m), u = fluid velocity (2.0 m/s), Q_v = volumetric flow rate (m^3/s).

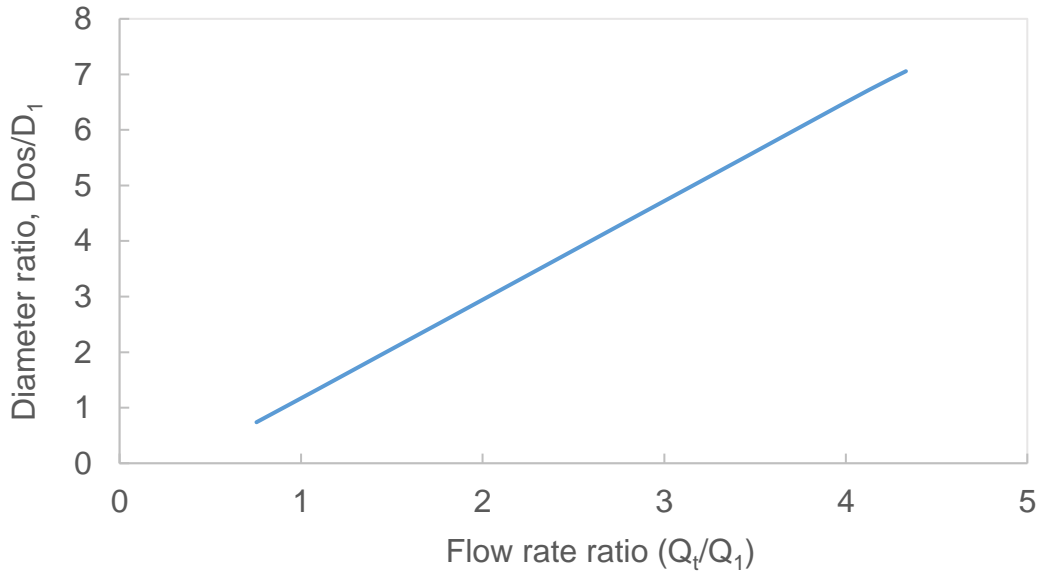


Figure 2.3: Relationship between flow rate ratio and diameter ratio ([Wang et al. 2014](#)).

The erosional velocity or maximum velocity of fluids in pipelines must be established to avoid excessive velocities capable of causing erosion of the pipeline inner wall. An empirical equation to calculate the maximum velocity is given in Equation 2.35 ([API 1991](#)).

$$u_e = 0.82 \frac{c}{\sqrt{\rho}} \quad (2.35)$$

where v_e = erosional velocity (m/s), c = empirical constant and ρ = gas/liquid density (kg/m^3). It is important to carefully choose a pipeline internal diameter so that the maximum velocity of the CO_2 stream does not cause erosion of the internal pipe wall or cause high pressure losses ([Barton 2003](#)). [Vandeginste and Piessens \(2008\)](#) arrived at a maximum flow velocity of 4.3 m/s after applying the

API-RP-14E formula for erosional velocity. The need to avoid high pressure losses limit the velocity to below erosional velocity ([Svedeman 1995](#))

2.4.4 Point-To-Point or Trunk/oversized pipelines

CO₂ sources may be close together requiring a decision to either design a large trunk pipeline or several point-to-point pipelines. The accepted decision is informed by purely economic reasons. A trunk, backbone or oversized pipeline may be constructed to connect the various CO₂ sources to single sink(s). On the other hand, point-to-point pipelines may be constructed to connect single CO₂ sources directly to a sink. Generally, collecting CO₂ fluids from several sources into a single trunk pipeline is more economical than running separate pipelines ([Luo et al. 2014b](#)). The preferred choice may depend on the distance between the sources and the distance between the sources and the sink. Trunk pipelines are usually less expensive ([Wetenhall et al. 2014b](#)) because less labour and material is used. ([Kuby et al. 2011](#)) also found that networked systems saved up to 6.5 % on cost when compared to single direct pipelines. But [Knoope et al. \(2014\)](#) found that point-to-point connections may be more economical if, for example, two sources are each 100 km from a sink and the two sources are more than 100 km apart. Three scenarios were analysed in [IEA GHG \(2010\)](#), “point – to – point”, “tree and branches” and “Hub and spoke” arrangement of two CO₂ sources and one sink, see Appendix B for a pictorial of the pipeline arrangements. The angles made by the two sources at the sink are given as 0°, 30°, 45°, 60° and 90°, see Appendix B. \$50,000 per km per inch and 5% of CAPEX was assumed for the annual OPEX to model the cost of the pipeline. Angles greater than 90° had no cost saving, between 30° and 60°, the radial hub and spoke arrangement was the best option and below 15°, the tree and branches

arrangement resulted in least cost. Their analysis agrees with the [Knoope et al. \(2014\)](#) conclusion.

[Wang et al. \(2014\)](#) presented Equation 2.36 that relates pipeline diameter ratio to the flow rate ratio (Equation 2.36 – 2.38). This equation is used to compute the diameter of a trunk pipeline in relation to the initial internal diameter of a single pipeline.

If $N = N^*$, then

$$\frac{D_t}{D_1} = 0.22 R_{flow} + 0.7 \quad (2.36)$$

If both sources start production at the same time (i.e. both Q_1 and Q_2 start flowing at the same time), then

$$D_{Q_1+Q_2} = R_{flow}^{0.39} D_{Q_1} \quad (2.37)$$

For the oversized pipeline, optimal diameter is:

$$\frac{D_t}{D_1} = \left[1 - 0.78 \left(\frac{N}{N^*} \right) \right] R_{flow}^{0.39+0.61(N/N^*)^{2.1}} + 0.7(N/N^*)^{0.53} \quad (2.38)$$

where N = actual time difference between the two CO₂ sources (years), N^* = trade-off point (years) or number of years after which duplicate pipelines become more cost effective. D_{Q_1} = optimal diameter for Q_1 and $D_{Q_1+Q_2}$ = optimal flow rate for $Q_1 + Q_2$ (Mtpa), D_1 = diameter of initial duplicate pipeline (mm) D_{os} = oversized pipeline diameter (mm), and R_{flow} = flow rate ratio.

There is a maximum pipeline diameter size. Where the flowrate is too high to be transported in a single pipeline, an additional pipeline may be used. The required pipeline inner diameter is calculated and where it does not correspond to available sizes, it is rounded up to the next higher available standard size. More

than one pipeline is only used when the required pipe size is larger than the largest available standard pipe size. The minimum number of pipelines required can be calculated from Equation 2.39 [Chandel et al. \(2010\)](#).

$$N_{pipe} = \left\lfloor \frac{Q}{Q_{max}} \right\rfloor + 1 \quad (2.39)$$

If $N_{pipe} - 1$ pipelines have diameter $D_{i_{max}}$, then N_{pipe}^{th} pipeline diameter is calculated from:

$$D_{i_{N_{pipe}^{th}}} = \sqrt{\frac{4 [Q - (N-1)Q_{max}]}{\pi U}} \quad (2.40)$$

where N_{pipe} = number of pipes, $\left\lfloor \frac{Q}{Q_{max}} \right\rfloor$ = the integer value of $\frac{Q}{Q_{max}}$ not greater than the enclosed ratio (magnitude), Q = the flow rate (m³/s) and Q_{max} = maximum flow rate of the largest diameter pipe (m³/s).

2.4.5 CO₂ pipeline wall thickness

The maximum expected operating pressure dictates the pipe resistance or wall thickness. Pipeline wall thickness is selected to withstand the pressures on the inside and outside of the pipeline. The burst pressure rating of the pipeline is the minimum pressure that can cause failure from the inside while the collapse pressure rating is the minimum pressure that can cause the pipeline to collapse from the outside. The risk of failure when the pipeline is exposed to high pressures is less when pipes with greater wall thickness is used. Pipelines having a wall thickness of at least 11.9 mm are resistant to damage with low failure rates and reduced risk to personnel around these pipelines ([Cooper and Barnett 2014](#)). The expected internal/burst and collapse/external pressures are computed, and values used to select pipes having adequate strength and wall thickness. Pipeline wall thickness is half the difference between the outer and inner pipe diameters.

Equations to calculate pipeline wall thickness are given in Equation 2.41 ([Witkowski et al. 2014b](#)) and Equation 2.42 ([Lazic et al. 2014](#)).

$$t = \frac{P_{mop} D_o}{2 S E F} \quad (2.41)$$

where t = pipe wall thickness (m), P_{mop} = maximum operating pressure (MPa), D_o = outer diameter of pipe (m), S = specific yield stress of pipe material (MPa), E = longitudinal joint factor (1.0) and F = design factor (0.72).

$$t = \frac{P_{max} D_i}{2(S*F*E - P_{max})} \quad (2.42)$$

where t = pipeline wall thickness (m), P_{max} = maximum design pressure (MPa), D_i = pipeline internal diameter, S = pipe yield strength (MPa), F = safety factor and E = seam joint factor.

Though pipes are specified in outer diameter or nominal diameter values, in actual design, the internal diameter and thickness are determined before selecting the outer diameter. [Chandel et al. \(2010\)](#) presented an equation for the calculation of pipeline outer diameter, Equation 2.43. The value arrived with this computation may not match available pipe size and may be rounded up to the next higher available size.

$$D_o = D_i + 2 t \quad (2.43)$$

2.4.6 CO₂ pipeline pressures, temperatures, and diameter

The choice of pipeline input pressure is made after careful consideration of the delivery pressure, preferred fluid state (single phase, supercritical or liquid), flange pressure ratings and economic factors. A minimum pressure at which recompression is required is specified after analysing the phase behaviour of the fluid to ensure that the fluid stays in a single state. Predicting the phase behaviour

is tricky because at supercritical pressures and temperatures, CO₂ fluid phase behaviour becomes unusual ([Lazic et al. 2014](#); [Zahid et al. 2014](#)). However, keeping the pressure in the supercritical region ensures that gaseous phase is avoided. Pressure variation along a pipeline is due to elevation change, friction and acceleration effects. Though the pressure losses due to elevation and acceleration can be zero for horizontal and constant density fluids respectively, there is always pressure loss due to friction. For long distance pipelines, there may be significant changes in temperature and pressure along a pipeline due to fluid friction, heat transfer between the fluid and the surrounding and expansion work done by the fluid ([Brown et al. 2015](#)).

Though there are variations in the pressure range in the literature, all reported pressures are in the supercritical region. [Forbes et al. \(2008\)](#) reported that pipeline pressures upper and lower limits are determined by economics and ASME-ANSI 900# flange rating and supercritical requirement respectively. [Patchigolla and Oakey \(2013\)](#) put the range of CO₂ operating temperatures from 15 to 30 °C and pressures from 10.0 to 15.0 MPa while [Forbes et al. \(2008\)](#) put pressures between 8.62 MPa and 15.17 MPa with the upper temperature limit as the discharge temperature of the compressor. The minimum pressure to transport CO₂ is 7.39 MPa ([Han et al. 2015](#)) which is the critical pressure of pure CO₂ but [Witkowski et al. \(2014b\)](#) raised it to 86 MPa to accommodate increased critical pressure due to impurities and avoid abrupt changes in specific heat and compressibility along the CO₂ pipeline due to temperature changes.

In the modelling paper by [Wetenhall et al. \(2014b\)](#), the minimum pressure was put at 10% above the cricondenbar with an assumed pressure gradient of 0.02 MPa/km. 0.02 MPa/km is an arbitrary assumption and not representative of actual

pipeline pressure drops. Pressure gradients need to be computed for each pipeline. Along a CO₂ pipeline, pressures are not linear and simple averaging between two pressure values may not yield accurate values for computation. [McCoy and Rubin \(2008\)](#) presented Equation 2.44 to compute average pressure between two pressure points in a pipeline.

$$P_{ave} = \frac{2}{3} \left(P_2 + P_1 - \frac{P_2 P_1}{P_2 + P_1} \right) \quad (2.44)$$

CO₂ pipelines are usually not heated nor cooled, except in some situations, where the compressor increases the temperature beyond the maximum design value or in very low climates where the temperature drops too low. However, there may be need to insulate them to reduce the temperature change along the length. The temperature limit is not a critical requirement in CO₂ pipelines, if pressures are above the critical value of the fluid ([Vandeginste and Piessens 2008](#)). To protect the anti-corrosion agents, a maximum temperature limit of 50 °C is set ([Nimtz et al. 2010](#)). Many models in the literature assumed isothermal conditions even though researchers recognise that the temperature varies along the pipeline, but they did not consider the effect of temperature changes along the pipeline due to heat transfer between the fluid and the surrounding. Pipelines are usually buried to about 1 m depth for protection from the weather and surface damages. Where compressors are used, they may increase the temperature of the fluid ([Forbes et al. 2008](#); [Nimtz et al. 2010](#)). Where this heat addition occurs and the surrounding temperature is significantly lower than the temperature of the fluid coming out of the compressor, the minimum and maximum temperatures occur immediately before and after the compressor. This situation is reversed if the maximum temperature of the pipeline fluid is lower than the surrounding temperature.

Pipeline pressure losses are lower in places with lower ambient temperatures than places with higher ambient temperatures. Where the ambient temperature is very low, the flowing fluid loses heat to the surrounding quickly and enters the subcritical state resulting to lower pressure losses. ([Teh et al. 2015](#)) concluded that cold climates are better suited for liquid CO₂ transportation and warm climates for supercritical CO₂ fluid transportation. However, the soil surrounding the pipeline is continually heated up and rises. When this happens, the effect of ambient temperature will be greatly reduced.

[Witkowski et al. \(2014b\)](#) presented a plot showing maximum safe pipeline length against ambient temperature (Figure 2.4). It shows that the difference between the length of fluid transport for the same pressure drop at 21 °C and 44 °C ambient temperatures is as much as 100 km. Where ambient temperature is very low, the fluid may enter the liquid or subcritical phase by losing heat to the environment.

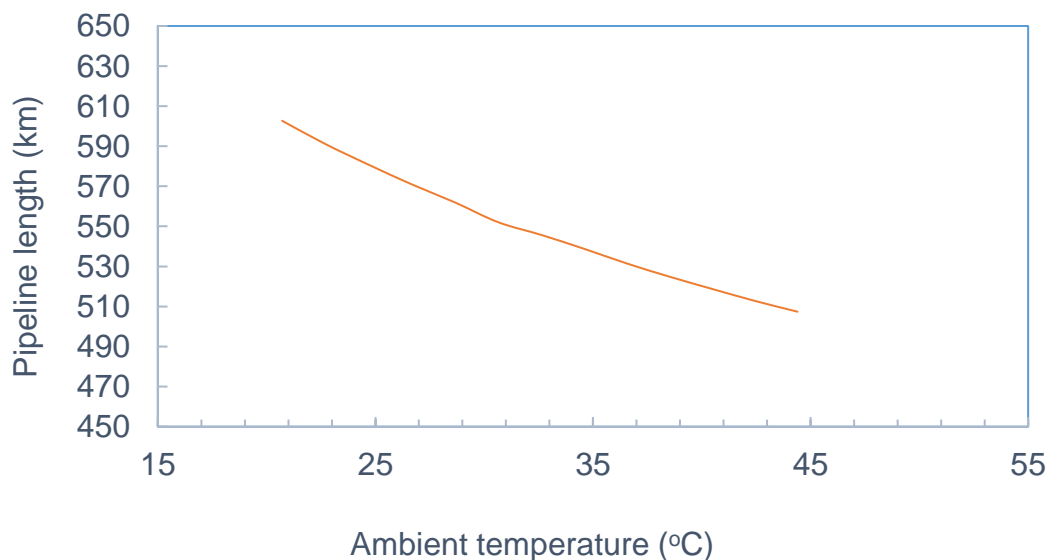


Figure 2.4: Maximum safe CO₂ pipeline length against ambient temperature ([Witkowski et al. 2014b](#)).

Several factors such as flowrates, cost, and velocity are considered when selecting pipeline internal diameter. A large internal diameter pipe would have been ideal to avoid excessive velocity that can cause erosion and minimise pressure drop but the cost of the pipes hinders this option. To select an optimum pipeline, pressure losses are calculated after specifying a maximum allowable velocity. An initial diameter may be selected and pressure losses, booster stations requirements and costs are computed.

This process is repeated with other diameter sizes and the optimum size selected. Equations for liquid flow rate (Equation 2.31) and gas flowrate (Equation 2.45) is given in [IEA GHG \(2002\)](#). In this report, the length of pipeline, diameter of pipeline, flowrate and fluid density were considered in the pressure loss calculations.

$$\Delta P = 2.252 \frac{f L \rho Q^2}{D_i^5} \quad (2.45)$$

where ΔP = pressure drop (bar), f = friction factor, L = pipeline length (km), ρ = fluid density (kg/m³), Q = flow rate (l/m) and D_i = pipeline inner diameter (mm).

$$q = 1.361 * 10^{-7} \sqrt{\left[\frac{P_1^2 - P_2^2}{f L S} \right]} D_i^5 \quad (2.46)$$

where q = standard gas flow rate (m³/h), P_1 , P_2 = inlet and outlet pressures respectively (Pa), f = friction factor, L = pipeline length (km), S = gas specific gravity and D_i = pipeline internal diameter (mm).

[McCoy and Rubin \(2008\)](#) held upstream and downstream pressures constant while calculating pipeline diameter. While deriving the internal diameter equation, they assumed that kinetic energy changes were negligible (constant velocity) and the gas compressibility was averaged over the pipeline length, see Equation 2.47

([Mohitpour et al. 2003a](#)). Most of the available models assume constant velocity but this is oversimplifying because when pressure reduces, the fluid expands and increases in velocity thereby increasing pressure losses due to acceleration effects. Though the pressure losses due to velocity change (acceleration effect) are lower than frictional and elevation losses, it should be considered.

$$D_i = \left\{ \frac{-64 Z_{ave}^2 R^2 T_{ave}^2 f_F \dot{m}^2 L}{\pi^2 [M Z_{ave} R T_{ave} (P_2^2 - P_1^2) + 2 g P_{ave}^2 M^2 (h_2 - h_1)]} \right\}^{1/5} \quad (2.47)$$

where D_i = pipe segment diameter (m), Z_{ave} = average fluid compressibility, R = universal gas constant (Pa.m³/mol K), T_{ave} = average fluid temperature (K), \dot{m} = molecular weight of flowing stream, $P_{1,2}$ = pressure at points 1 and 2 respectively, h = pipeline elevation.

[Chandel et al. \(2010\)](#) neglected the effect of impurities on the flow characteristics and assumed that pipelines are buried at depths of 1m underground with the fluid having a constant density and temperature of 27 °C. They assumed a constant input pressure of 13MPa for all CO₂ sources and only CO₂ velocity and flow rate were used as input variables in the model. The assumptions include a density of 827 kg/m³, constant temperature of 27 °C and a constant average pressure of 11.5 MPa. The pipe inner diameter was calculated from Equation 2.48. Even with insulated pipelines, there is always some form of heat transfer between the surrounding medium and the flowing fluid. The assumption of constant temperature therefore introduces inaccuracies into the results. The density of CO₂ pipeline fluids changes as the fluid losses pressure along the pipeline. Assuming a constant density adds to the inaccuracies.

$$D_i = \sqrt{\frac{4 Q_v}{\pi u}} \quad (2.48)$$

where D_i = inner diameter (m), u = fluid velocity (2.0 m/s), Q_v = volumetric flow rate (m^3/s).

The Bernoulli equation for pressure drop in a pipeline (Equation 2.49) and the Darcy – Weisbach equation (Equation 2.50) for frictional head loss was presented in [Chandel et al. \(2010\)](#). These two equations can be combined to give a pressure drop equation (Equation 2.51) accounting for losses due to friction and elevation changes but not losses due to acceleration.

$$\Delta P = \rho g (h_L + \Delta Z) \quad (2.49)$$

$$h_L = f \cdot \frac{L u^2}{D 2 g} \quad (2.50)$$

$$\Delta P = \frac{f \rho L v^2}{2 D} + \rho g \Delta Z \quad (2.51)$$

where ΔP is pressure drop, ρ is fluid density, g is gravitational constant, h_L is frictional head loss, ΔZ is elevation change, u is velocity and D is internal diameter.

There is always pressure loss when fluids flow in an uphill pipeline due to frictional and elevation effects. However, there could be pressure gain when fluids flow downhill due to gravity effects. If the pressure gain due to gravity effect is higher than pressure loss due to frictional effects, the pipeline could actually gain in pressure. When supercritical CO_2 flows in horizontal or inclined pipelines, the pressure drops and CO_2 expands causing a reduction in density and sometimes formation of gas, resulting to two-phase flow. [Zhang et al. \(2006\)](#) refers to the condition where gas forms and causes increased velocity resulting to high pressure losses and/or no flow condition, a choking point. In their analysis, the safe distance to transport the CO_2 fluid before the choking point is specified at

90% of the choking distance. The equation for optimum pipeline diameter considering flowrate, density and viscosity is given in Equation 2.52 ([Zhang et al. 2006](#)).

$$D_{i,opt} = 0.363 Q_v^{0.45} \rho^{0.13} \mu_c^{0.025} \quad (2.52)$$

Equation 2.53 used to determine the diameter of pipelines presented in [Vandeginste and Piessens \(2008\)](#) incorporates elevation changes into the Darcy-Weisbach formula for diameter calculation.

$$D_i = \left[\frac{8 f Q^2 L}{\rho \pi^2 [\rho g (z_1 - z_2) + (P_1 - P_2)]} \right]^{\frac{1}{5}} \quad (2.53)$$

where D_i = diameter (m), f = Darcy - Weisbach friction factor, Q = mass flow rate (kg/s), ρ = density (kg/m³), $P_1 - P_2 = \Delta P$ = pressure drop (Pa), L = length (m), and z_1, z_2 = place height at inlet and outlet respectively (m).

Whenever fluids flow in pipes, there are always frictional pressure losses. The friction factor needs to be computed to calculate the pressure drop due to friction. Equation 2.54 is an iterative equation to calculate the friction factor ([Vandeginste and Piessens 2008](#)). The Swanee – Jain friction factor, Equation 2.55, is preferred because it eliminates the iterations of the White – Colebrook equation.

$$\frac{1}{\sqrt{f}} = -2 \log \left(\frac{e}{14.8 R} + \frac{2.51}{R_e \sqrt{f}} \right) \quad (2.54)$$

where f = Darcy – Weisbach friction factor = $4f_F$, e = pipe roughness height (m), R_e = Reynold's number.

$$f = \frac{1.325}{\left\{ \ln \left[\left(\frac{e}{3.7 D_i} \right) + \left(\frac{5.74}{R_e^{0.9}} \right) \right] \right\}^2} \quad (2.55)$$

where f = Darcy – Weisbach friction factor = $4f_F$, e = pipe roughness (m), R_e = Reynold's number, D_i = pipe internal diameter (m).

Another friction factor equation is that by Zigrang and Sylvester (1962) presented as Equation 2.56 ([McCoy and Rubin 2008](#)).

$$\frac{1}{2\sqrt{f_F}} = -2.0 \log \left\{ \frac{\epsilon/D_i}{3.7} - \frac{5.02}{R_e} \log \left[\frac{\epsilon/D_i}{3.7} - \frac{5.02}{R_e} \log \left(\frac{\epsilon/D_i}{3.7} + \frac{13}{R_e} \right) \right] \right\} \quad (2.56)$$

2.5 Chapter conclusion

Impurities affect the density, viscosity, enthalpy (heat transfer), fluid velocity, pressure and temperature losses. In other words, the thermodynamic properties are affected by the impurities in the stream. Each impurity affects the properties to varying degrees and the effect should be clearly understood for analysis of CO₂ pipeline transportation. Since CO₂ fluids usually contain more than two gas components, a representative model for multicomponent gases is required.

The bulk of CO₂ pipeline design uses pure CO₂ fluids, but no CO₂ fluid is 100 % pure. Assuming a pure CO₂ fluid while designing pipeline transportation is inaccurate. Furthermore, a complete analysis of the impact of all common impurities on the transportation of CO₂ fluids in pipelines could not be found in the open literature. There is also no clear preference for CO₂ fluid phase in pipeline transportation. Supercritical phase is sometimes specified but some authors have indicated that subcritical (liquid) phase is more economical

The effects of all common impurities found in CO₂ fluids at their maximum allowable concentrations have not been studied. This thesis seeks to bridge that gap and provide a quick reference for each impurity in CO₂ fluids flowing in pipelines. Analysis of the effect from zero to the maximum concentration is done

for all impurities. The impact of each impurity on the parameters are presented for reference.

Temperature effects were generally ignored in the models studied. Temperature changes affect the pressure behaviour, fluid density and viscosity. Understanding the effect of impurities on temperature behaviour of the fluid will improve the accuracy of the design of CO₂ pipeline transportation.

No pressure loss model included pressure losses due to acceleration of the fluid. This component always contributes to pressure changes in CO₂ pipelines as the fluid expands when pressure reduces and should be incorporated. The fluids either expand or contract when pressure and temperature change in the pipeline, contributing to the pressure variations. A good model should therefore include these effects for accuracy. An analysis is carried out in this thesis to investigate if it is justified to ignore the acceleration component.

Chapter 3: Research Methodology

3.1 Introduction

In this chapter, the procedure and methodology of determining the effect of impurities on CO₂ fluids flowing in pipelines is outlined. Various equations of state are used to calculate the gas compressibility factor. This factor is used to calculate the density and fluid viscosity is computed with available correlations. The results are compared to available data and the most accurate correlation is chosen to be used in the calculation of the Reynolds number and the friction factor. These are then used in the pressure drop equation coupled with temperature variation correlations to calculate the pressure and temperature drop along the pipeline. The effect of each impurity is computed in each stage of the analysis and the effect of multiple impurities of some pipelines are also analysed.

The transportation of rich CO₂ fluids in pipelines could be in the gaseous, dense liquid, or supercritical phase. It is more economical to transport CO₂ in pipelines in subcritical or supercritical phases than in gaseous phase. CO₂ fluids are different from conventional pipeline fluids. The modelling challenges are therefore different from natural gas pipelines ([Aursand et al. 2013](#)). This difference is due to presence of impurities, higher operating pressures, thermodynamic behaviour of the fluid, etc. ([Lazic et al. 2014](#)). CO₂ fluids are commonly transported in a dense liquid phase while natural gas is transported in a dense gaseous phase. The transportation pressures of CO₂ pipelines are much higher than those of natural gas pipelines and CO₂ is generally impure. Pipelines have been transporting CO₂ for enhanced oil recovery operations in the USA and Canada for decades and is a mature technology ([Luo et al. 2014b](#)). Knowledge can also

be tapped from the vast literature of oil and gas pipeline transportation. The operating pressure of CO₂ pipelines must be above the critical pressure of pure CO₂ (7.38 MPa), though this pressure changes with impurities, to keep it in the supercritical or subcritical phases. CO₂ fluids with impurities may have critical pressures higher than that of pure CO₂, above 7.38 MPa. To avoid two-phase flow, the minimum pressure assumed in this work is at least 1 MPa higher than the critical pressure of any pipeline fluid considered. The maximum pressure is also assumed to be 20 MPa, which is also representative of some existing pipelines.

Pipelines are designed to operate effectively both in terms of operational ease and cost. The flowing fluid thermodynamic properties therefore needs to be evaluated correctly for optimal operations. However, as the experimental data is scarce on the thermodynamic properties of rich CO₂ fluids in pipelines, the use of equations of state (EoS) is employed in calculating the properties to fill this gap. The complete design of the pipeline is achieved by first identifying the most appropriate EoS for rich CO₂. This is done by evaluating simulation results by comparing to data if available. The most accurate thermodynamic properties are used to calculate the effect of impurities on the binary CO₂ fluids and some existing CO₂ pipelines. In this research, Aspen HYSYS (ver. 10.0) and gPROMS (ver. 5.1.1), are used to compute z – factor, viscosity, density, temperature changes and pressure drop along the pipeline. Aspen HYSYS being an industry standard software is used to validate the gPROMS results where practical data is not available.

It is desired to identify the best correlations/equations to determine each parameter of CO₂ pipeline transportation. These correlations are then built into a

comprehensive gPROMS program that can be used to design CO₂ pipelines with high accuracy. To achieve this, a gas compressibility factor is firstly determined and used to calculate the density. Available correlations for density are also used and the values compared. Next, the viscosity is computed with available equations and the most accurate equation selected after comparing to available data. This viscosity value is then used to calculate the friction factor. These are then coupled into a single correlation for the determination of pressure drop in CO₂ pipelines.

A one – dimensional horizontal flow is assumed in this thesis. Pipelines are rarely horizontal along the entire length but considering changes in elevation would make the problem too complex. However, changes in elevation is also considered to show the impact of impurities on the flow parameters. The following assumptions are made:

- Flow is one – dimensional.
- No change in pipeline cross – sectional area.
- Pressures are held above critical values.
- Start-up and shutdown are not considered. CO₂ pipelines are pressurized with N₂ above the critical pressure of CO₂ before it is introduced into the pipeline.
- Both uninsulated pipelines to allow rapid heat loss and insulated pipelines are considered.

The flow of the fluid could be laminar, transitional, or turbulent. At high pressure and high flow velocities, the flow is considered turbulent. Reynold's number (Re)

is used to determine if the flow is laminar, transitional, or turbulent. It is generally accepted that R_e less than 2100 is laminar, greater than 4000 is turbulent and in between is transitional ([Rehm et al. 2008](#)). Though in ([White 2011](#)), laminar flow is considered up to R_e of 2300. CO₂ pipelines are not smooth walled, and vibrations occur enabling transition to turbulence at much lower R_e . A formula to calculate R_e is shown in Equation 3.1. Turbulent flow is assumed in this work, though R_e is calculated to show that the flow is in the turbulent region.

$$R_e = \frac{\rho u D}{\mu} \quad (3.1)$$

where R_e = Reynold's number, ρ = density (kg/m³), u = velocity (m/s) and μ = viscosity (cP).

In thesis report, the input pressure shall be between 15 MPa and 20 MPa and input temperature at 35 °C in line with values in the existing literature. Minimum pressure and temperature shall be 9 MPa and 7 °C respectively. The maximum temperature (35 °C) is above the critical temperature of all CO₂ fluid compositions. The input pressure and temperature ensure that the fluid is in the supercritical state at the beginning of flow. However, during flow the temperature is allowed to drop below the critical value and enter subcritical flow. The pressure is always maintained above the critical value (at a minimum of 9 MPa) to avoid two-phase flow in the pipeline.

For CO₂ to remain in a single supercritical state, both flowing pressure and temperature must be above the critical values. The critical pressure and temperature of pure CO₂ is 7.38 MPa and 31.1 °C respectively. The critical pressure and temperature of CO₂ fluids with impurities deviate from these values according to the concentration and type of impurities. This difference is

considered when assigning the minimum pipeline operating pressure and temperature. There is no need to specify a minimum temperature because it is not a critical requirement as long as pressures are above the critical value. There is research work that considered temperatures far below critical values, e.g. [Wetenhall et al. \(2014a\)](#). CO₂ fluids enter the subcritical phase whenever temperatures drop below the critical value if pressures remain in the supercritical region. There is also an evidence that subcritical pipeline transportation is more economical than supercritical pipeline transportation.

Pressure losses in pipeline fluid transportation is the single most important factor in the process design of CO₂ pipelines. The loss of pressure in the pipeline is due to friction among the fluid particles and friction between the fluid particles and the pipeline wall, elevation changes along the pipeline route and acceleration of the flow. The pressure loss due to friction is always present during flow of fluids in pipelines. The pressure change due to elevation is zero for horizontal pipelines and the pressure loss due to acceleration is zero for an incompressible fluid flowing in a constant diameter pipeline. The pressure loss due to acceleration, though present in compressible fluid (as in CO₂ fluids) is very small and ignored in most pressure loss calculations.

In the study of the effect of single impurities on the pressure drop, three different scenarios of pipelines that incline at different angles to the horizontal from inlet to outlet were analysed (See Figures 3.1, 3.2, and 3.3). The binary composition consists of the maximum allowed concentration of the impurity (N₂, CH₄, H₂S, SO₂, O₂, CO, H₂, Ar, NH₃ and H₂O) and the balance of CO₂. Some existing pipelines (Cortez, Choctaw, Canyon Reef and Weyburn) were also studied.

3.2 Aspen HYSYS

A process simulation software in design and operations, Aspen HYSYS (V. 10), was used to determine pressure drop, critical temperature, critical pressure, phase envelope, and hydrate formation profile in CO₂ pipelines. Aspen HYSYS is very convenient, as it only requires the selection of appropriate EoS and the input parameters. [Besong et al. \(2013\)](#) used the Peng - Robinson EoS in Aspen HYSYS to study low temperature processes for producing high pressure and high purity CO₂ from oxy – fuel flue gas. Available EoS were used to simulation flow parameters in Aspen HYSYS. Results for critical pressure, critical temperature and phase envelope were also obtained. These values were plotted and compared with the ones obtained with gPROMS or HydraFLASH.

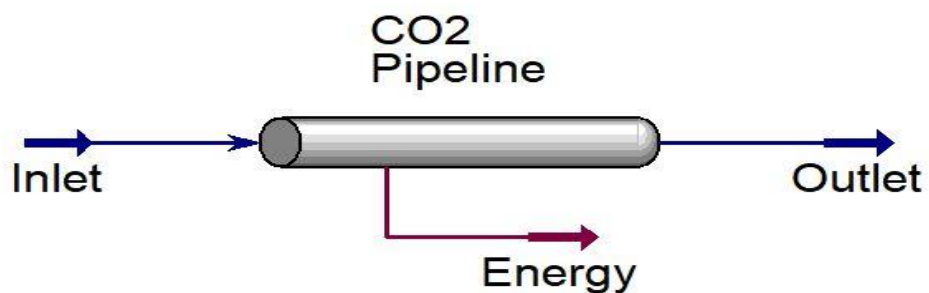


Figure 3.1: CO₂ pipeline flow sheet created in Aspen HYSYS.

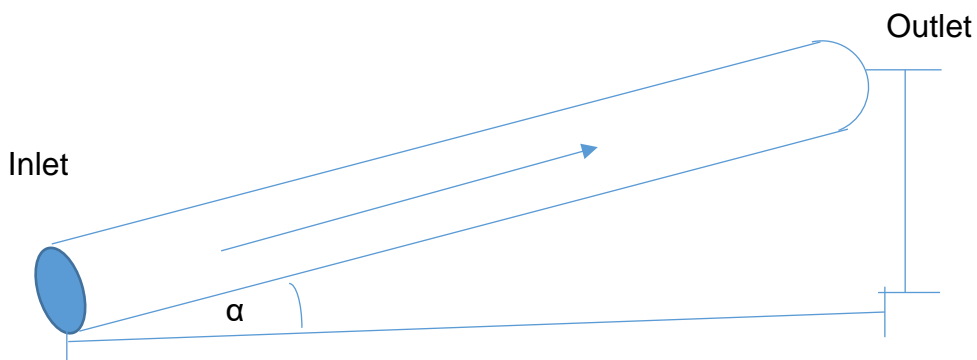


Figure 3.2: Inclined CO₂ pipeline

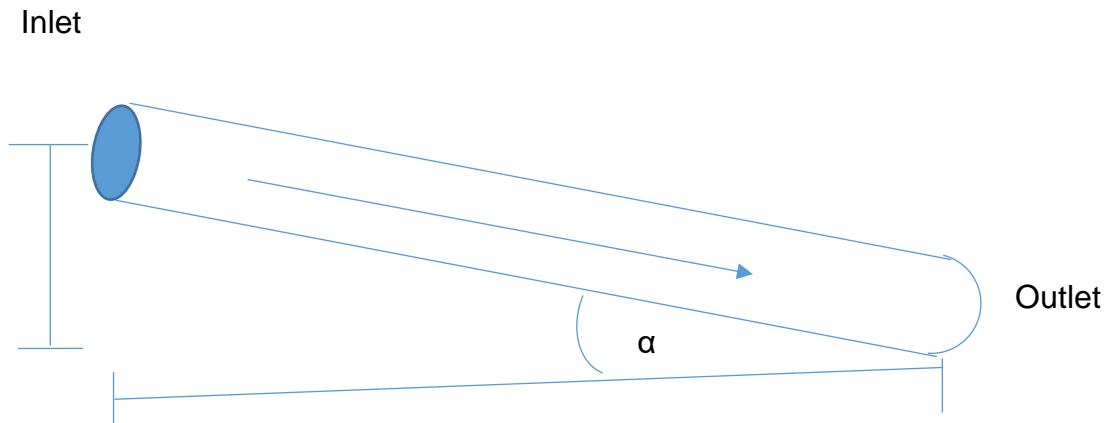


Figure 3.3: Downhill CO₂ pipeline profile

3.3 Process System Enterprise (gPROMS)

gPROMS which stands for “general process modelling system” is an equation-based software that models, simulates, and runs optimisation on chemical processes. gPROMS is adequate in modelling the pressure drop in CO₂ pipelines if the correct set of defining equations are used. Complex, controlled or hybrid systems can be adequately described and simulated by gPROMS ([Agut et al. 2010](#)). [Alhajaj et al. \(2013\)](#) used gPROMS to simulate energetic and economic performance of capture plant to handle flue gases from amine post – combustion CO₂ capture from different sources. They used the information with mathematical optimization model to develop a data base of information for designing an integrated transportation, capture and storage CO₂ networks.

Several equations of state were used in gPROMS (v 5.1.1) to simulate the gas deviation factor of CO₂ fluids. The calculated z-factors were used to compute the fluid density using the real gas equation. Other equations specifically developed for CO₂ fluids in the open literature were also used. Different correlations were used to compute the fluid viscosity, Reynold’s number (Re) and friction factor (f). Heat loss equations were also used in the analysis of heat transfer from the

flowing fluid to the surrounding. The calculated parameters were then used in the pressure drop equation to compute the decline in pressure.

Some pipelines used in the analysis include Cortez pipeline, Weyburn pipeline, Canyon Reef pipeline and Sheep Mountain pipeline in the USA. Location of these pipelines and their fluid compositions are shown in Figure 3.4 and Table 2.1, respectively.



Figure 3.4: : Location of Selected CO₂ Pipelines ([PowerPlantCCS 2010](#)).

3.4 Equations of state and gas compressibility factor

There is a long history of the development of equations of state (EoS). Robert Boyle found in 1662 that the volume of a gas was inversely proportional to its pressure. This means that for a specific composition of gas, the product of the pressure multiplied by the volume is a constant (see Equation 3.2). Charles in 1787 found that at constant pressure, the volume of a gas is directly proportional to its temperature or that the volume divided by the temperature was a constant (Equation 3.3). John Dalton in 1801 proposed that the total pressure of a mixture of gases is the combined pressure of the individual gases (Equation 3.4) ([Ramdharee et al. 2013](#)). In 1808, Joseph Louis Gay-Lussac found that the

pressure exerted by a mass of gas on the sides of its container is directly proportional to its absolute temperature (Equation 3.5). Johannes Diderik van der Waals' important contribution to the continuous development of EoS in 1873 was the generalization of the ideal gas equation. Van der Waals replaced the volume, V by $(V_m - b)$, (Equation 3.6). He also recognized that gas molecules also attract one another, and real gases were more compressible than ideal gases. His equation, the basis for all modern EoS is given in Equation 3.7.

$$PV = \text{constant} \quad (3.2)$$

$$\frac{V}{T} = \text{constant} \quad (3.3)$$

$$P_T = P_1 + P_2 + P_3 + \dots + P_n \quad (3.4)$$

$$\frac{P_1}{T_1} = \frac{P_2}{T_2} \quad (3.5)$$

$$P(V_m - b) = RT \quad (3.6)$$

$$\left(P + a \frac{1}{V_m^2}\right) (V_m - b) = RT \quad (3.7)$$

where P is Pressure, V is molar volume, V_m is molar volume, R is universal gas constant, T is temperature, a is constant depending on the gas and b is volume occupied by one mole of the molecules.

Designing engineering operations requires the use of EoS to calculate VLE properties of fluids ([Li and Yan 2009](#)). Peng-Robinson (PR), Soave-Redlich-Kwong (SRK), Stryjek-Vera-Peng-Robinson (PRSV), Patel – Tega (PT), and SRK – TWU EoS were used. The PR EoS and SRK EoS are the most common cubic EoS used in research ([Valderrama and Silva 2003](#)). The PR EoS is preferred to others because it is ideal for VLE calculations of liquid densities for hydrocarbon

systems and performs better than other EoS at supercritical pressures and temperatures ([Böttcher et al. 2012](#)). It solves single, double and three phase fluids reliably within temperatures greater than – 271 °C and pressures less than 100 MPa. The PRSV EoS is a modification of the PR EoS, with better predictions of phase behaviour and matches vapour pressure curves better than the PR EoS. The PRSV EoS can equally predict non-ideal systems with good accuracy. The SRK EoS is comparable to PR EoS but with a limited range of applicability; temperatures greater than -143 °C and pressures lower than 5.0 MPa. For some EoS that were not used in this work due to the lack of wide usage, please see ([Mangold et al. 2019](#)).

The gas compressibility factor (or z – factor) is an essential property of gases applied in many engineering applications. The formula for z - factor is given for each EoS. The real gas equation of state is the simplest way to compute the z -factor and it is given in Equation 3. 8.

$$z = \frac{P V}{n R T} \quad (3.8)$$

where z is the gas deviation factor, P is pressure, V is volume, n is number of gas molecules, R is gas constant and T is temperature.

3.4.1 van der Waals (vdW) EoS

Alexander van der Waals in 1873 proposed an equation representing the vapour-liquid coexistence. The critical compressibility factor predicted by this equation is 0.375. This equation is the foundation on which future EoS were built on. The vdW EoS is presented in Equation 3.9 ([Kwak and Mansoori 1986](#)) and z - factor form in Equation 3.10. Several researchers have made changes to the attractive

and repulsive terms but only the most widely used modifications are discussed here.

$$P = \frac{RT}{V-b} - \frac{a}{V^2} \quad (3.9)$$

$$Z = \frac{V}{V-b} - \frac{a}{VRT} \quad (3.10)$$

where z is the compressibility factor, V is the molar volume (cm^3/mol), P is the pressure (bara), R is the universal gas constant ($\text{J/mol} \cdot \text{K}$) and T the temperature (K). The parameter, a represents the attractive forces between the molecules and b represent volume occupied by the molecules.

3.4.2 Ridlich Kwong (RK) EoS

Ridlich and Kwong made the first modification to the vdW EoS in 1949 ([Li and Yan 2009](#)). They retained the hard-sphere term but added a temperature dependent attraction term. This EoS has a critical compressibility factor of 0.333. The Ridlich-Kwong EoS can be used for mixtures after applying appropriate mixing rules ([Wei and Sadus 2000](#)), see Equations 3.11 to 3.15. Note that the RK EoS is adequate only when $\frac{P}{P_c} < \frac{T}{2T_c}$

$$P = \frac{RT}{V-b} - \frac{a}{V(V+b)\sqrt{T}} \quad (3.11)$$

$$a = 0.42747 \left(\frac{R^2 T_c^2}{P_c} \right)^{\frac{5}{8}} \quad (3.12)$$

$$b = 0.08664 \left(\frac{RT_c}{P_c} \right) \quad (3.13)$$

$$z^3 - z^2 - (qz) = -AB \quad (3.14)$$

$$z = \frac{V}{V-b} - \frac{a}{RT^{1.5}(V+b)} \quad (3.15)$$

3.4.3 Soave Redlich Kwong (SRK) EoS

Soave replaced the attractive term, a , with a temperature dependent one, $a(T)$, see Equations 3.16 to 3.19. The SRK EoS could be the most widely used equation to correlate and predict phase behaviour and fluid properties ([Valderrama and Silva 2003](#)). The SRK EoS was able to predict phase behaviour of mixtures around the critical region ([Wei and Sadus 2000](#)). However, [Lopez-Echeverry et al. \(2017\)](#) showed that SRK EoS was not very accurate when used to predict properties near the critical point.

$$P = \frac{RT}{V-b} + \frac{a_c \alpha(T)}{V(V+b)} \quad (3.16)$$

$$Z = \frac{V}{V-b} - \frac{a(T)}{RT(V+b)} \quad (3.17)$$

$$a(T) = 0.4274 \left(\frac{R^2 T_c^2}{P_c} \right) \left\{ 1 + m \left[1 - \left(\frac{T}{T_c} \right)^{0.5} \right] \right\}^2 \quad (3.18)$$

$$m = 0.480 + 1.57\omega - 0.176 \omega^2 \quad (3.19)$$

$$b = 0.08664 \left(\frac{RT_c}{P_c} \right) \quad (3.13)$$

where ω is the acentric factor.

3.4.4 Peng Robinson (PR) EoS

Peng and Robinson further modified the attractive term in 1976 ([Ghanbari et al. 2017](#)). The use of a critical compressibility factor (0.307) improves the prediction of liquid volumes. See Equations 3.20 to 3.26. However, [Woolley et al. \(2014\)](#) stated that the PR EoS is only satisfactory for predicting CO₂ gas phase properties but didn't perform so well when compared to Span and Wagner EoS when applied to condensed phase. But [Valderrama and Silva \(2003\)](#) affirmed that the SRK EoS and PR EoS are the most widely used EoS in research, simulations

and optimisations for VLE and thermodynamic properties. [Li and Yan \(2009\)](#) also found that with properly calibrated binary interaction parameter (k_{ij}), cubic EoSs produced better accuracy on liquid volumes than gas volumes, and that PR and PT EoSs were superior to others in volume calculations.

$$P = \frac{RT}{V-b} - \frac{a(T)}{V(V+b)+b(V-b)} \quad (3.20)$$

$$a(T) = a \alpha \quad (3.21)$$

$$a = 0.45724 \frac{R^2 T_c^2}{P_c} \quad (3.22)$$

$$\alpha = \left[1 + k \left(1 - \left(\frac{T}{T_c} \right)^{0.5} \right) \right]^2 \quad (3.23)$$

$$k = 0.37464 + 1.54226 \omega - 0.26992 \omega^2 \quad (3.24)$$

$$b = 0.0778 \frac{R T_c}{P_c} \quad (3.25)$$

$$z = \frac{V}{V-b} - \frac{a(T)V}{RT[V(V+b)+(V-b)]} \quad (3.26)$$

where P is absolute pressure, R is gas constant, T is absolute temperature, V is the molar volume, and T_c is the critical temperature, P_c is the critical pressure, and ω is the Pitzer acentric factor.

3.4.5 Peng Robinson Stryjek Vera (PRSV) EoS

Stryjek and Vera further modified the attractive term of the PR EoS. The PRSV EoS, which is similar to the PR EoS is given in Equations 2.27 to 3.31 ([Van der Stelt et al. 2012](#)).

$$P = \frac{RT}{V-b} - \frac{a}{v^2 + 2bv - b^2} \quad (3.27)$$

$$a = \left(\frac{0.457235 R^2 T_c^2}{P_c} \right) \alpha \quad (3.28)$$

$$\alpha = [1 + k(1 - \sqrt{T_R})]^2 \quad (3.29)$$

$$k = k_o + k_1(1 + \sqrt{T_R})(0.7 - T_R) \quad (3.30)$$

$$k_o = 0.378893 + 1.489753 \omega - 0.17131848\omega^2 + 0.0196554\omega^3 \quad (3.31)$$

where k_1 is a pure component parameter. k_1 and ω are in Table 3.2 ([Stryjek and Vera 1986](#); [Proust and Vera 1989](#)). For T_R values up to 0.7, it is recommended that k_1 values in Table 3.2 be used and for T_R greater than 0.7, $k_1 = 0.0$.

Table 3.1: k_1 and ω values for CO_2 and impurities

Component	k_1	ω	Component	k_1	ω
CO ₂	0.04285	0.22500	CO	0.04279	0.04830
CH ₄	-0.00159	0.01045	H ₂ O	-0.06635	0.34380
N ₂	0.01996	0.03726	NH ₃	0.00100	0.25170
H ₂ S	0.03160	0.10000	O ₂	0.01512	0.02128
SO ₂	0.03963	0.25630			

3.4.6 Patel Tega (PT) EoS

Patel and Tega extended the SRK, and PR EoS. Their EoS is applicable to non-polar fluids and some polar fluids such as NH₃, alcohols and water, Equation 3.32 ([de Almeida et al. 2014](#)).

$$P = \frac{RT}{V-b} - \frac{a(T)}{V(V+b)+c(V-b)} \quad (3.32)$$

$$z^3 + (\gamma - 1)z^2 + (\alpha - 2\beta\gamma - \beta - \gamma - \beta^2)z + (\beta\gamma + \beta^2\gamma - \alpha\beta) = 0 \quad (3.33)$$

$$\alpha = (0.66121 - 0.76105z_c) \left(\frac{P_R}{T_R^2}\right) [1 + m(1 - \sqrt{T_R})]^2 \quad (3.34)$$

$$\beta = (0.02207 + 0.20868z_c) \left(\frac{P_R}{T_R}\right) \quad (3.35)$$

$$\gamma = (0.57765 - 1.87080z_c) \left(\frac{P_R}{T_R}\right) \quad (3.36)$$

$$m = (-6.608 + 70.43 z_c - 159.0 z_c) \left(\frac{P_R}{T_R} \right) \quad (3.37)$$

where b and c are constants, and z_c is critical compressibility constant. Equation 3.32 reduces to PR EoS if $c = b$ and to SRK if $c = 0$.

3.5 Mixing rules

The accuracy of using equations of state strongly depends on the application of mixing rules ([Twu et al. 2002](#)). Van der Waals one-fluid mixing rule is a common way to extend the EoS to non-polar mixtures. The parameters a and b in $z = \frac{V}{V-b_m} - \frac{a_m}{V R T}$ can be combined as:

$$a_m = \sum_i \sum_j x_i x_j a_{ij} \quad (3.38)$$

$$b_m = \sum_i \sum_j x_i x_j b_{ij} \quad (3.39)$$

The parameter a_{ij} is defined as

$$a_{ij} = \sqrt{a_i a_j} (1 - k_{ij}) \quad (3.40)$$

And parameter b_{ij} is defined as

$$b_{ij} = (b_i + b_j)/2 \quad (3.41)$$

Where, a_m and b_m represent mixture parameters, and k_{ij} is the binary interaction parameter of the two molecules.

Where the molecules are strongly polar, a modification of the van der Waals mixing rule by ([Twu et al. 2002](#)), Equation 3.42 can be used.

$$a = \sum_i \sum_j x_i x_j \sqrt{a_i a_j} (1 - k_{ij}) + \sum_i x_i \left[\sum_j x_j (a_i a_j)^{1/6} (k_{ji} - k_{ij})^{1/3} \right]^3 \quad (3.42)$$

Note that in Equation 3.42, k_{ij} is not equal to k_{ji} . If they are equal it reduces to the van der Waals mixing rule. Though the modified vdW mixing rule is applicable to complex mixtures including non-ideal systems, it no longer satisfies the second virial coefficient ([Twu et al. 2002](#)). Some mixing rules developed include, the Huron-Vidal mixing rule (Equation 3.43 to 3.47). This mixing rule is not widely used due to lack of parameters in the open literature for excess Gibbs energy at very high pressures, and the poor accuracy when used for non-polar hydrocarbon mixtures.

$$a^* = b^* \left[\sum_i x_i \frac{a_i^*}{b_i^*} + \frac{1}{c_1} \left(\frac{G_{\infty}^E}{RT} \right) \right] \quad (3.43)$$

$$a^* = \frac{P a}{R^2 T^2} \quad (3.44)$$

$$b^* = \frac{P b}{R T} \quad (3.45)$$

$$c_1 = -\frac{1}{(w-u)} \ln \left(\frac{1+w}{1+u} \right) \quad (3.46)$$

$$b = \sum_i \sum_j x_i x_j \left[\frac{1}{2} (b_i + b_j) \right] \quad (3.47)$$

where w and u are constants dependent on the EoS.

3.6 Density of CO₂ fluids

Knowledge of fluid pressure and temperature, environmental temperature and heat transfer along the pipeline is required for accurate prediction of the density of CO₂ fluids in pipelines. The results of z – factor calculated with the EoS were used in Equation 3.38, to calculate density.

$$\rho = \frac{P * M}{Z * R * T} \quad (3.38)$$

where ρ is the density, P is the pressure, and M is the molar mass.

Equation 3.39 is used to calculate density by calculating the density at a higher pressure and temperature and at a lower pressure and temperature ([McCullum and Ogden 2006](#)). To determine the density at the desired pressure and temperature, Equation 3.40 is used to interpolate between the densities at the higher pressure and the lower pressure, see Appendix D, Table D1. However, if the desired density corresponds to a given pressure and temperature value, there would not be any need for interpolation.

$$\rho = a * P_{op}^6 + b * P_{op}^5 + c * P_{op}^4 + d * P_{op}^3 + e * P_{op}^2 + f * P_{op} + g \quad (3.39)$$

$$\rho_{op} = \{(\rho_{high} - \rho_{low}) * (T_{op} - T_{low}) * (T_{high} - T_{low})\} + \rho_{low} \quad (3.40)$$

where ρ_{op} is the desired density, ρ_{high} is the density at a higher pressure and temperature, ρ_{low} is the density at a lower pressure and temperature, P_{high} and T_{high} are the pressure and temperature at which ρ_{high} is calculated, and P_{low} and T_{low} are the pressure and temperature at which ρ_{low} is calculated.

To calculate the density of a gas mixture, it is required that the correct gas deviation factor and molecular weight be determined. The gas deviation factor of gas mixtures was covered in section 3.4 and 3.5. The mixture molar mass can be calculated by using the molecular fractions of the component gases and their molecular masses.

3.7 Viscosity of CO₂ fluids

The viscosity of pure CO₂ in both liquid and gas phases have been reported in some studies. Some references exist in the literature that use correlations to measure the viscosity of CO₂ ([Heidaryan et al. 2011](#)). The correlation developed

by [Heidaryan et al. \(2011\)](#) for pure CO₂ in the pressure range of 7.5 to 101.4 MPa and temperature range of 31.85 and 626.85 °C is given in Equation 3.41 .

$$\mu = \frac{A_1 + A_2 P + A_3 P^2 + A_4 \ln(T) + A_5 (\ln(T))^2 + A_6 (\ln(T))^3}{1 + A_7 P + A_8 \ln(T) + A_9 (\ln(T))^2} \quad (3.41)$$

where μ is viscosity (cP), P is pressure (bara) and T is temperature (K). Values for A_1-9 are given in Table 3.3 below.

Table 3.2: Tuned coefficients for Equation 3.8 ([Heidaryan et al. 2011](#)).

Coefficients	Tuned coefficients
A ₁	-0.01146067
A ₂	0.0000006978380
A ₃	0.0000000003976765
A ₄	0.06336120
A ₅	- 0.01166119
A ₆	0.0007142596
A ₇	0.000006519333
A ₈	-0.3567559
A ₉	0.03180473

The ([Ouyang 2011](#)) viscosity equation is given in Equation 3.42.

$$\mu = c_0 + c_1 P + c_2 P^2 + c_3 P^3 + c_4 P^4 + c_5 P^5 \quad (3.42)$$

Where μ is viscosity (cP), P is pressure (psia), and T is temperature (°C) and

$$c_0 = d_{00} + (d_{01} * T) + (d_{02} * T^2) + (d_{03} * T^3) + (d_{04} * T^4)$$

$$c_1 = d_{10} + (d_{11} * T) + (d_{12} * T^2) + (d_{13} * T^3) + (d_{14} * T^4)$$

$$c_2 = d_{20} + (d_{21} * T) + (d_{22} * T^2) + (d_{23} * T^3) + (d_{24} * T^4)$$

$$c_3 = d_{30} + (d_{31} * T) + (d_{32} * T^2) + (d_{33} * T^3) + (d_{34} * T^4)$$

$$c_0 = d_{40} + (d_{41} * T) + (d_{42} * T^2) + (d_{43} * T^3) + (d_{44} * T^4)$$

The Arrhenius equation can be used to calculate the viscosity of fluid mixtures, requiring only the component viscosities, see Equation 3.43 ([Yener et al. 1998](#)).

$$\mu_m = \mu_1^{x_1} \mu_2^{x_2} \quad (3.43)$$

where μ_m is the viscosity of the mixture, μ_1 and μ_2 are the viscosities of the gas components, x_1 and x_2 are the component mole fractions.

([Al-Syabi et al. 2001](#)) presented the JST correlation for viscosity for non-polar substances, see Equation 3.44.

$$[(\mu - \mu^o)\lambda + 10^{-4}]^{1/4} = 0.10230 + 0.023364\rho_r + 0.058533\rho_r^2 - 0.040758\rho_r^3 + 0.0093324\rho_r^4 \quad (3.44)$$

$$\rho_r = \frac{v_c}{v} \quad (3.45)$$

If $T_r \leq 1.5$,

$$\mu^o = 34 * 10^{-5} T_r^{0.94} / \lambda \quad (3.46)$$

If $T_r > 1.5$,

$$\mu^o = 17.78 * 10^{-5} (4.58 T_r - 1.67)^{5/8} / \lambda \quad (3.47)$$

where μ is viscosity (cP), v_c is the critical molar volume and v is the molar volume.

Similar to the density equation, ([McCollum and Ogden 2006](#)) presented viscosity Equations 3.48 and 3.49. See Appendix D, Table D2 for the viscosity correlation parameters.

$$\mu = a * P_{op}^6 + b * P_{op}^5 + c * P_{op}^4 + d * P_{op}^3 + e * P_{op}^2 + f * P_{op} + g \quad (3.48)$$

$$\mu_{op} = \{(\mu_{high} - \mu_{low}) * (T_{op} - T_{low}) * (T_{high} - T_{low})\} + \mu_{low} \quad (3.49)$$

3.8 Pipeline heat transfer

There is heat exchange between the pipeline and the surrounding as CO₂ fluids flow in pipelines. The rate of heat transfer from the fluid to the surrounding can be calculated. Equation 3.50 represents the first law of thermodynamics for a pipeline ([Mohitpour et al. 2003b](#))

$$\Delta \left\{ \left(H + \frac{1}{2} u_m^2 + g Z \right) dm \right\} = \Sigma \delta Q - \delta W \quad (3.50)$$

where u_m is the mean velocity, g is the gravitational constant, Z is the elevation, δQ is the heat transferred to or from the pipeline, and δW is the work done to the fluid.

The driving factor in heat transfer between two media is the difference in temperature. The total amount of heat transfer (for a steady state) between the pipeline fluid and the surrounding soil may be written as in Equation 3.51 ([Wetenhall et al. 2017](#)).

$$Q = 2 \pi k_g S \Delta T \quad (3.51)$$

where Q is the heat transferred, S is the shape factor, k_g is the thermal conductivity of the surrounding soil, and ΔT is the difference in temperature between the two media. A good analysis of heat transfer from a CO₂ pipeline to the surrounding soil and atmosphere is given in ([Wetenhall et al. 2017](#)). Some formulae are presented below.

$$S = \frac{Bi_p a_{bur}}{\sqrt{\left(\cosh a_o - Bi_p a_{bur} \alpha_o = \frac{Bi_p}{Bi_g} \right)^2 - \left(1 + \frac{Bi_p}{Bi_g} \right)^2}} \quad (3.52)$$

$$a_o = -\cosh^{-1} \frac{2Z}{D_o}$$

$$a_{bur} = 4 \frac{Z^2}{D_o^2} - 1$$

$$Bi_p = \frac{U_{pipe} D_o}{2 k_g}$$

$$Bi_g = \frac{h_a D_o}{2 k_g}$$

$$\frac{1}{U_{pipe}} = \frac{1}{h_{film}} + \frac{1}{h_{pipe}}$$

where Bi_p is the Biop number of the pipeline, Bi_g is the Biop number of the surrounding ground, h_a is the heat transfer coefficient of the fluid film of the ground surface and ambient air at the surface, U_{pipe} is combined heat transfer coefficients of the pipeline h_{pipe} and fluid film h_{film} .

3.9 Other parameters

Some input parameters into the pressure drop equation include velocity/flow rate, friction factor (f), pipeline internal diameter (D), elevation (h), density, gravitational constant (g), etc. Of these, the diameter, velocity, and friction factor have not been discussed. The pressure drop in a pipeline is heavily dependent on the internal diameter. Therefore, both parameters can be calculated from the available correlations if one is given. Several equations can be used to calculate a suitable diameter given the pressure drop but the one given by ([Zhang et al. 2006](#)) is independent of pressure drop and may be used to select an initial optimal pipeline diameter.

$$D_{opt} = 0.0363 Q_v^{0.45} \rho^{0.13} \mu^{0.025} \quad (3.53)$$

The velocity of a fluid flowing in a circular pipe is easily calculated with;

$$vel = \frac{q_v}{A} \quad (3.54)$$

$$A = \pi \frac{D^2}{4} = \pi r^2 \quad (3.55)$$

where q_v is volumetric flow rate (m³/s), A is the cross-sectional area of the pipeline (m²), D is the internal diameter of the pipeline and r is the radius of the pipeline.

To calculate the friction factor, the Reynold's number is required. Reynolds number is the ratio of the inertial forces to the viscous forces of the fluid.

$$R_e = \frac{\rho v D}{\mu} \quad (3.56)$$

The Colebrook and White friction factor (f) equation is widely used in industry ([Kiijarvi 2011](#)). The Darcy friction factor is four times the Fanning friction factor.

The Darcy friction factor equation and Fanning friction factor equation are given in Equations 3.57 and 3.58 ([McCollum and Ogden 2006](#))

$$\frac{1}{\sqrt{f}} = -2.0 \log \left(\frac{\varepsilon/D}{3.7} + \frac{2.51}{R_e \sqrt{f}} \right) \quad (3.57)$$

$$f_F = \left\{ 4 \left[-1.8 \log \left(\frac{6.91}{R_e} + \left(\frac{12(\varepsilon/D)}{3.7} \right)^{1.11} \right) \right] \right\}^{-2} \quad (3.58)$$

where (ε/D) is the relative roughness of the pipe.

The Nikuradse friction factor for fully developed turbulent flow according to [Mohitpour et al. \(2003b\)](#) is given in Equation 3.59.

$$\sqrt{1/f} = 4 \log \left(\frac{3.7 D}{k} \right) \quad (3.59)$$

where k is pipe roughness.

3.10 CO₂ Pipeline pressures

The pressure drop in pipelines is simulated with Equation 3.60. The effect of impurities on all input parameters into the equation is analysed. Equation 3.60 ([Chandel et al. 2010](#)) is used to compute the pressure drop.

$$\Delta P = \frac{f \rho L u^2}{2 D} + \rho g \Delta h \quad (3.60)$$

where ΔP is pressure drop between inlet and outlet, f is dimensionless friction factor, L is length of pipeline (m), u is velocity (m/s), D is pipeline internal diameter (m), ρ = fluid density (kg/m³), g = acceleration due to gravity (m/s²) and ΔZ is change in elevation (m).

To calculate the pressure at any point along the pipeline, the pressure drop is subtracted from the initial pressure, Equation 3.61.

$$P_{outlet} = P_{inlet} - \Delta P \quad (3.61)$$

([Ogden et al. 2004](#)) presented an equation to determine the steady state flow of CO₂ at supercritical conditions as a function of diameter, pressure, temperature, pipeline length, and fluid composition.

$$Q_v = C_1 \sqrt{(1/f)} \left[\frac{(P_i^2 - P_o^2 - C_2 \left\{ G \frac{\Delta h P_{ave}^2}{z_{ave} T_{ave}} \right\})}{G T_{ave} z_{ave} L} \right]^{0.5} D^{0.5} E \quad (3.62)$$

where Q_v is volumetric flow rate (Nm³/s), P_i , P_o are inlet and outlet pressures (kPa), G is specific gravity, T_{ave} is average temperature, z_{ave} is gas deviation factor at average pressure, L is pipeline length (km), E is pipeline efficiency factor and C_1 , C_2 are constants, 18.921 and 0.06835 respectively.

3.11 Chapter conclusion

Various equations for the estimation for the parameters and properties of CO₂ fluids flowing in pipelines are presented in this chapter. Equations of state used in the Aspen HYSYS and gPROMS simulations were presented. Several correlations were used in gPROMS to calculate the parameters of both pure and impure properties of CO₂ fluids. The results from Aspen HYSYS and gPROMS are compared and presented in chapter 6. Equations are developed to account for the effect of each impurity on each of the parameters studied.

Chapter 4: Simulation of the effects of single impurities in CO₂ pipelines

4.1 Introduction

CO₂ pipeline minimum pressure is specified at about 10 % above the critical pressure ([Lemontzoglou et al. 2017](#)). Above the critical pressure, CO₂ fluid does not become a gas while flowing in the pipeline. Transporting CO₂ fluids in supercritical pressure and supercritical temperature ensures that the fluid remains in the supercritical state. However, the flowing fluid changes to the dense subcritical phase if the temperature drops below the critical value while the pressure remains above the critical value. Several authors gave varying ranges of pressure and temperature of CO₂ pipelines. [Wetenhall et al. \(2014a\)](#) put it at between 8.5 MPa and 20 MPa and 12 °C and 44 °C, [Mohitpour et al. \(2003b\)](#) at between 8.6 MPa and 15.1 MPa and 12.7 °C and 43.3 °C and 8.6 MPa to 15 MPa in [Kang et al. \(2014\)](#). However, similar to the NEFL study, an inlet pressure of 15 MPa ([IEA GHG 2014](#)) and temperature of 33 °C are assumed in this section. All reported CO₂ pipeline pressures are higher than the critical pressure of pure CO₂ (7.39 MPa) but the temperature is not always higher than the critical temperature (31.1 °C). This is because CO₂ remains in the dense phase if the pressure is maintained above the critical value. An analysis of the transportation of CO₂ as a subcritical fluid (below critical temperature) and supercritical fluid (above critical temperature) is given in chapter 5.

4.2 Effects of single impurities at 10 mol %

For every captured CO₂, the impurities are different and occur in different concentrations. However, for a fair comparison, all impurities are assumed to constitute 10 mol % in this section.

4.2.1 Methodology

CO₂ fluids with single impurities (0.9 mol fraction CO₂ and 0.1 mol fraction) were simulated with Aspen HYSYS (Ver. 10). The Peng Robinson equation of state was used in this analysis because it has the lowest absolute average deviation (AAD) when used to calculate density of binary CO₂ fluids ([Mazzocolia et al. 2013](#)). [Yang et al. \(2014\)](#) also stated that the PR EoS was better than others when used in calculating the critical temperature and critical pressure of CO₂ fluids. Four CO₂ pipelines, Cortez pipeline, Canyon Reef Carriers, Weyburn pipeline and Sheep Mountain pipeline, are selected for the analysis. The parameters simulated include pressure drop (ΔP), critical pressure (P_c), critical temperature (T_c), temperature change (ΔT), and phase envelope. HydraFlash was also used to simulate the phase envelope and the results compared to those obtained from Aspen HYSYS. It should be noted that only N₂ and CH₄ may be constituent up to 0.1 mol concentration in actual pipelines. In CCS operations, only N₂ is greater than 0.065 mol concentration. Table 4.1 shows the hypothetical pipeline and Table 4.2 shows the actual composition of the pipelines (CO₂ pipelines for oil recovery in the USA) used in the analysis.

Table 4.1: Hypothetical pipeline specification.

Length	50,000 m	Material	Mild steel
Outer diameter	0.324 m	Elevation change	0 m
Inner diameter	0.289 m	Pipe wall conductivity	45 W/(m. °C)
Inlet pressure	15 MPa	Mass flow rate	74 kg/s
Inlet temperature	33 °C	Pipe roughness	0.0000457 m

Table 4.2: Actual fluid composition of CO₂ pipelines ([Patchigolla and Oakey 2013](#))

Component	Cortez Pipeline	Canyon Reef Carriers	Weyburn pipeline	Sheep Mountain Pipeline
CO ₂	0.95	0.8991	0.9600	0.9700
CH ₄	0.01	0.0997	0.0070	0.0170
N ₂	0.0378	0.0050	0.0003	0.0079
CO	-	-	0.0010	-
H ₂ S	0.002	0.0002	0.0090	-
O ₂	-	-	0.0001	-
C ₂₊	-	-	0.0225	0.0050
H ₂ O	0.0002	0.0005	0.0001	0.0001

4.2.2 Effects impurities on critical point

Pressure and temperature may decline when CO₂ fluids flow in pipelines due to frictional, acceleration or elevation change effects. The change in temperature may be ignored if pressure remains above critical value as the fluid will remain in the dense phase. However, the fluid changes from supercritical phase to subcritical phase if the temperature falls below the critical value while pressure remains above the critical value. To specify the minimum pressure of a CO₂ stream, the critical pressure must first be ascertained. The minimum pressure is usually a value slightly above the critical pressure. The increase in critical pressure is less than 5 % if the concentration of impurities is below 2.5 % ([Kaufmann 2011](#)). Though 5 % increase is small, it still requires careful analysis and most CO₂ pipelines constitute greater than 2.5 % impurity concentration. Table 4.3 shows the values of the critical pressures of the binary fluids from both Aspen HYSYS and HydraFLASH. Some values did not converge on HydraFLASH. The critical pressure of the selected CO₂ pipelines is shown in Table 4.4.

Table 4.3: Critical temperature and pressure of binary CO₂ fluids.

Components	Critical pressure (MPa)		Critical temperature(°C)	
	Aspen HYSYS	HydraFLASH	Aspen HYSYS	HydraFLASH
10 mol %				
Pure CO ₂	7.37	7.35	30.95	30.85
CH ₄	7.94	7.66	23.25	23.14
N ₂	8.82	7.71	23.61	22.09
H ₂ S	7.45	6.22	33.29	-
O ₂	8.64	-	24.41	-
% SO ₂	8.51	8.39	49.84	49.87
CO	8.78	8.64	23.48	23.85
H ₂ O	8.91	-	24.83	-
H ₂	10.77	10.90	28.34	29.02
Ar	8.37	-	24.39	-
NH ₃	8.04	-	41.91	-

Fluids with high critical pressure increase the minimum pressure of the pipeline and consequently increase both the capital cost (higher cost for stronger pipes) and the operational cost (higher energy for compression). Therefore, impurities that increase the critical pressure also increase the cost of transportation. A reduced critical temperature increases the temperature range for supercritical flow. The flowing fluid becomes a supercritical fluid at lower temperatures, hence may eliminate the need for heating the pipeline fluid to attain supercritical phase.

Therefore, impurities that reduce the critical temperature have positive effect in terms of their impact on temperature, if supercritical transportation is specified. Impurities that increase the critical temperature make liquid or subcritical transportation possible at higher temperatures. The temperature of the flowing fluid declines below the critical temperature as it travels along the pipeline. This could be a positive effect, if supercritical phase is not a requirement, because the

fluids flows for longer distances under subcritical conditions. However, if supercritical phase transportation is specified, such impurities have negative impact as pipelines may require heating to attain supercritical state, mostly in colder climates. Heating the pipeline fluid would significantly increase the cost of transportation.

Table 4.4: Critical temperature and pressure of selected pipelines.

Pipelines	Software	Critical Pressure (MPa)	Critical Temperature (°C)
Pure CO ₂	Aspen HYSYS	7.37	30.95
	HydraFLASH	7.34	30.85
Cortez	Aspen HYSYS	7.88	27.57
	HydraFLASH	8.01	27.41
Weyburn	Aspen HYSYS	7.34	29.17
	HydraFLASH	6.54	23.65
Sheep Mountain	Aspen HYSYS	7.56	28.92
	HydraFLASH	7.56	29.03
Canyon Reef	Aspen HYSYS	8.03	22.46
	HydraFLASH	7.92	23.35

4.2.3 Effects of impurities on phase envelope

A two-phase region forms below the VLE line of pure CO₂ if the impurities have higher critical pressure while those with lower critical pressure will form two-phase regions above the VLE line of pure CO₂ ([Wetenhall et al. 2014b](#)). The results obtained with Aspen HYSYS and HydraFlash simulations were similar and confirmed that the two – phase region of fluids with higher critical pressure forms above the VLE line of pure CO₂. Figures 4.1 shows the phase envelopes from Aspen HYSYS of binary CO₂ fluids and Figure 4.2 shows Aspen HYSYS and HydraFlash plots of the phase envelopes for the selected pipelines. The phase envelope of Weyburn pipeline fluid did not converge on HydraFlash.

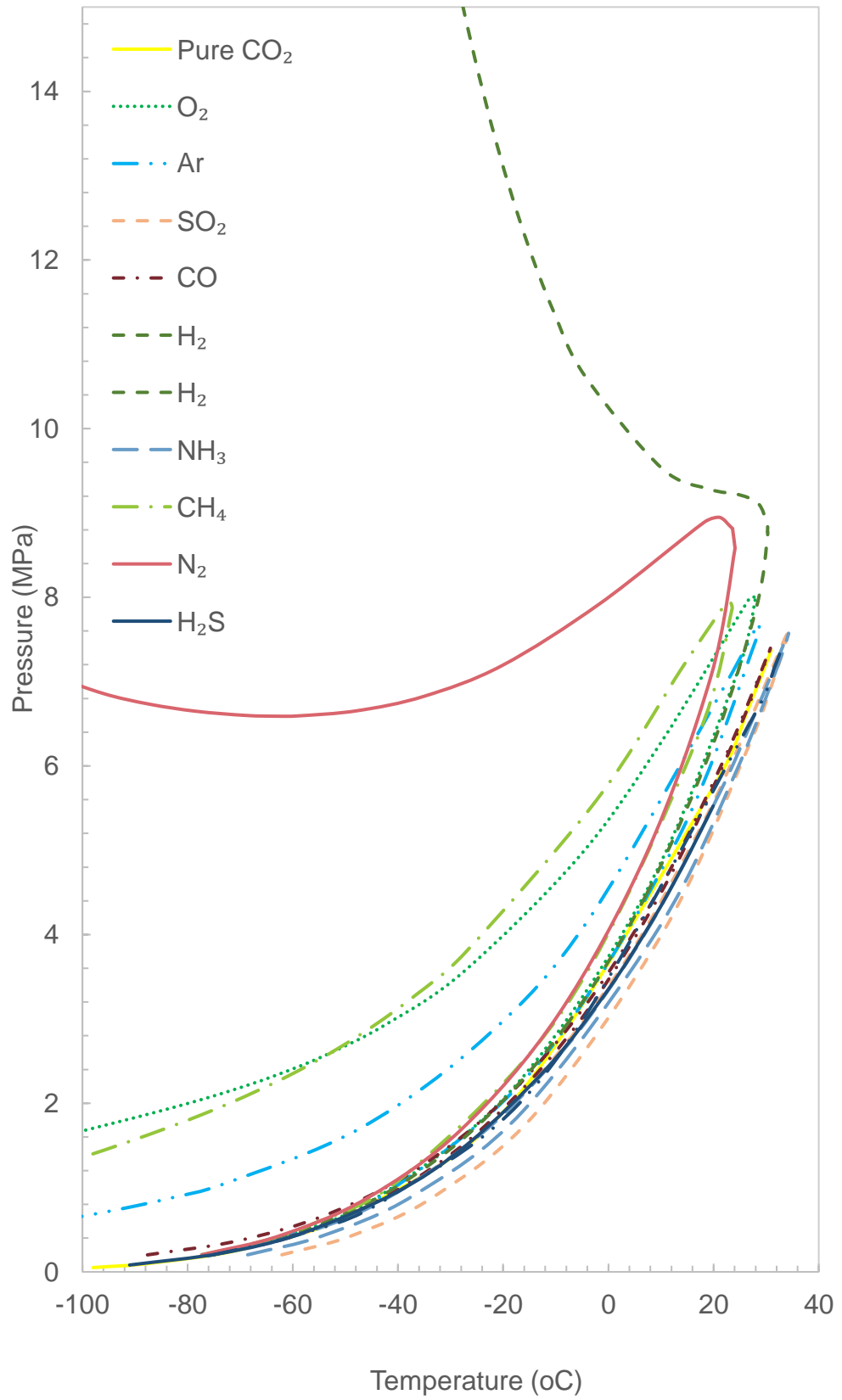
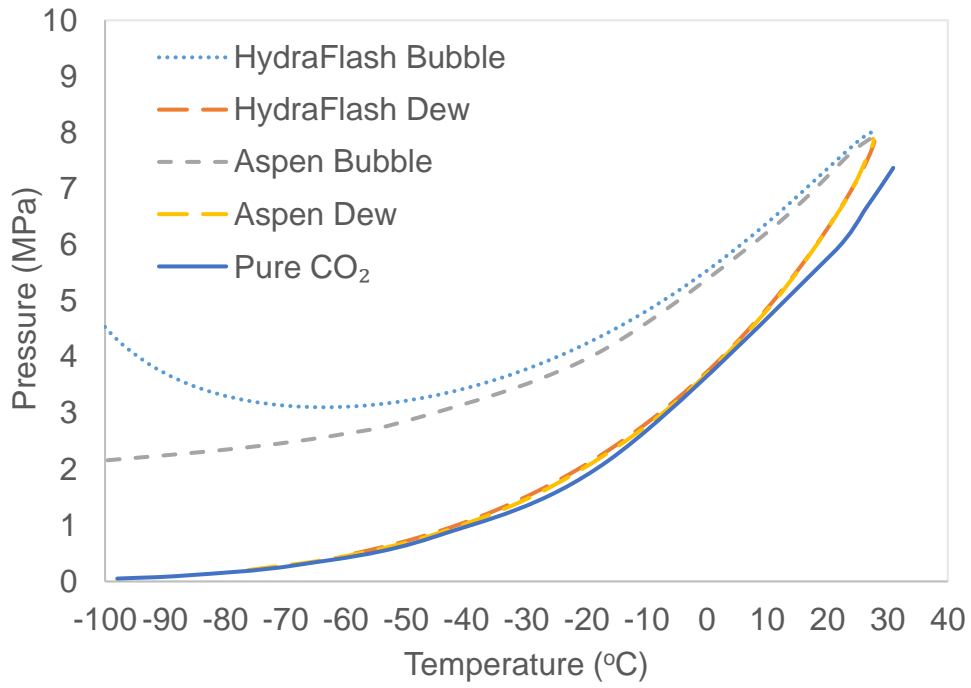
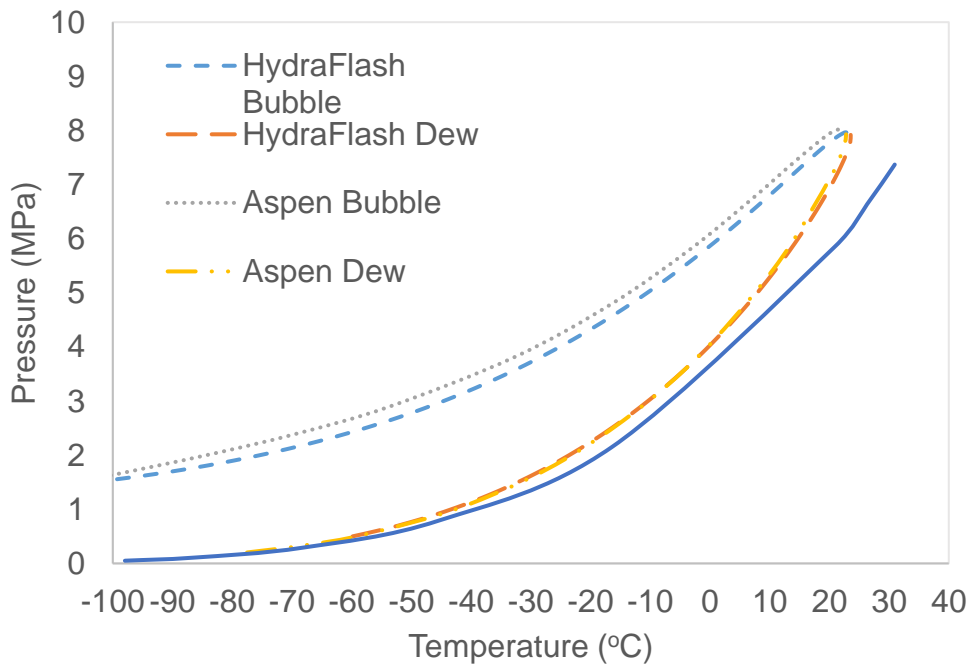


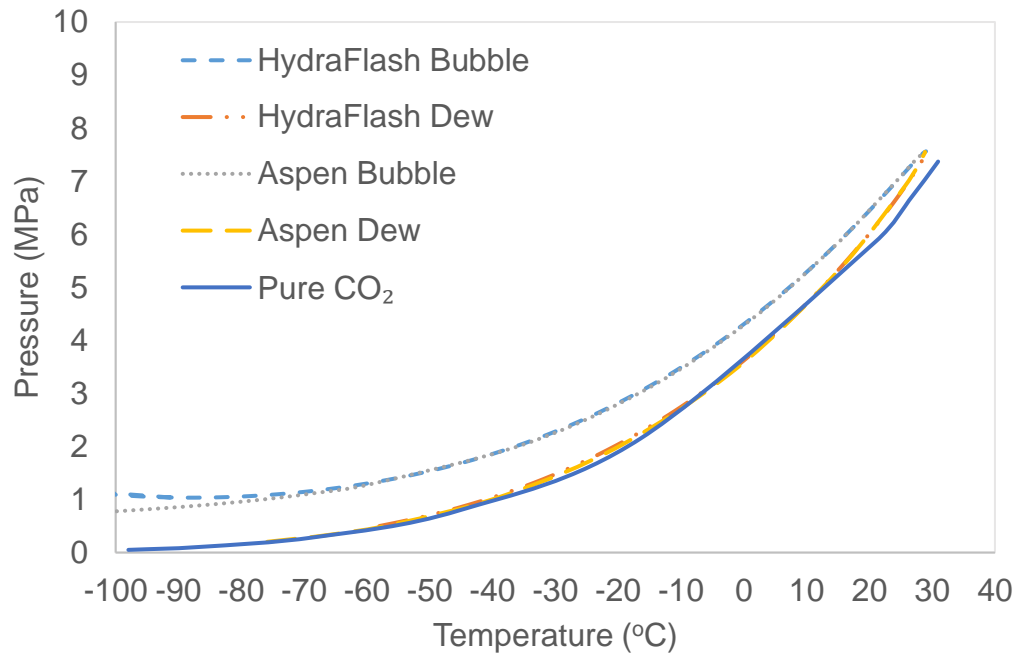
Figure 4.1: *P – T phase diagram of binary fluids at 10 mol % impurity concentration.*



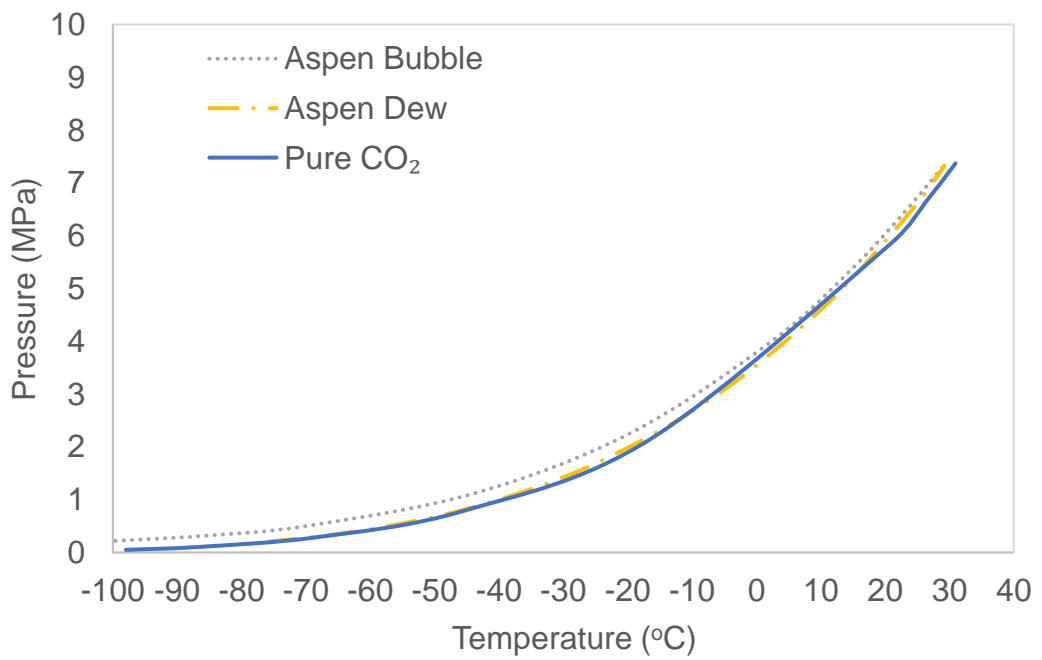
(a) Cortez pipeline



(b) Canyon Reef Pipeline fluid



(c) Sheep Mountain pipeline fluid



Weyburn pipeline

Figure 4.2: *P – T phase diagram of selected pipelines fluids.*

H₂ formed the widest two – phase region and H₂S the narrowest. The two – phase region of SO₂ and NH₃ occur below the VLE line of pure CO₂ while others occur about it. The VLE line of pure CO₂ lies close to the dew – point curves of all pipelines. The two – phase region of all pipeline fluids except that of Weyburn

pipeline lie above the VLE of pure CO₂. This is because the critical pressure of Cortez, Sheep Mountain and Canyon Reef CO₂ fluids have higher critical pressure than pure CO₂, but the Weyburn pipeline fluid has about the same critical pressure. The two – phase region of the Weyburn pipeline fluid is also the narrowest because it has the smallest concentration of impurities. Two – phase region is wider for fluids with higher concentration of impurities. The comparative width of the bubble and dew point curves at 20 °C is given in Table 4.5, as a measure of the width between the two lines. HydraFlash predicted a wider two – phase region than Aspen HYSYS. The percentage difference of the width between the Aspen HYSYS and HydraFlash predictions for the Cortez, Canyon Reef and Sheep Mountain pipeline fluids are 14.4 %, 3.3 %, and 6.0 %, respectively. The Cortez pipeline fluid has the widest two – phase region followed by the Canyon Reef pipeline fluid.

Table 4.5: Comparative width of bubble and dew point lines at 20 °C.

Pipelines	Aspen HYSYS	HydraFLASH	Difference
Cortez (MPa)	0.913	1.066	0.153
Canyon Reef (MPa)	0.823	0.850	0.027
Sheep Mountain (MPa)	0.409	0.435	0.026
Weyburn (MPa)	0.118	-	-

The possibility of fluids with wide two – phase regions to form a gaseous phase during transportation is higher than those with narrower two – phase region. Above the bubble point curve and below the critical pressure, the fluid exists in the subcritical region. Fluids with higher bubble point pressure are therefore more suitable for subcritical phase transportation while fluids with lower bubble point pressure are more suitable for supercritical phase transportation. Very low ambient temperatures favour subcritical phase transportation because the

flowing fluid would lose heat quickly and enter the subcritical phase. Fluids with very high critical temperatures are also suitable for subcritical flow. For example, the Sheep Mountain CO₂ pipeline fluid exists in subcritical state at temperatures below 29 °C but the Canyon Reef pipeline fluid would remain in supercritical state until the temperature drops below 23 °C.

4.2.4 Effects of impurities on density

Density positively correlates with pressure but negatively correlates with temperature. At supercritical temperatures and pressures pure gases may have liquid - like densities and low gas - like viscosities ([Koga et al. 2005](#)). [Liu et al. \(2017\)](#) measured density of 0.8988-mol % CO₂ and 0.1012-mol % CH₄ and showed that within the temperature and pressure ranges of CO₂ pipelines, pressure changes had milder effects than temperature changes. A 26.38 % decrease in density was observed for a 10 % increase in temperature and only a 6.08 % increase in density for an increase of 10 % in pressure. The results for CO₂ + CH₄ fluid was similar in the supercritical phase. The density of pure CO₂ at the specified condition of pressure and temperature is 805.46 kg/m³. Figure 4.3 shows the densities of the binary fluids at equal concentration of 10 mol %.

Density also changes as the fluid flows along the pipeline. This change results from the change in the fluid temperature and pressure. In horizontal pipelines, the pressure will decline, and the fluid will expand reducing the density. However, the temperature also declines along the direction of flow and the fluid contracts increasing the density. The overall change in density will depend on the parameter with the greater effect on density at the prevailing conditions.

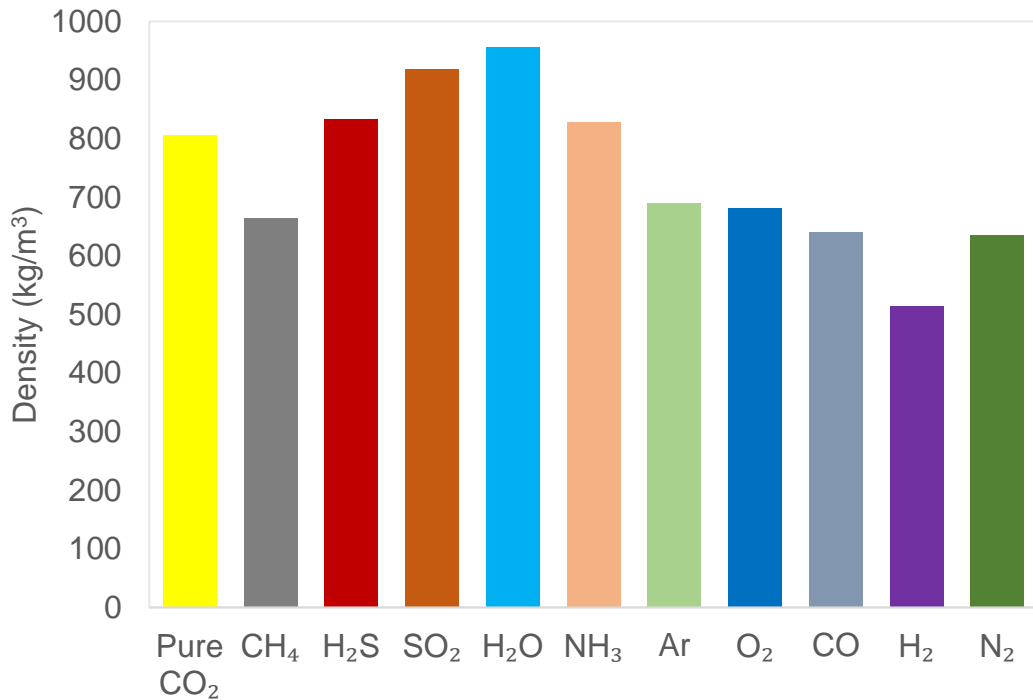


Figure 4.3: Density of binary fluids at 10 mol % impurity concentration.

Figure 4.4 shows plots of density variations with temperature of a post combustion capture fluid (see Table 2.3) at five different pressure values. From the figure, it can be deduced that at high pressures, i.e. pressures higher than critical, density varies linearly with temperature. At lower pressures, below critical value, the effect of temperature on density is greatly reduced. At very low pressures, a drop in temperature from 20 °C to 10 °C shows a sharp increase in density. But at higher pressures, the change of density from 20 °C to 10 °C is smaller than a 10 °C change at higher temperatures. For example, a change of temperature from 40 °C to 30 °C at 13 MPa results to an increase in density of 97.85 kg/m³ while a change from 20 °C to 10 °C resulted in only 71.19 kg/m³ increase. But a change of temperature from 20 °C to 10 °C at 5.4 MPa resulted in an increase in density of 668.80 kg/m³ and only an increase of 14.46 kg/m³ from 40 °C to 30 °C. The impact of temperature on density is higher at lower pressures and lower temperatures than at lower pressures and higher

temperatures. The impact of temperature on density is also increased at higher pressures and higher temperatures than at higher pressures and lower temperatures.

CO₂ fluid impurities also affect the change in density along the pipeline. All impurities increased the drop in density of the fluid as it flows along the pipeline. H₂O caused the highest increase in density drop while H₂ caused the lowest. The decrease in density of pure CO₂ from the inlet of the pipeline to the outlet was 12.36 kg/m³ while that of CO₂/H₂ binary fluid was 63.41 kg/m³ and that of CO₂/H₂O was 97.09 kg/m³. See Figure 4.5 for the density change of all the binary fluids.

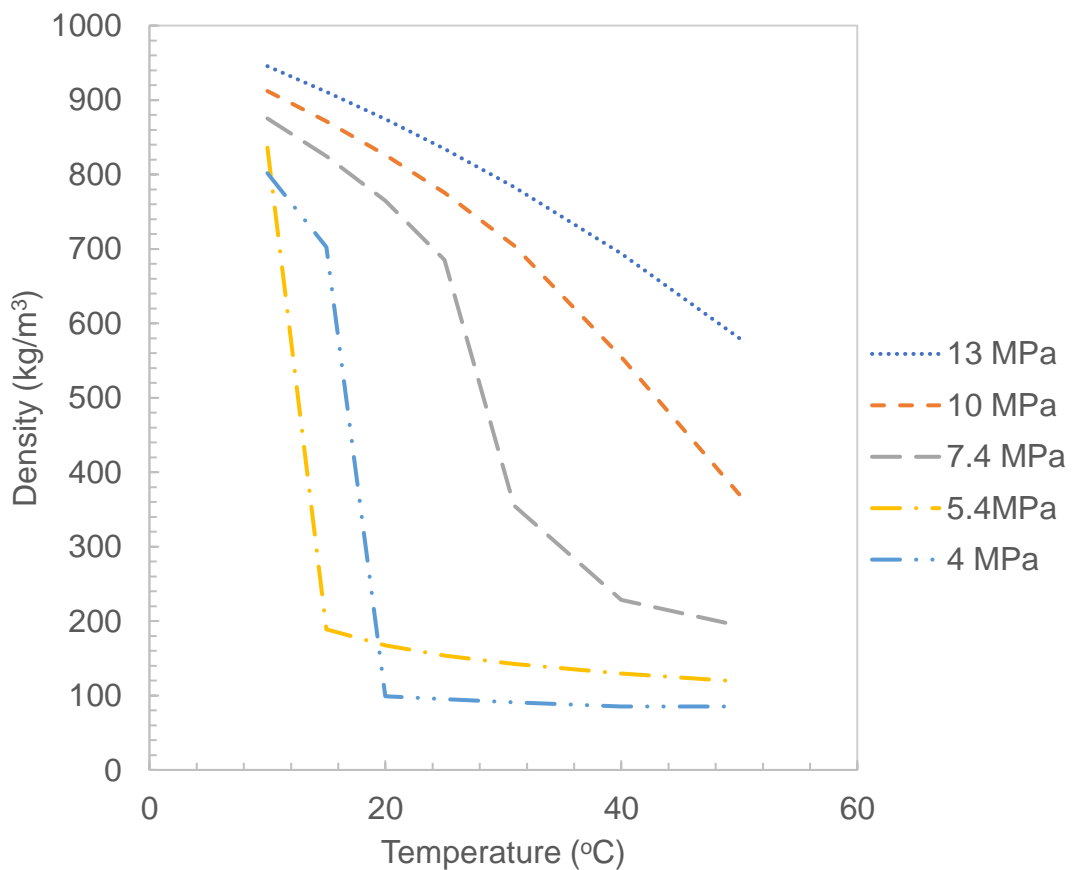


Figure 4.4: Temperature effect on density at different pressure values of a post combustion fluid.

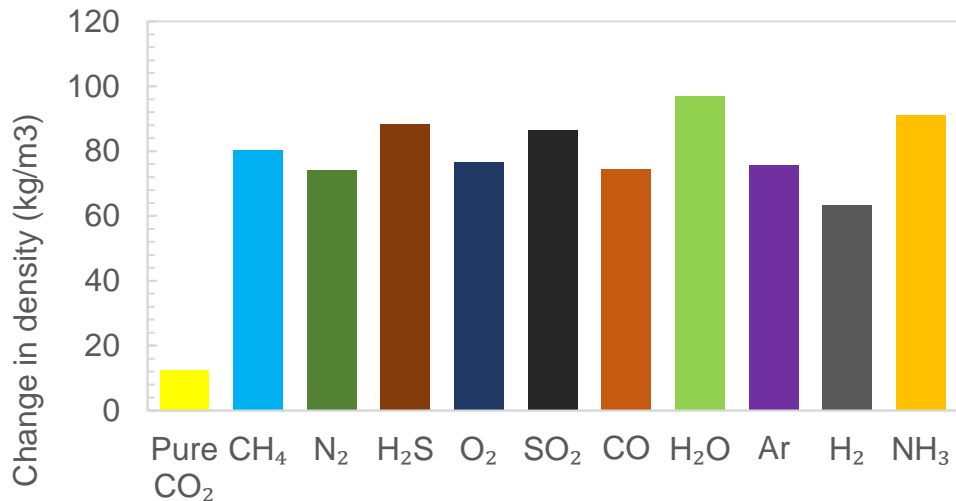


Figure 4.5: Density change along pipeline.

4.2.5 Effects of impurities on temperature

An ambient temperature of 25 °C was assumed in the simulation of temperature changes in Aspen HYSYS. The inlet pressure of the pipeline is 33 MPa, and the pipeline is uninsulated. Heat transfer from the pipeline to the ground may reduce the temperature below supercritical value. The fluid becomes a subcritical fluid when the temperature drops below the critical value. Supercritical CO₂ fluid transportation is usually specified for pipelines but the reason for this preference is not clear. The advantages of transporting CO₂ at lower temperatures include the use of pipelines with thinner wall thickness (capital cost saving), smaller diameter pipes (capital cost saving), pumps for compression instead of compressors (energy saving) ([Teh et al. 2015](#)) and increased density of fluid (more volume) ([Zhang et al. 2006](#)). Figure 4.6 shows the temperature drop due to single impurities and Figure 4.7 shows the temperature drop due to actual pipeline fluids and pure CO₂.

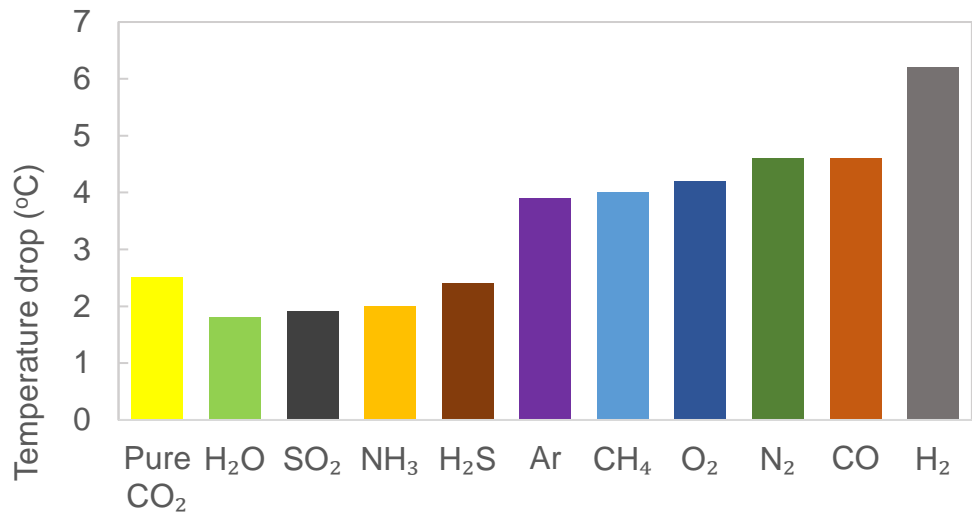


Figure 4.6: Temperature drop of CO₂ binary fluids (at 10 % impurity concentration) from inlet to outlet of pipeline.

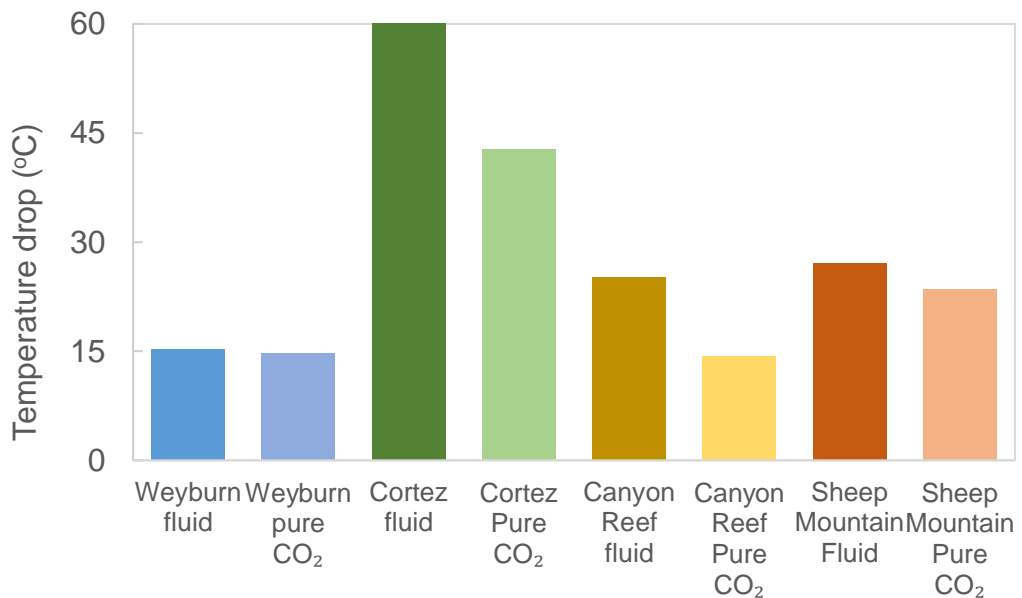


Figure 4.7: Temperature drop of actual pipeline and pure CO₂ fluids.

H₂O, SO₂, NH₃, and H₂S reduced the heat losses in the binary fluid pipelines while all other impurities increased the heat loss over that of pure CO₂. All actual pipeline fluids showed higher heat losses than pure CO₂. Increased heat loss may reduce fluid temperatures and change the fluid state from supercritical to subcritical. At subcritical state, the pressure losses are reduced, and the fluid can be transported for longer distances before recompression.

4.2.6 Effects of impurities on pressure drop

When CO₂ fluids are transported in pipelines as supercritical fluids, there is no discontinuity in the fluid properties even when the temperature falls below the critical value ([Raimondi 2014](#)). However, if the pressure drops below the critical value, there may be drastic changes in phase. For this reason, the fluid pressure is maintained above the critical point by re-pressurizing at a specified minimum fluid pressure value. The pressure drop is calculated, and transportation distances ascertained for the installation of pressure boosting stations. Several different forms of similar equations exist for the determination of pressure drop. Equation 2.45, a frictional pressure drop equation given in [IEA GHG \(2002\)](#) is suitable for only horizontal pipelines. Pressure drop equation for both frictional pressure loss and elevation change are given in Equation 4.1 ([Chandel et al. 2010](#)). The complete pressure drop equation, for frictional, elevation and acceleration effects is rarely used in design. Figures 4.8 and 4.9 show the pressure drop of the binary fluids and the selected pipeline fluids, respectively.

$$\Delta P = \frac{f L \rho u^2}{2 D} + \rho g \Delta Z \quad (4.1)$$

where ΔP is the pressure drop (MPa), L is the pipeline length (m), u is the velocity of the fluid (m/s), g is acceleration constant (m/s²), ΔZ is the change in elevation from the inlet to the outlet (m).

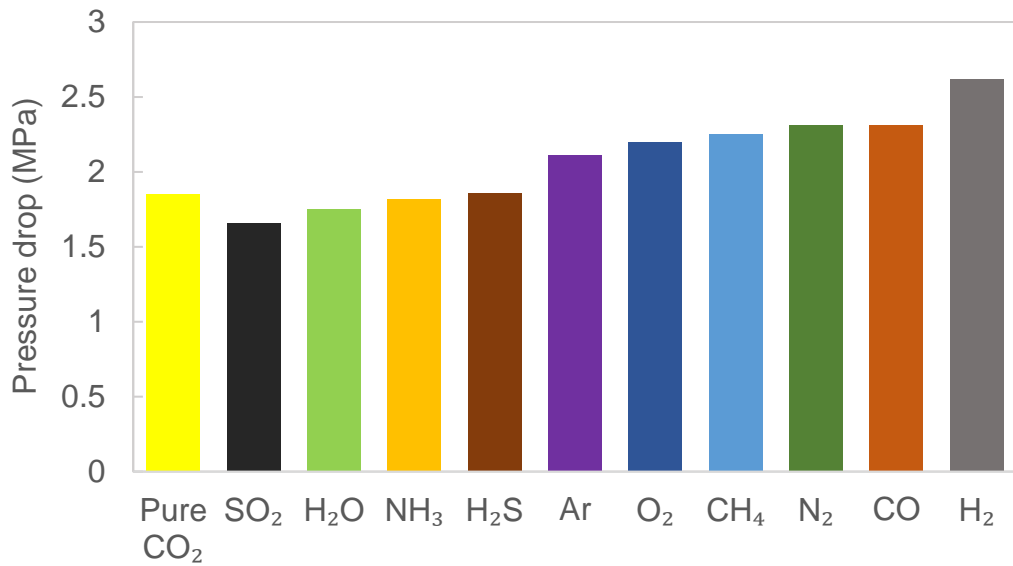


Figure 4.8: Pressure drop of CO₂ binary fluids from inlet to outlet of pipeline.

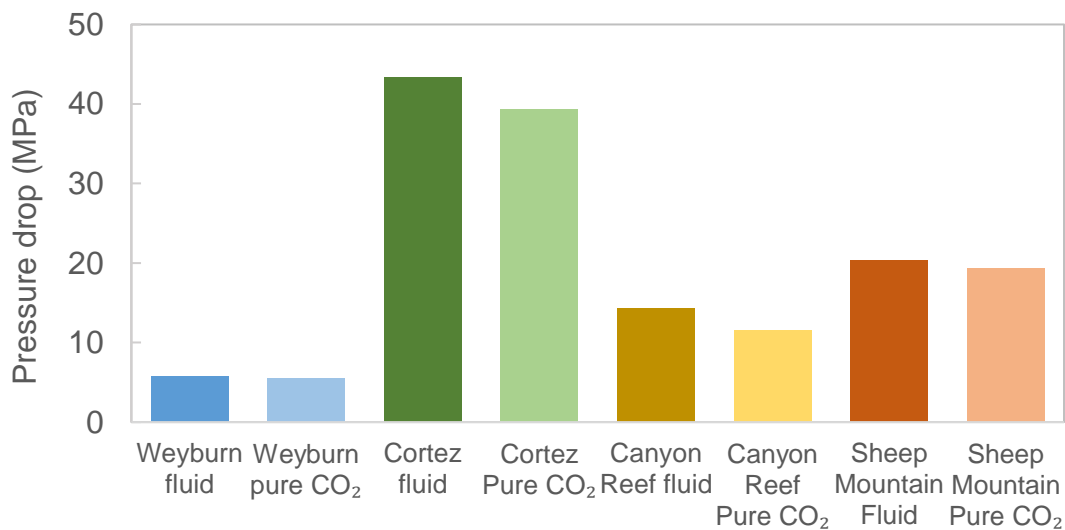


Figure 4.9: Comparison of pressure drop of actual pipeline fluids and pure CO₂.

Three impurities (SO₂, H₂O and NH₃) reduced the pressure losses. SO₂ impurity resulted to the highest reduction in pressure loss while H₂ resulted to the highest increase of pressure loss. All actual pipelines showed increased pressure loss due to the impurities. The Weyburn pipeline had the smallest increase while the Cortez pipeline had the highest increase in pressure loss due to the impurities. However, it should be noted that the Cortez pipeline is longer than all other pipelines and would have higher pressure loss than others.

4.2.7 Effects of impurities on pressure in non-horizontal pipelines

Two pipelines rising and falling 300 m from inlet to outlet were analysed to study the effect of impurities on the pressure behaviour of non – horizontal CO₂ pipelines. The pipeline is the same as the one in Table 4.1 except that the elevation is + 300 m for the inclined pipeline and – 300 m for the declined pipeline. Figure 4.7 shows the pressure drop of the two pipelines. The bars above 0 or positive values show a pressure loss while bars below 0 or negative values show a pressure increased.



Figure 4.10: Pressure drop of non – horizontal pipelines.

In the inclined pipeline, pressure drop for all binary fluids increased compared to the horizontal pipeline because of the elevation component of the pressure drop, (see Equation 4.2). For non – horizontal pipeline, the elevation component plays

a significant role in pressure changes. For pipelines going downslope, the pressure may increase depending on the angle of elevation and the impurity. In this case, pure CO₂ and 10 mol % of H₂S, SO₂, H₂O and NH₃ caused an increase in pressure. The magnitude of the impact of the impurities is also dependent on the pipeline profile. The percentage increase in pressure due to H₂ impurity is 41.7 % for horizontal pipeline, 8.83 % for the inclined pipeline and 263 % for the declined pipeline. H₂S impurity which barely had any effect on the pressure drop in horizontal pipeline showed an 8.21 % increase in pressure gain in declined pipeline. The impact of the impurities is smallest for inclined pipeline and largest for declined pipeline, see Table 4.6. It is generally understood that H₂ and H₂S has the highest and smallest impact in CO₂ pipeline transportation, but this is only true in horizontal pipelines. In this simulation, changing the elevation from 300 to 350 m in the inclined pipeline makes SO₂ to have the highest increase in pressure drop. Due to the elevation component, higher pressure losses are expected from fluids with higher densities in inclined pipelines. In pipelines going downslope, the pressure will increase if the elevation component is higher than the frictional component. Therefore, SO₂ has the highest pressure gain of 0.995 MPa in the pipeline running downslope.

Table 4.6: Percentage of impurity induced pressure change in pipeline profiles.

Elevation	SO ₂	CH ₄	H ₂ S	CO	O ₂	Ar	NH ₃	N ₂	H ₂ O	H ₂
300 m	2.43	0.33	0.43	0.02	0.52	0.69	0.5	0.05	1.22	8.83
0 m	10.15	22.08	0.54	25.23	18.93	14.27	1.52	25.01	5.53	41.67
- 300 m	82.12	151.4	8.21	169.7	130.3	100.5	7.85	168.2	46.7	263.0

4.2.8 Results and discussion

All common impurities increased the critical pressure of the fluid. H₂S caused the smallest increase and H₂ the highest increase. All pipeline fluids have critical

pressures higher than pure CO₂ except the Weyburn pipeline which contains a C₂₊ fraction. Canyon Reef pipeline fluid has the highest concentration of impurities and the highest critical pressure. In terms of critical pressure, no impurity has a positive effect because all would require a higher minimum pipeline pressure than pure CO₂.

An undesirable two – phase region is created by all impurities. A two – phase region will form in a combination of gases having different condensation or vaporisation pressure/temperature combinations. H₂ formed the widest two – phase region while H₂S, the narrowest. Canyon Reef with the highest concentration of impurities also has the widest two – phase region followed by Cortez. Due to the two – phase region formed by impurities, the pressure and temperature combinations for subcritical flow is also reduced. For example, pure CO₂ is a subcritical fluid at a pressure of 7 MPa and 20 °C but the Cortez pipeline fluid will be in two – phases at this pressure and temperature.

All pipelines showed increased temperature drop due to impurities. The temperature drop increased for Cortex pipeline from 42.79 °C (pure CO₂) to 60.28 °C (with impurities), for Weyburn pipeline, from 14.80 °C (pure CO₂) to 15.24 °C (with impurities), for Canyon Reef pipeline, from 14.34 °C (pure CO₂) to 25.15 °C (with impurities) and for Sheep Mountain pipeline from 23.48 °C (pure CO₂) to 27.04 °C (with impurities). Since lower fluid temperatures result to lower pressure losses, all impurities have positive effect in terms of temperature. However, if supercritical state transportation is specified, the impurities may increase the likelihood of heating the pipeline fluid to attain supercritical conditions, thereby incurring additional cost.

All impurities increased the pressure losses except SO₂, H₂O and NH₃. The smallest increase in pressure loss was due to H₂S and the largest was due to H₂. All pipelines showed increased pressure drop compared to pure CO₂ fluids in the pipelines. Additional pressure losses for Weyburn pipeline was 0.24 MPa, for Cortez pipeline was 3.98 MPa, for Canyon Reef pipeline was 2.69 MPa and for sheep Mountain pipeline was 1.05 MPa. These additional pressure losses may increase capital and operational costs. If a minimum pressure of 10 MPa is assumed, the number of booster stations for the pipelines will increase from 8 to 9 for Cortez, 4 to 5 for Sheep Mountain but no change at 2 for Weyburn and 3 for Canyon Reef.

Table 4.7 shows the percentage deviation due to the single impurities for each parameter studied and Table 4.8 shows the deviation from pure CO₂ due to the impurities in the pipelines.

Table 4.7: Percentage change in horizontal pipelines due to 10 mol % impurities.

Parameter	Pressure drop (%)	Temperature drop (%)	Density increase (%)	Critical pressure (%)
H ₂ S	0.54	-0.04	3.36	1.1
NH ₃	1.6	-0.20	2.72	9.2
H ₂ O	-5.4	-0.28	18.70	20.0
SO ₂	-10.3	-0.24	14.04	15.5
CO	24.9	0.84	-20.55	19.1
Ar	14.1	0.56	-14.30	13.6
CH ₄	21.6	0.60	-17.41	7.70
O ₂	18.9	0.68	-15.50	17.3
N ₂	24.8	0.84	-21.13	19.6
H ₂	41.6	1.48	-36.23	46.1

Table 4.8: Percentage of pressure and temperature change due to impurities

Pipeline	Pressure drop (%)	Temperature drop (%)
Weyburn	4.48	2.95
Cortez	10.13	40.85
Canyon Reef	23.29	75.40
Sheep Mountain	5.44	15.16

4.3 Impact of single impurity at maximum allowed concentrations

Impurities with concentrations that are less than 0.1 % are inconsequential and are ignored. Though some impurities concentrations may be as low as 0.001 mol %, others could be as high as high as 10-mol %. The total concentration of impurities in CO₂ pipelines is rarely above 10 mol %. In this section, the maximum concentration of CH₄ is 4-mol %, but it could be much higher. For example, it is as high as 15 mol % in the Canyon Reef Carrier pipeline in the USA ([Patchigolla and Oakey 2013](#)).

4.3.1 Methodology

A chemical process simulator, Aspen HYSYS (V10) is used to simulate the parameters studied; z - factor, density, phase envelope, critical pressure, critical temperature, viscosity, temperature, and pressure. gPROMS was also used to simulate z – factor, density, viscosity, temperature, and pressure. Peng – Robinson (PR) EoS was utilised in both gPROMS and Aspen HYSYS to calculate thermodynamic properties of CO₂ mixture state, temperature, and pressure losses. Results obtained from both software were compared and analysed. CO₂ and single impurity fluids at maximum concentrations were simulated. Specification for the hypothetical pipeline is shown in Table 4.9. The inlet pressure is assumed to be 15 MPa and minimum pressure to be 9 MPa. If the pressure drops below the minimum, not in this simulation, recompression is

required. An inlet temperature of 33 °C is assumed to keep the fluid in supercritical state at the inlet. No minimum temperature is specified since the fluid will remain in the dense phase. All impurities are studied at their specified maximum concentrations and their effects on the fluid parameters at the same conditions as pure CO₂ are recorded. The impurities are graded according to the magnitude of their effect.

Table 4.9: CO₂ Pipeline specification for impurities at maximum concentration.

Pipeline length (m)	100,000
Inner diameter (m)	0.711
Outer diameter (m)	0.885
Mass Flow (kg/h)	2,200,600
Angle of elevation (°)	+0.287/0/-0.287
Pipe Wall Roughness (m)	4.57E-05
Pipe Wall conductivity (W/ (m K))	45
Inlet Pressure (MPa)	15
Inlet Temperature (°C)	33

4.3.2 Impact of impurities on density variation

Each impurity affects the fluid density according to its molecular mass. Expectedly, the heavier gases increased the density and the lighter gases reduced the density. The densities of pure CO₂ and binary fluids are shown in Figure 4.11. Due to its high concentration, 10 mol % N₂ resulted to the lowest density (650 kg/m³), against H₂ at equal concentrations. 6.5-mol % H₂O has the highest increase of density at 6.11 %. The density of the fluid was reduced by 10.71 % by 4-mol % H₂.

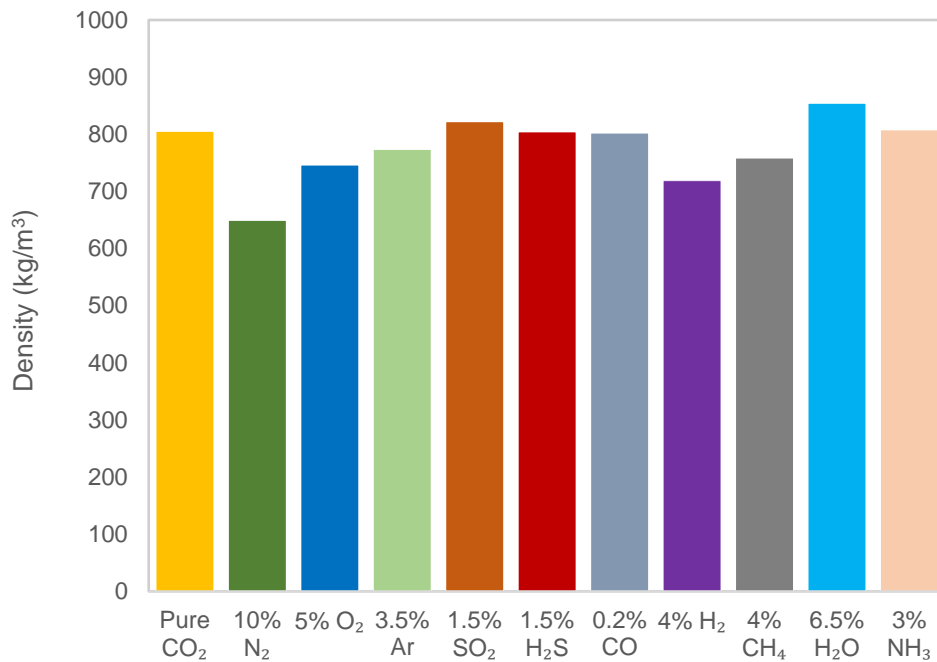


Figure 4.11: Densities of CO₂ binary mixtures.

4.3.3 Impact of impurities on critical pressure and temperature

To achieve supercritical state, the CO₂ fluid is compressed and the pipeline insulated to reduce the heat lost to the surrounding. Since it is expensive to compress and heat the fluid, lower critical pressures are desired because they require less compression work and consequently lower energy cost. All binary CO₂ fluids have higher critical pressure than pure CO₂ fluid. Since the critical pressure dictates the minimum pressure of the pipeline, a high critical pressure increases the operational cost of CO₂ pipelines. The highest critical pressure was due to 10-mol % N₂ and the lowest was due to 1.5-mol % H₂S. As seen above, at equal mol %, H₂S still has the lowest critical pressure but the highest critical pressure is due to H₂. Impurities resulting in higher critical pressures therefore increases the cost of fluid compression and transportation.

Increases in critical temperature were observed with only NH₃, SO₂, and H₂S. A low critical temperature favours supercritical flow since a wider temperature range is then within the supercritical region. High critical temperature decreases the

temperature range for supercritical fluid transportation. However, it was found that the lower transportation temperatures are more economical (see chapter 5). Fluids at subcritical state generally have higher densities than at supercritical state. Therefore, CO₂ fluids transported at subcritical state result to lower pressure losses than when transported at supercritical state. The lowest critical pressure resulted from 10-mol % N₂ while the highest critical temperature resulted from 3-mol % NH₃. It is noted that a high critical temperature may necessitate heating the pipeline fluid if supercritical state is specified. In this case, impurities resulting to lower critical temperature are beneficial as the need for heating to attain supercritical state may be eliminated. The critical temperature and pressure of the binary CO₂ fluids is shown in Table 4.10.

Table 4.10: Critical pressure and temperature of CO₂ fluids

Impurity	Pure CO ₂	4% CH ₄	10% N ₂	4% H ₂	5% O ₂	1.5% SO ₂	1.5% H ₂ S	0.2% CO	3% NH ₃	3.5% Ar
P _c (MPa)	7.37	7.99	8.82	7.86	7.40	7.56	7.38	7.60	7.57	7.71
T _c (°C)	30.9	27.8	23.6	28.5	30.8	34.0	31.2	28.0	34.3	28.8

4.3.4 Impact of impurities on viscosity

Viscosity of a gas is important in determining the friction factor while calculating pressure losses in CO₂ pipelines. The Reynold's number used in the determination of the friction factor is a function of fluid viscosity. Viscosity changes may be non-linear within the range of pressure and temperature of pipeline CO₂ transportation. Pressure, temperature, and composition strongly affect the viscosity of gases. Viscosity of CO₂ fluids show nonlinearity at supercritical temperatures, so [McCollum and Ogden \(2006\)](#) recommended the use of complex equations. At high densities, viscosity reduces with increase in temperature but at low densities it increases with increase in temperature

([Zabaloy et al. 2005](#)). At pressures between 10 MPa and 60 MPa, the viscosity of 0.56-mol % and 99.44-mol % CO₂ pentaerythritol tetra-2-ethylhexanoate (PEB3) decreased with increase in temperature ([Pensado et al. 2008](#)). Viscosity will therefore decrease with increase in temperature because the density of CO₂ is high, usually higher than 8 MPa at supercritical pressures. Figure 4.9 shows the actual viscosity values of the fluids.

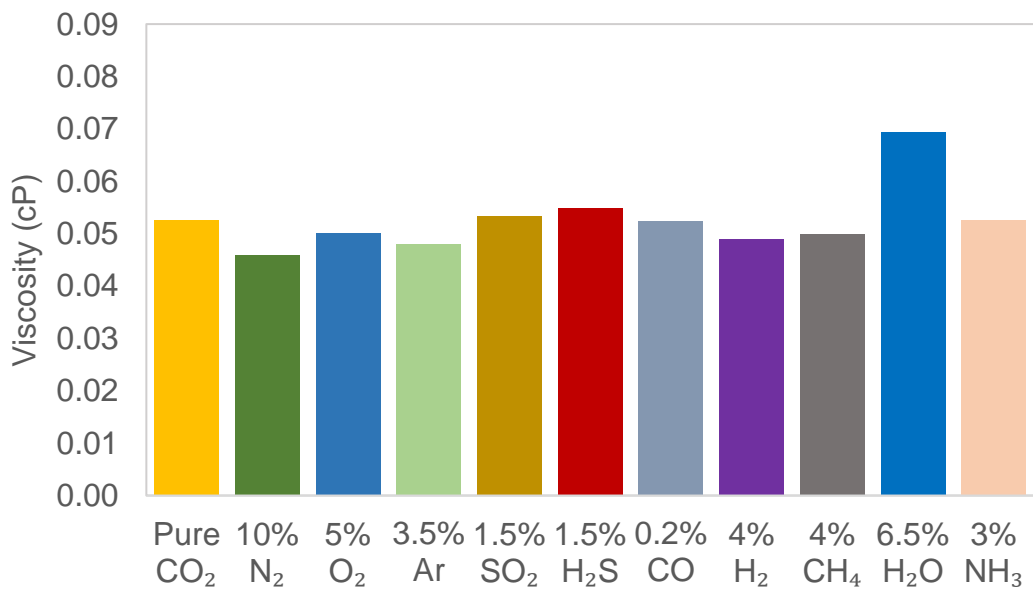


Figure 4.12: Viscosity of binary CO₂ fluids at 15MPa and 33 °C.

The highest viscosity value is due to 10-mol % N₂ and the lowest viscosity value is due to 6.5-mol % H₂O. An increase in viscosity increases the friction between subsequent layers of the flowing fluid and tends to increase pressure drop. H₂O, SO₂, and H₂S had negative impacts on viscosity though they resulted to less pressure losses due to other effects. Higher pressure losses are expected with higher viscous fluids if all other parameters are the same.

4.3.5 Impact of impurities on fluid pressure

The pressure decline in CO₂ fluids flowing in pipelines is dependent on viscosity, density ([Tan et al. 2015](#)) and velocity among others. In inclined pipelines, the

effect of density may become the major determinant factor in pressure changes. The elevation component of the pressure loss term may outweigh the effect of frictional pressure loss. For this reason, high-density fluids will result in higher pressure losses than low density fluids. The reverse is true in horizontal pipelines where lighter fluids result to high pressure losses at the same mass flow rate because of higher velocities. In declining pipelines, higher density fluids also result to higher pressure gains for the same reason of the elevation component. See Equation 3.59

$$\Delta P = \frac{f \rho l v^2}{2D} + \rho g \Delta z \quad (3.60)$$

In horizontal pipelines, gases heavier than CO₂ decreased the pressure losses while lighter gases increase the pressure losses. This is due to the increased velocity of the lighter gases. The effect due to the increased velocity outweighs the reduced density when squared (see Equation 3.59). Pressure loss during flow determines the distance fluids can be transported in pipelines before recompression. The cost of CO₂ pipelines increases when there are high pressure losses. Increase in capital cost to install more pressure boosting stations and increased operational cost in running the boosting stations. [Elahi et al. \(2014\)](#) gives a transportation cost model and [Kemp and Sola Kasim \(2010\)](#) gives a model for optimising cost of transportation in CO₂ pipelines. Analysis for obtaining minimum pipeline transportation cost is given in [Benson and Ogden \(2003\)](#). Where pipelines are expected to gain in pressure, they may be designed to minimize pressure increase. High fluid pressures may cause erosion of the pipeline inner wall, affect pipeline joints/seals, cause leakages, or even require pressure reducing stations to be installed.

At the permitted maximum concentrations, only H₂O and SO₂ impurities resulted to lower pressure losses than pure CO₂ in horizontal pipelines. Therefore, binary CO₂ fluids with H₂O and SO₂ impurities will be transported for longer pipeline distances than pure CO₂ before requiring recompression, thereby reducing transportation cost. The minimum pressure loss occurred with H₂O (1.54 MPa) and the maximum with N₂ (2.04 MPa). The difference between the maximum and minimum losses is 0.50 MPa.

Pressure losses are significantly affected by pipeline profile. The pressure drop in an inclined pipeline is higher than that in horizontal pipeline. This is due to the elevation component of the pressure loss equation. Though pressure losses in inclined pipelines are higher than horizontal pipelines, the effect of impurities is slightly reduced. The maximum decline of pressure at the studied inclination is 5.28 MPa, due to H₂O and the minimum is 4.86 MPa due to N₂. The difference between the maximum pressure loss and minimum pressure loss is 0.42 MPa. Impurities heavier than CO₂ also increased the pressure losses in the uphill pipeline.

In pipelines running downhill, the pressure increased in all cases studied. This increase is because the gain in pressure from the elevation component outweighed the frictional pressure loss. Pipelines with negative inclination angles showed reduced pressure gain/loss. However, the net effect due to the impurities increased. The difference between the maximum pressure gain was due to H₂O (2.30 MPa) and the minimum pressure gain due to N₂ (0.88 MPa) is 1.42 MPa.

Figure 4.13 shows the pressure changes of the CO₂ fluids in the three pipeline scenarios. Here, negative values (bars) indicate pressure increases. Pressure

increase is also not desired as pressure reducing stations may be required to control the pressure.

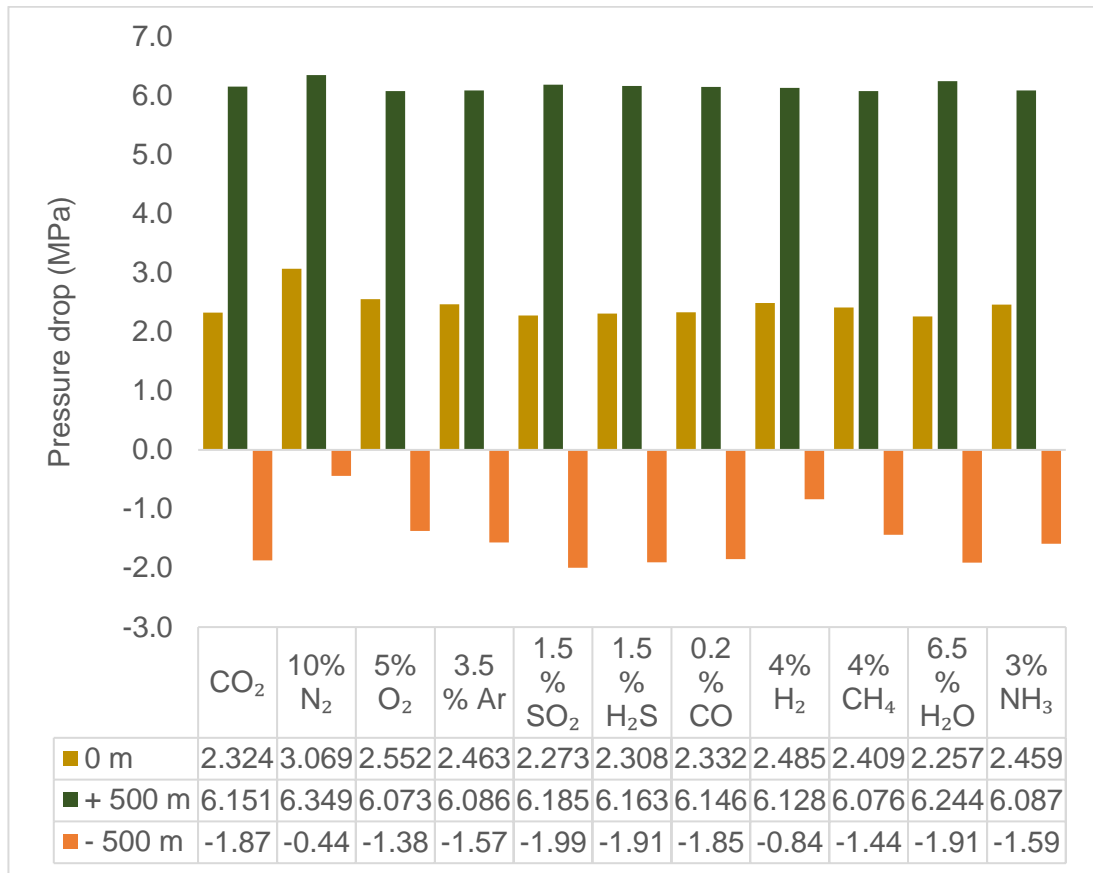


Figure 4.13: Pressure change of CO₂ binary fluids in horizontal, uphill and downhill pipeline

4.3.6 Impact of impurities on fluid temperature

As CO₂ flows in the pipeline, heat is transferred from the flowing fluid to the soil or surrounding. Heat transfer out of the pipeline is in three components, convective heat transfer between the fluid and the inner pipeline wall, the heat conduction from the inner pipeline wall to the outer pipeline wall and the heat emission to the surrounding (Na et al. 2012). Compressors can generate heat and increase the fluid temperature which is dissipated to the surrounding. Though, multistage compression for CO₂ fluids is usually combined with intercooling (Porter et al. 2016). If the fluid temperature is higher than the

surrounding temperature, the maximum and minimum flowing fluid temperatures occur immediately after exiting the compressor and just before entering the compressor. Flowing fluid temperature also affects the performance of CO₂ pipelines (see Chapter 5 below). There may be transfer of heat from the surrounding to the pipeline during depressurisation, as the CO₂ cools due to vaporisation and the Joule-Thompson effect ([de Koeijer et al. 2011](#)) or if the surrounding soil temperature is higher than the pipeline temperature. This (reverse) heat transfer usually occurs during start-up or shut down for a short time or during a leak. CO₂ pipelines are therefore first pressured with N₂ during start-up to avoid the cooling effect of expanding CO₂.

The temperature variations of the binary CO₂ fluids were studied. The temperature loss of each CO₂ fluid flowing in a horizontal pipeline is shown in Figure 4.11. Lower flowing temperatures are desired because it results in less pressure loss and higher volumes transported due to increased density ([Zhang et al. 2006](#)). It may then be understood that impurities which increase heat loss have positive effects. To ensure adequate heat loss pipelines may not be insulated. The highest heat loss (4.03 °C) was due to 10-mol % N₂, and the minimum heat loss (1.60 °C) was due to 6.5-mol % H₂O. 1.5-mol % H₂S had a negligible effect on temperature.

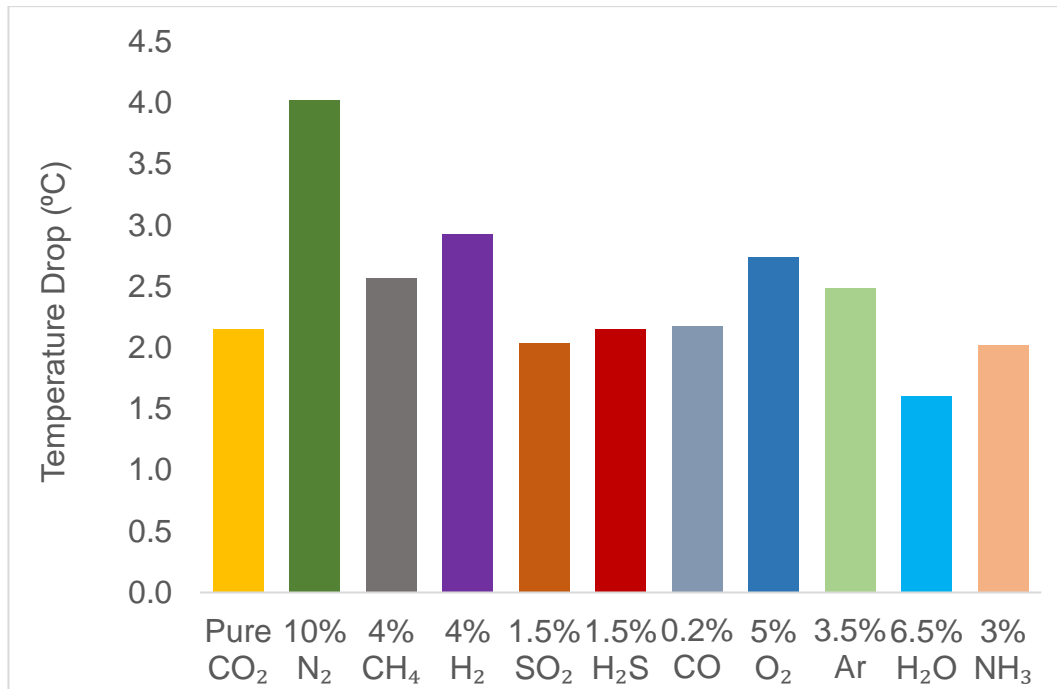


Figure 4.14: Temperature drop of binary mixtures.

4.3.7 Impact of impurities on phase envelope

Transporting CO₂ fluids above the critical pressure prevents the formation of the gaseous phase. The phase envelopes of the binary fluids are shown in Figure 4.15 where the bubble point curve is shown as a solid line and the dew point curve as a dashed line. The widest two – phase envelope was created by 4-mol % H₂ and the narrowest by 1.5-mol % H₂S. Impurities in the CO₂ fluid increase the likelihood of a two-phase forming as pressure and temperature decline in the pipeline. To indicate the effect of each impurity on the formation of a two – phase flow, the (dimensionless) area enclosed by the dew point and bubble point lines intersected by a vertical line drawn at 0 °C is given in Table 4.11.

Table 4.11: Dimensionless area of two-phase region of binary fluids at their maximum concentrations from 0 °C to critical temperature.

Impurity	CH ₄	SO ₂	H ₂ S	O ₂	H ₂	CO	NH ₃	N ₂	Ar
Dimensionless	18.0	12.4	2.3	31	26	2.4	6.5	60.0	22.0

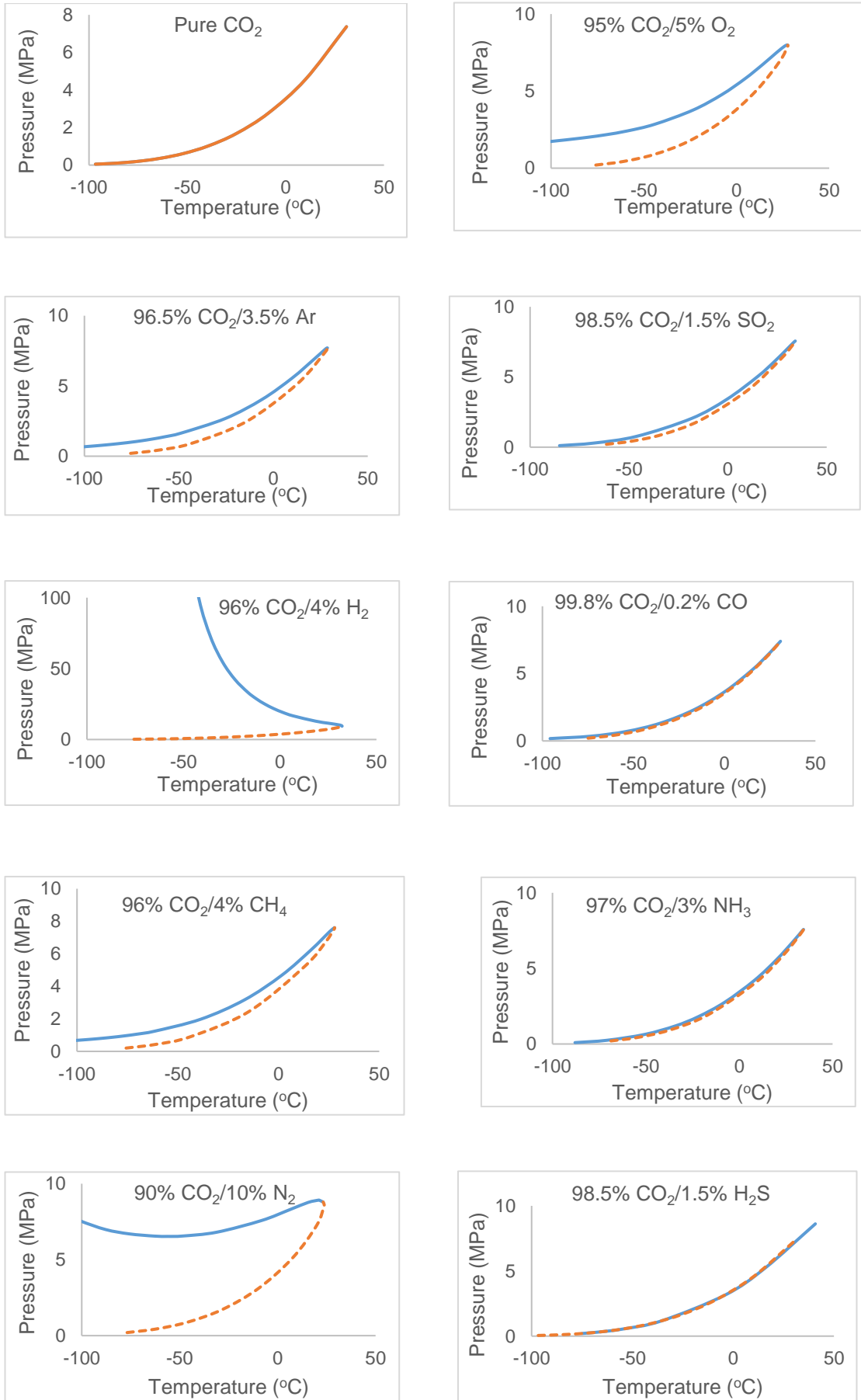


Figure 4.15: Phase envelope of binary CO₂ fluids.

4.3.8 Grading of impurities

Impurities take up some volume of CO₂ fluid thereby reducing the actual volume of CO₂ transported. However, some impurities, as stated above, seem to have some positive impact on the overall transportation process. Table 4.12 presents the percentage increase of each property due to each impurity.

Table 4.12: Percentage increase of fluid properties due to each impurity.

Param.	N ₂	CH ₄	Ar	SO ₂	H ₂ S	O ₂	H ₂	CO	NH ₃	H ₂ O
ΔP (%)	32.0	8.0	6.0	-2.2	-0.7	9.8	6.9	0.3	5.8	-2.9
ρ (%)	-19.4	-5.8	-3.9	2.1	-0.1	-7.3	-	-0.4	-0.3	6.1
P _c (%)	19.67	3.2	4.6	2.6	0.1	8.4	6.7	0.4	2.8	-
T _c (%)	-23.7	-9.6	-7.1	9.8	0.9	-10.1	-8.0	-0.44	10.7	-
P-T*	60.0	18.0	22.0	12.4	2.3	31.0	260	2.4	6.5	-
μ (%)	-12.9	-5.1	-8.8	1.3	4.4	-4.9	-6.9	-0.2	-0.1	-31.8
ΔT (%)	87.2	19.3	15.5	-5.1	-0.1	27.3	36.3	1.1	-5.9	-25.5

* P-T (Two – phase envelope) is in dimensionless area.

From Table 4.12 a list showing the relative impact of impurities on each property given in order of increasing negative effect is given below. Impurities at the beginning of the list may have positive impact on transportation.

- Pressure: H₂O, SO₂, H₂S, CO, NH₃, Ar, CH₄, O₂, H₂, N₂
- Heat loss: N₂, H₂, O₂, CH₄, Ar, CO, H₂S, SO₂, NH₃, H₂O
- Density: H₂O, SO₂, H₂S, NH₃, CO, Ar, CH₄, O₂, H₂, N₂
- Viscosity: H₂O, N₂, Ar, H₂, CH₄, O₂, CO, NH₃, SO₂, H₂S
- Phase envelope: H₂O, H₂S, CO, NH₃, SO₂, CH₄, Ar, O₂, N₂, H₂
- Critical pressure: H₂O, H₂S, CO, SO₂, NH₃, CH₄, Ar, H₂, O₂, N₂
- Critical temperature: H₂O, NH₃, SO₂, H₂S, CO, Ar, H₂, CH₄, O₂, N₂

All impurities increased the critical pressure with N_2 having the most increase at more than 19.6 % while H_2S increased it by just 0.11 %. Since higher critical pressure also requires higher minimum pressure, N_2 had the highest negative impact and H_2S has the least negative impact. No impurity has positive impact on critical pressure.

Impurities that reduce pressure decline have positive effects on transportation. These impurities will enable the fluid to be transported for longer distances when compared to pure CO_2 . In terms of pressure loss, H_2O and SO_2 have positive impact. No actual CO_2 pipeline has up to 6.5 mol % water concentration, and it should be noted that free H_2O causes corrosion and is therefore undesirable. All pipelines running downslope gained in pressure. A pressure increase is also undesirable because high pressures may affect pipeline joints/seals and cause leakages.

4.4 Chapter conclusion

The impact of impurities at equal concentrations and at the maximum specified concentrations were studied. Impacts on density, critical pressure, P – T diagram, temperature and pressure have been considered in this chapter. At equal concentrations, it was found that H_2 has the worst impact while H_2S has the mildest impact. All impurities studied increased the critical pressure of the fluid. The critical pressure of the Weyburn pipeline was however, less than that of pure CO_2 . This low value can be attributed to the presence of C_{2+} components, which are not significant impurities in CCS fluid streams. Some impurities have positive impact on the flowing streams, so both positive and negative impacts and the percentage change from pure CO_2 were considered. It is recognised that CO_2 pipeline fluids usually have multiple impurities and binary fluids are considered

only for the purpose of comparing the impact of each impurity. The grading for pressure changes is done only for horizontal pipelines because the impact of impurities on pressure changes in the pipeline is a function of the impurity, the concentration, and the angle of inclination of the pipeline. It becomes difficult to grade the impact of the impurities when non – horizontal pipelines are considered. Impurities that cause high pressure losses in horizontal pipelines may result to lower pressure losses in inclined pipelines and less pressure gain in pipelines with a negative inclination angle. Generally, the effect of impurities on pressure is reduced in pipelines with positive inclination angles and increased in pipelines with negative inclination angles.

Chapter 5: CO₂ Pipeline Transportation: Supercritical or Subcritical Flow

5.1 Introduction

Captured CO₂ from industrial processes is mostly transported in pipelines in the dense phase (sub-cooled liquid or supercritical fluid) ([Teh et al. 2015](#)). CO₂ could also be transported in the gaseous phase but this is uneconomical due to the high pressure losses and low density ([Zhang et al. 2006](#)). According to [Knoope et al. \(2013a\)](#), gaseous phase transportation is economical at low flow rates, low pressures and short distances. The definition of CO₂ pipeline fluid in [Forbes et al. \(2008\)](#) suggests that the fluid phase must be supercritical. [Leung et al. \(2014\)](#) recognized supercritical state as the preferred state in CO₂ pipeline transportation. The need or otherwise for this preference is investigated in this chapter by comparing the two modes of transportation by analyzing oxy–fuel, pre–combustion and post combustion fluids at four different temperatures.

5.2 Methodology and modelling

Pressures and temperatures maintained above 7.3 MPa and 31.1 °C keep pure CO₂ in supercritical state. But pressure and temperature decline along the pipeline during transportation and the flowing fluid may enter the gas phase if the pressure falls below the critical value. Two-phase (liquid and gas) flow may also result if the fluid contains impurities (as in most pipelines) and gaseous and liquid phases co-exist in the pipeline.

The Peng Robinson EoS was used in Aspen HYSYS (V10), in steady state mode on a 50 km insulated hypothetical pipeline with a mass flow rate of 1,080,000 kg/hr. Typical fluids from the three major capture methods (oxy–fuel, pre–combustion and post–combustion) are used in this analysis. The transportation of the fluids from the three capture methods are separately simulated. Table 5.1

shows the specification of the pipeline used in the analysis. The phase envelopes of the fluids are shown in Figure 5.1. In Figure 5.1, the (red) rectangle encloses the range of pressure and temperature considered in this study.

Four pressure and temperature points are selected for this analysis. Two points each for supercritical and subcritical phases. First, the critical pressure and temperature are determined for the three fluids. This is to ensure that two of the temperature points selected for the fluids are above the critical value and two below the critical value for all three fluids. The composition of the fluids is shown in Table 5.2. The maximum (inlet) pressure for the analysis is 17 MPa. The selected temperatures are 40 °C and 33 °C (for supercritical) and 26 °C and 19 °C (for subcritical). Only horizontal pipelines are considered, and the ambient temperature is assumed to be 10 °C. To ensure that the fluid remains in the dense phase, the minimum pressure is specified at 10.0 MPa, which is higher than the highest critical pressure (that of oxyfuel).

Table 5.1: Pipeline specification

Parameter	Value
Internal diameter (m)	0.4556
Outer diameter (m)	0.5080
Material	Mild steel
Roughness (m)	0.0000457
Length (m)	50,000
Elevation (m)	0
Pipe wall conductivity (W/m.K)	45
Insulation - Urethane Foam (m)	0.10

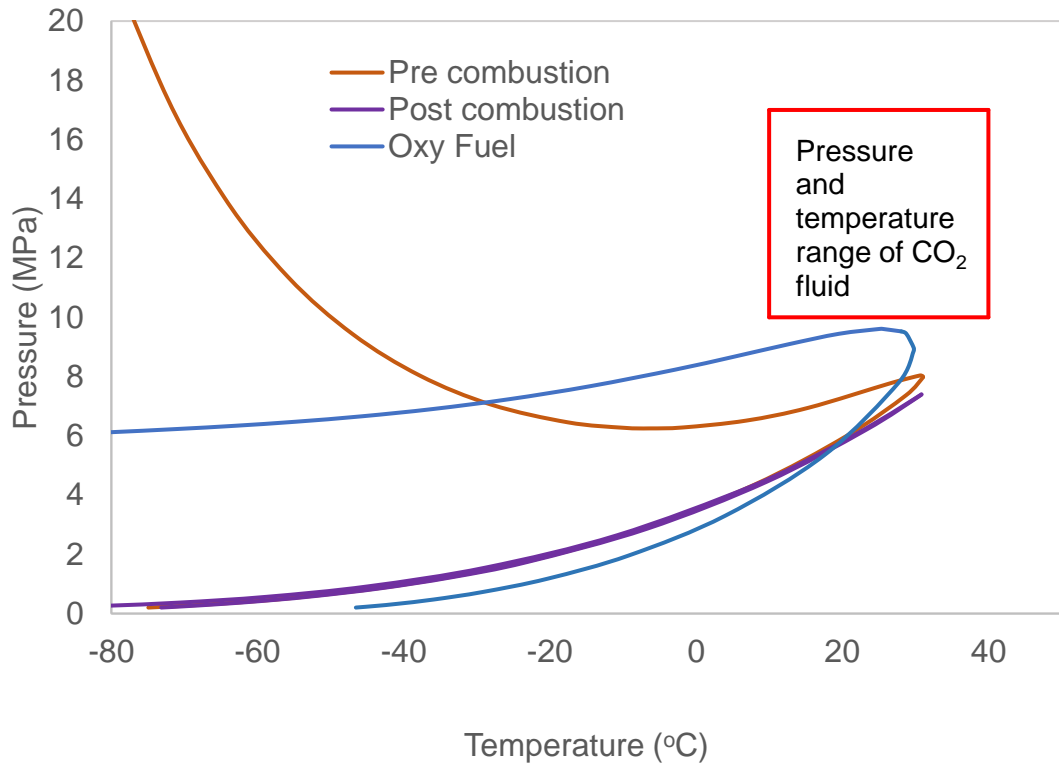


Figure 5.1: Phase envelopes of CO₂ capture fluids.

Table 5.2: Concentration of Impurities for the capture methods ([Antonie Oosterkamp 2008](#); [Seevam et al. 2008](#)).

Component	Oxyfuel	Pre-combustion	Post combustion
CO ₂	85.00	96.05	99.78
N ₂	6.00	0.05	0.17
CH ₄	-	0.03	0.01
H ₂ S	-	2.00	-
H ₂	-	1.70	-
Ar	4.00	0.04	-
O ₂	2.23	-	0.01
CO	0.07	0.03	-
C ₂₊	-	-	0.01
NO ₂	0.24	-	0.01
SO ₂	2.45	0.05	-
H ₂ O	0.01	0.05	0.01
Total	100.00	100.00	100.00

5.3 Results and discussion

The results for critical pressure, density, pressure loss, temperature change, volume of fluid transported, relative distance transported, and viscosity are presented below.

5.3.1 CO₂ critical pressure

The critical pressure and temperature of the three fluids are shown in Figure 5.2. Oxy – fuel has the highest critical pressure but the lowest critical temperature. At all inlet temperature, the fluid with the highest critical pressure had the highest pressure drop. Post combustion fluid with the lowest critical pressure had the lowest pressure loss. It can be found from this that fluids with higher critical pressure also result to higher pressure losses. Therefore, impurities that increase the critical pressure not only increase the cost of compression to attain supercritical state but may also increase the number of pressure boosting stations. The effect of critical temperature on pressure drop cannot be inferred because post combustion and oxy - fuel fluids with lower critical temperatures than pre – combustion fluid had lower and higher pressure drop, respectively.

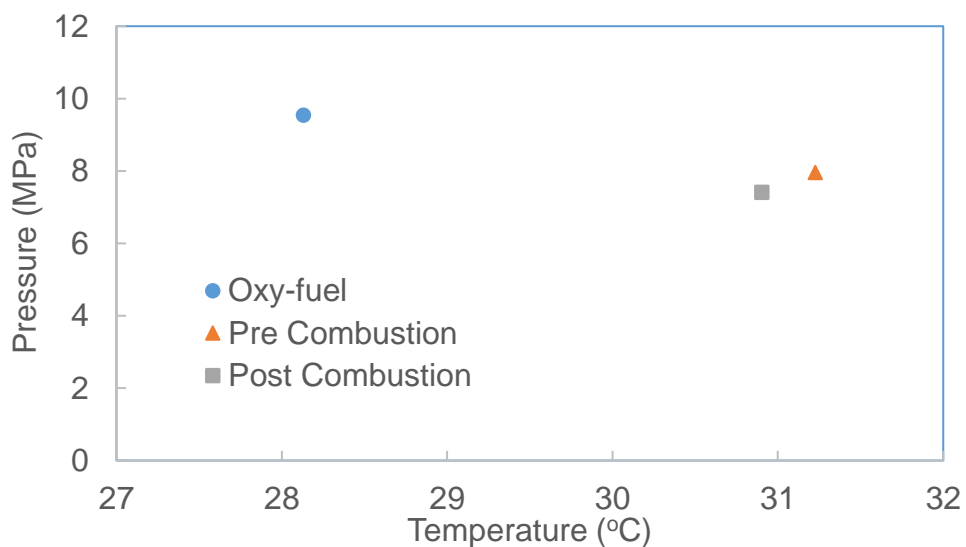


Figure 5.2: Critical points of typical CO₂ capture fluids.

5.3.2 CO₂ fluid density

The density at the inlet of the pipeline increased as the inlet temperature was reduced. A total increase of 163.48 kg/m³ or 24.50 % (for oxy-fuel), 134.88 kg/m³ or 18.02 % (for pre-combustion) and 135.79 kg/m³ or 17.38 % (for post-combustion fluid) at the minimum temperature of 19 °C. This increase in density could be explained as an increase in volume transported. Increased density implies smaller volume and may reduce the size of the pipeline used ([Li and Yan 2009](#)). It should be noted that there is no actual increase in volume transported because the flow rate is held constant. The supposed increase in volume transported shows as reduced pressure drop and slower velocity. However, if the flow rate is not kept constant, the indicated percentage increase in volume (shown as flowrate) can be transported at the lower temperatures, see Table 5.3. A flowrate of 1,116,576 kg/hr at 33 °C or 1,141,880kg/hr at 27 °C or 1,173,930 kg/hr at 19 °C will result in the same pressure loss as 1,080,000 kg/hr at 40 °C for post – combustion fluid in the pipeline.

Table 5.3: Percentage increase of mass flow for lower temperatures.

Fluid	33 °C (supercritical)	26 °C (liquid)	19 °C (liquid)
Oxy-fuel	3.31 %	5.92 %	8.85 %
Pre combustion	3.90 %	6.68 %	8.93 %
Post combustion	3.39 %	5.73 %	8.70 %

5.3.3 CO₂ pipeline flowing pressures

As stated earlier, pressure losses are lower at lower temperatures. For the oxy-fuel fluid, the pressure loss was 3.48 MPa at 40 °C, 3.18 MPa at 33 °C, 2.94 MPa at 26 °C and 2.76 MPa at 19 °C. The other two fluids show the same trend of lower pressure losses at the lower inlet temperatures. This means that the fluids

will flow for longer distances before requiring recompression. See Figure 5.3 for the pressure profile for the four temperature values of the oxy-fuel fluid. The lines are extrapolated to show the transportation distance for each inlet temperature to reach the minimum pipeline pressure of 10 MPa. The fluid will be transported for 100.9 km at 40 °C, 110.2 km at 33 °C, 119.0 km at 26 °C and 126.9 km at 19 °C in the specified pipeline for the pressure to decline to 10 MPa. Table 5.4 shows the pressure losses of each fluid at all inlet temperatures. Table 5.5 presents the percentage increase in transportation distance for the reduced inlet temperature values.

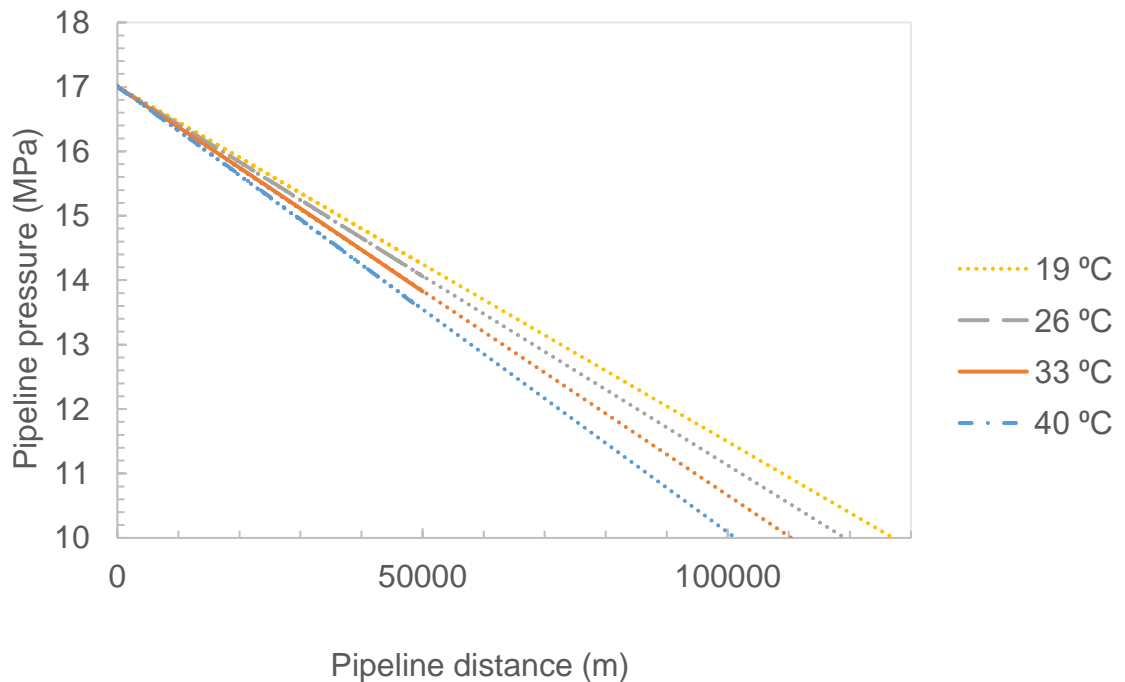


Figure 5.3: Oxy-fuel pipeline pressure profiles at indicated temperature.

Table 5.4: Pipeline pressure drop.

Fluid	40 °C (supercritical)	33 °C (supercritical)	26 °C (liquid)	19 °C (liquid)
Oxy-fuel	3.48	3.18	2.94	2.76
Pre combustion	3.07	2.86	2.72	2.58
Post combustion	2.93	2.74	2.62	2.49

Table 5.5: Percentage increase in fluid transport length for lower temperatures.

Fluid	33 °C (supercritical)	26 °C (liquid)	19 °C (liquid)
Oxy-fuel	8.45 %	15.28 %	20.64 %
Pre combustion	6.94 %	11.41 %	15.79 %
Post combustion	6.53 %	10.57 %	15.20 %

5.3.4 Viscosity and temperature

The viscosity of the fluid increases with reduced temperature. However, this increase is too small to significantly affect the flow or raise pressure losses. Table 5.6 shows the viscosity of the fluids at the four temperatures. Heat is lost to the surrounding soil as the fluid flows along the pipeline. At lower temperatures, the heat loss is smaller because the temperature difference between the flowing fluid and the surrounding is reduced. Reduced heat loss keeps the temperature of the flowing fluid at a higher value and may cause higher pressure losses. However, the differences between the inlet temperatures of any two subsequent fluids (7 °C) is higher than the temperature change due to heat loss of any pipeline (see Table 5.7). Therefore, the effect of the heat loss on the performance of the pipeline cannot be understood in this study.

Table 5.6: Viscosity of fluids at the inlet.

Fluid	40 °C	33 °C (supercritical)	26 °C (liquid)	19 °C (liquid)
Oxy-fuel	0.0439	0.0457	0.0473	0.0599
Pre combustion	0.0501	0.0517	0.0648	0.0766
Post combustion	0.0523	0.0538	0.0678	0.0808

Table 5.7: Temperature drop along the pipeline

Fluid	40 °C	33 °C (supercritical)	26 °C (liquid)	19 °C (liquid)
Oxy-fuel	6.34	4.61	3.34	2.39
Pre combustion	4.05	2.96	2.18	1.55
Post combustion	3.55	2.61	1.92	1.35

5.3.5 Volume and velocity

Even though the volume of fluid transported is the same for all temperatures because the flow rate is fixed at 1,080,000 kg/hr, the velocity is different at the various temperatures. The fluid velocity reduces with decrease in temperature because the fluid contracts. This reduced velocity translates into less pressure loss at lower temperatures. Every pipeline has erosional velocity and the reduced velocity due to lower temperatures reduces the likelihood that the erosional velocity is attained. The erosional velocity is the bulk fluid velocity that can remove pipeline protective scales present in the inside of the pipeline ([Bai and Bai 2005](#)). The API formula for erosional velocity according to ([Sani et al. 2019](#)) is given in Equation 5.1. Table 5.8 shows the inlet velocities of the three fluids. The velocities of the three fluids are different because the densities are different. The velocity/pressure - drop ratio is a constant for any flowrate and pipe diameter. For example, the initial velocity/pressure - drop ratio for this pipeline is 0.8. The linear relationship between pressure drop and velocity of a fluid flowing at a rate of 1,080,000 kg/hr in a 0.4556m pipeline for three different pipeline lengths is given in Figure 5.4. The ratio increases with decrease in pipeline length. In other words, the ratio of pressure – drop versus initial velocity increases with increase in pipeline length. This ratio is independent of fluid inlet temperature.

$$u_e = \frac{c}{\sqrt{\rho_m}} \quad (5.1)$$

where u_e is the erosional velocity (m/s), ρ_m is the density of the fluid and c is API RP factors. $c = 100$ for solid free continuous flow and $c = 125$ for intermittent flow.

Table 5.8 Pipeline inlet velocity at different inlet temperatures

Fluid	40 °C (supercritical)	33 °C (supercritical)	26 °C (liquid)	19 °C (liquid)
Oxy – fuel	2.76	2.54	2.36	2.21
Pre – combustion	2.46	2.30	2.17	2.08
Post – combustion	2.35	2.21	2.12	2.01

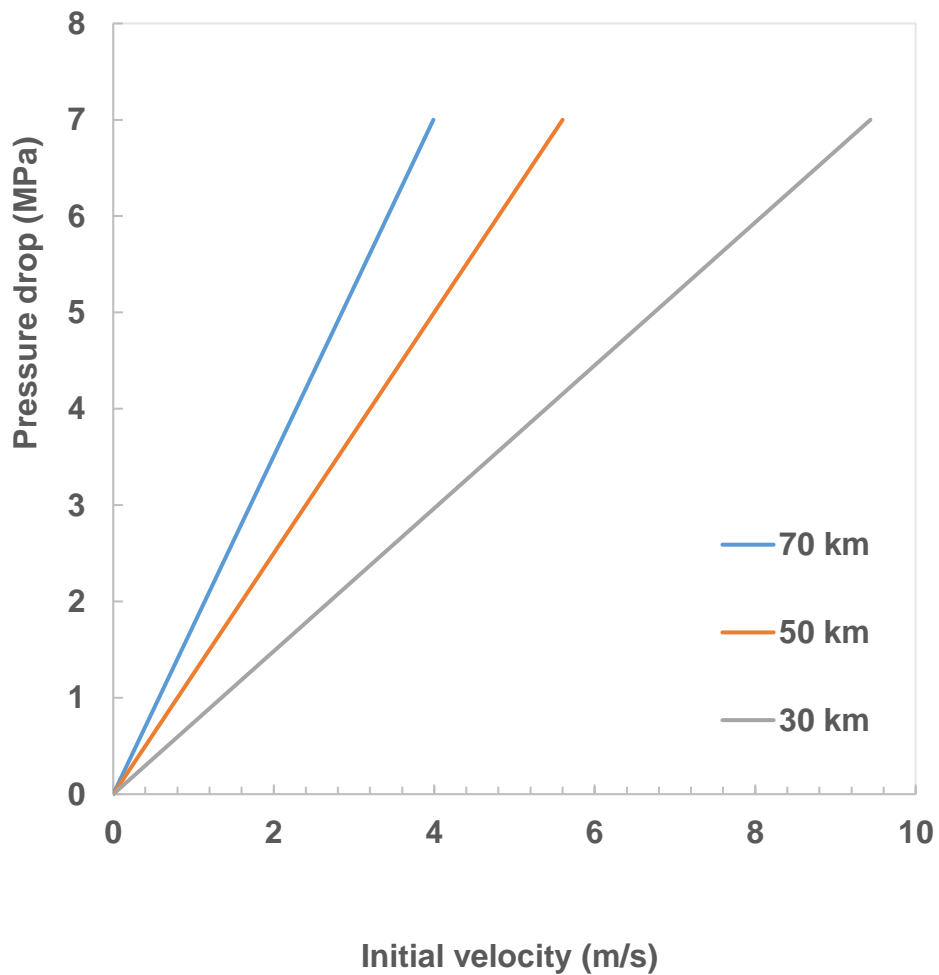


Figure 5.4: Plot of pressure - drop versus velocity.

5.4 Chapter conclusion

Fluids from the major capture methods, oxy – fuel, pre – combustion and post – combustion, were analyzed to see the effect of transporting CO₂ fluids in pipelines at the same inlet pressure while varying the temperature. The results show that lowering the temperature improved the performance of the pipeline. The density of the fluid increased when the temperature is reduced, making it possible to transport higher volumes of fluid. The velocity also reduced with decreasing temperature. The reduced velocity is beneficial in terms of erosional velocity and lower pressure loss. Fluids flow for longer distances at lower temperatures thereby reducing the number of pressure boosting stations and the cost of running them. Subcritical fluids performed better than supercritical fluids in all parameters examined. It is therefore more economical to transport CO₂ as an uncooled liquid than as a supercritical fluid. [Teh et al. \(2015\)](#) after analyzing the effect of ambient temperature on liquid CO₂ pipeline also concluded that transporting liquid CO₂ is better than transporting supercritical CO₂. The preference for transporting supercritical fluid over subcritical fluid in CO₂ pipelines is not justified because subcritical CO₂ flow is more economical.

Chapter 6: Modelling of effects of impurities

6.1 Introduction

This chapter presents the impact of each impurity on the properties of CO₂ fluids flowing in pipelines. The properties considered include gas compressibility factor (z – factor), density, viscosity, temperature, and pressure. Several equations of state are used in the computation of the z – factor. The most accurate equation is selected and used in the analysis of other parameters. Researchers have evaluated several EoS for CO₂ mixtures but a clear advantage of one over the rest has not been established. The EoS considered in the gPROMS simulation include Peng – Robinson (PR), Peng – Robinson Stryjek Vera (PRSV), Patel – Tega PT), Redlich – Kwong RK), and Soave Redlich – Kwong SRK). However, in the Aspen HYSYS simulation, only PR, SRK and PRSV are considered because the others have not yet been included in the software. A 20km hypothetical pipeline with internal diameter of 0.500 m and external diameter of 0.550 m is selected for the analysis. The fluid flowrate is 500 kg/s and the inlet temperature and pressure are 33 °C and 15 MPa, respectively. Table 6.1 shows the composition of each binary fluid.

Table 6.1: Binary fluid composition.

<i>Fluid</i>	<i>CO₂ mol %</i>	<i>Impurity mol %</i>	<i>Fluid</i>	<i>CO₂ mol %</i>	<i>Impurity mol %</i>
<i>Pure CO₂</i>	<i>100</i>	<i>0</i>	<i>CO₂/Ar</i>	<i>95</i>	<i>5</i>
<i>CO₂/CH₄</i>	<i>95</i>	<i>5</i>	<i>CO₂/H₂</i>	<i>95</i>	<i>5</i>
<i>CO₂/N₂</i>	<i>95</i>	<i>5</i>	<i>CO₂/NH₃</i>	<i>95</i>	<i>5</i>
<i>CO₂/H₂S</i>	<i>95</i>	<i>5</i>	<i>CO₂/SO₂</i>	<i>95</i>	<i>5</i>
<i>CO₂/O₂</i>	<i>95</i>	<i>5</i>	<i>CO₂/H₂O</i>	<i>95</i>	<i>5</i>
<i>CO₂/CO</i>	<i>95</i>	<i>5</i>			

6.2 Z factor of CO₂ pipeline fluids

Z – factor is used in the computation of density. The use of binary interaction parameters has minimal effect on the values obtained. Though binary interaction parameters are volume, composition and temperature independent and therefore taken as constants ([Li and Yan 2009](#)), they differ for different EoS. The z – factor values obtained from the various equations are shown in Table 6.2. The maximum change for the z – factor from that of pure CO₂ in the gPROMS simulation using the PR EoS occurs with H₂ (-0.0524) and the minimum with H₂S (0.0089). The minimum change of z – factor with Aspen HYSYS is zero. 5 mol % H₂S impurity and pure CO₂ is the same.

Table 6.2: z - factors for different EoS.

Fluid	gPROMS					Aspen HYSYS		
	RK	SRK	PR	PRSV	PT	PR	PRSV	SRK
CO ₂	0.3513	0.3556	0.3220	0.3221	0.2811	0.3221	0.3218	0.3577
CO ₂ /CH ₄	0.3638	0.3724	0.3415	0.3384	0.3218	0.3423	0.3421	0.3778
CO ₂ /N ₂	0.3696	0.3828	0.3529	0.3475	0.3475	0.3492	0.3487	0.3853
CO ₂ /H ₂ S	0.3437	0.3472	0.3131	0.3186	0.2514	0.3221	0.3494	0.3548
CO ₂ /O ₂	0.3653	0.3717	0.3443	0.3442	0.3442	0.3428	0.3423	0.3783
CO ₂ /CO	0.3691	0.3737	0.3523	-	0.3478	0.3495	0.3521	0.3897
CO ₂ /Ar	0.3658	0.3720	0.3452	0.3446	0.3449	0.3401	0.3396	0.3759
CO ₂ /H ₂	0.3760	0.3874	0.3744	0.3636	0.3768	0.3548	0.3708	0.3959
CO ₂ /NH ₃	0.3374	0.3423	0.3079	0.3079	0.2487	0.3119	0.3349	0.3425
CO ₂ /SO ₂	0.3416	0.3445	0.3077	0.3116	0.2424	0.3127	0.3228	0.3379
CO ₂ /H ₂ O	0.3043	0.3213	0.2858	0.2855	0.1940	-	-	-

The z – factors for the binary fluids using the PR EoS are plotted in Figure 6.1 from 1 mol% to 5 mol% impurity concentration. The change in value from pure CO₂ is used as a benchmark to compute the equations for the effect of the impurities on the z – factor. Impurities that decreased the gas deviation factor are SO₂, NH₃, and H₂S. The lowest z – factor occurred with SO₂. CH₄, N₂, O₂, CO

and Ar increase the z – factor. The maximum and minimum change in z – factor occurred with H₂, and H₂S, respectively. The z – factor for binary CO₂ fluids at 15 MPa and 33 °C can be approximated with Equations 6.1 to 6.9.

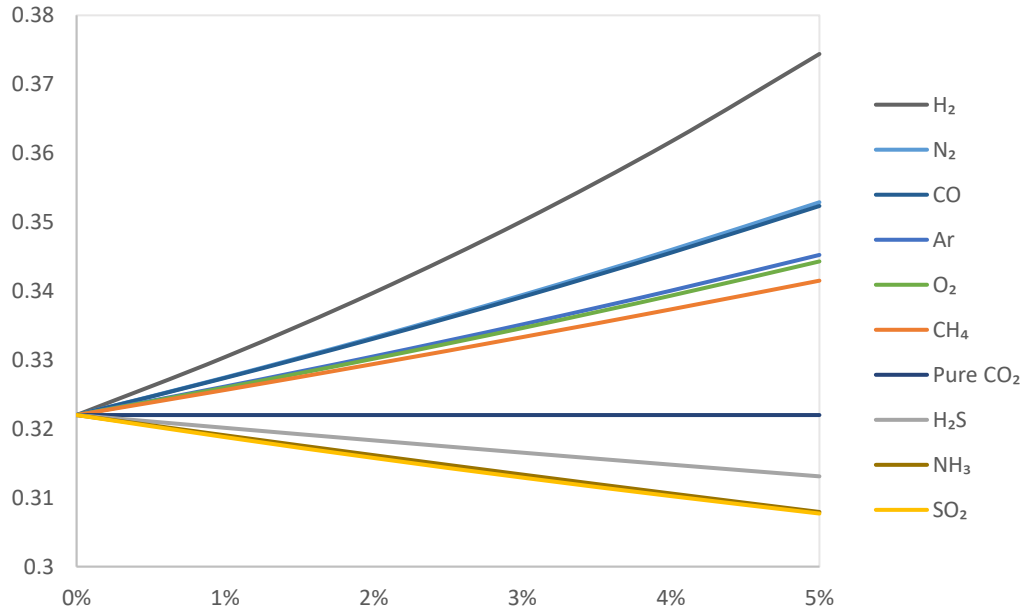


Figure 6.1: Gas deviation factors at 15 MPa and 33 °C (PR EoS).

$$\text{N}_2 \quad z = z_{\text{CO}_2} + 0.6172 \text{N}_2\% \quad (6.1)$$

$$\text{CH}_4, \quad z = z_{\text{CO}_2} + 0.3899 \text{CH}_4\% \quad (6.2)$$

$$\text{H}_2\text{S}, \quad z = z_{\text{CO}_2} - 0.1779 \text{H}_2\text{S}\% \quad (6.3)$$

$$\text{SO}_2, \quad z = z_{\text{CO}_2} - 0.2856 \text{SO}_2\% \quad (6.4)$$

$$\text{Ar}, \quad z = z_{\text{CO}_2} + 0.4644 \text{Ar}\% \quad (6.5)$$

$$\text{O}_2, \quad z = z_{\text{CO}_2} + 0.4455 \text{O}_2\% \quad (6.6)$$

$$\text{CO}, \quad z = z_{\text{CO}_2} + 0.6063 \text{CO}\% \quad (6.7)$$

$$\text{H}_2, \quad z = z_{\text{CO}_2} + 1.0459 \text{H}_2\% \quad (6.8)$$

$$\text{NH}_3, \quad z = z_{\text{CO}_2} - 0.2813 \text{NH}_3\% \quad (6.9)$$

The z – factor of an impure CO₂ mixture can be approximated with Equation 6.10, after determining the z – factor of a pure CO₂ fluid at the same pressure and temperature.

$$\begin{aligned}
 z_{mix} = & z_{CO_2} + 0.6172 N_2\% + 0.3899 CH_4\% - 0.1779 H_2S\% \\
 & - 0.2856 SO_2\% + 0.4644 Ar\% + 0.4455 O_2\% + 0.6063 CO\% \\
 & + 1.0459 H_2\% - 0.2813 NH_3\% - 0.7236 H_2O\% \quad (6.10)
 \end{aligned}$$

where z is gas deviation factor, z_{CO_2} is pure CO₂ gas deviation factor at specific pressure and temperature, and (N₂, CH₄, SO₂, H₂S, Ar, O₂, CO, H₂, NH₃) % is the concentration in mol% of the impurity.

Table 6.3 shows the z – factor values for binary CO₂ fluids and some pipelines, simulated with Aspen HYSYS and calculated with Equation 6.10. The maximum percentage difference occurs with H₂ at 5.54 % and the minimum with CH₄ at 0.20 %. The highest percentage difference for pipelines is 4.83 %.

Table 6.3: z – factors with Aspen HYSYS and gPROMS.

Fluid	Aspen HYSYS	Equation 6.10	% difference
CO ₂ /N ₂	0.3492	0.3530	1.09
CO ₂ /CH ₄	0.3423	0.3416	0.20
CO ₂ /H ₂ S	0.3221	0.3132	2.74
CO ₂ /O ₂	0.3428	0.3444	0.46
CO ₂ /SO ₂	0.3127	0.3079	1.55
CO ₂ /CO	0.3495	0.3524	0.84
CO ₂ /H ₂	0.3548	0.3744	5.54
CO ₂ /Ar	0.3401	0.3446	1.31
CO ₂ /NH ₃	0.3119	0.3081	1.23
Sheep Mountain pipeline	0.2768	0.2634	4.83
Canyon Reef pipeline	0.3524	0.3652	3.64
Cortez pipeline	0.3461	0.3490	0.85

6.3 Density of CO₂ pipeline fluids

Fluid pressure and temperature reduce along the pipeline and affect the density of the fluid. If the effect due to decrease in temperature outweighs the effect due to decrease in pressure, the density increases but if the reverse happens, the density decreases. CO₂ fluid density increased because the effect due to a reduced temperature was higher than that due to reduced pressure in the pipeline considered in [Nimtz et al. \(2010\)](#), which also resulted to a reduced flow velocity. Fluid density is also useful in calculating fluid volumes transported in pipelines. Abrupt changes in density during flow may cause fluid phase changes and booster stations may need to be installed to prevent this from happening. Density changes may be large for small changes in pressure and temperature close to the critical point. Accuracy of calculated density values also depend on the accuracy of the gas compressibility factor.

Equations of state used in the computation of z – factors are critical. In the analysis of [Wilhelmsen et al. \(2012\)](#), the Peng-Robinson EoS had the lowest AAD for density of binary CO₂ gases at the liquid state among the EoS considered in the study. When results from EoS are compared to practical data, the PR EoS has comparable accuracy to more advanced EoS ([Luo et al. 2014a](#)). Table 6.3 shows the density values calculated with the z – factor values obtained with different EoS and Figure 6.2 shows the density of binary fluids with PR EoS. Equations 6.11 to 6.20 can be used to approximate density values for binary CO₂ fluids if the value for pure CO₂ is known at the pressure and temperature. These equations are generated with a maximum of 5 mol % impurity concentration and may not be valid for higher concentrations of impurities.

Table 6.4: Density values from different EoS.

	gPROMS				Aspen HYSYS		
	SRK	PR	PRSV	PT	SRK	PR	PRSV
Pure CO ₂	726.3	805.5	805.4	922.8	725.0	805.1	805.8
N ₂	659.7	721.6	725.0	732.8	660.9	729.2	730.2
CH ₄	668.6	735.3	738.7	780.4	664.7	733.6	733.9
H ₂ S	736.5	819.0	820.1	1019.9	722.7	796.2	733.9
SO ₂	771.5	862.0	857.7	1094.1	785.1	848.3	821.7
Ar	682.0	747.8	747.6	748.6	686.8	759.1	760.2
O ₂	677.4	743.0	742.5	743.3	676.3	746.1	747.2
CO	660.5	722.7	727.4	732.1	653.4	728.5	723.2
H ₂	609.5	659.7	668.4	655.5	623.8	696.1	666.1
NH ₃	732.3	816.4	821.2	1010.9	734.1	806.0	750.7
H ₂ O	783.8	880.8	919.9	1297.5	782.6	853.3	661.3

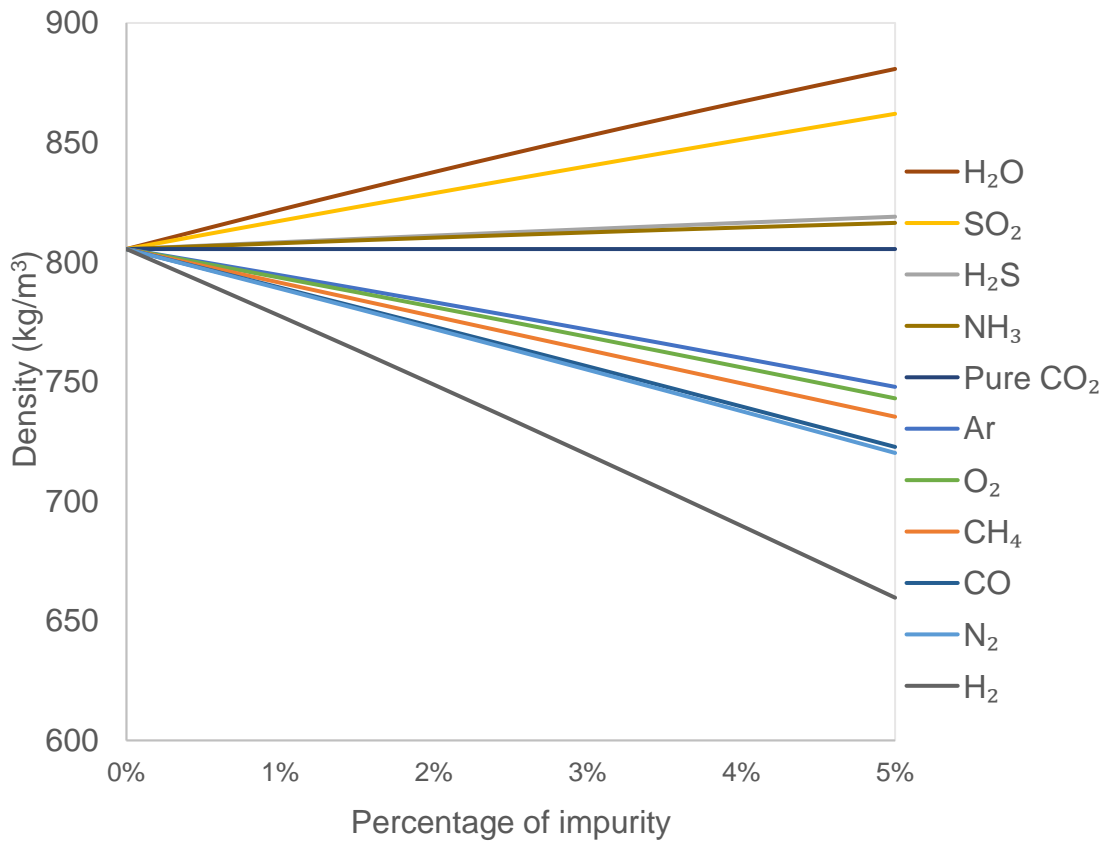


Figure 6.2 Density of binary mixtures

$$N_2 \quad \rho_{N_2} = \rho_{CO_2} - 1705.5 N_2\% \quad (6.11)$$

$$CH_4, \quad \rho_{CH_4} = \rho_{CO_2} - 1402.5 CH_4\% \quad (6.12)$$

$$H_2S, \quad \rho_{H_2S} = \rho_{CO_2} + 270.72 H_2S\% \quad (6.13)$$

$$SO_2, \quad \rho_{SO_2} = \rho_{CO_2} + 1131 SO_2\% \quad (6.14)$$

$$Ar, \quad \rho_{Ar} = \rho_{CO_2} - 1152.7 Ar\% \quad (6.15)$$

$$O_2, \quad \rho_{O_2} = \rho_{CO_2} - 1248 O_2\% \quad (6.16)$$

$$CO, \quad \rho_{CO} = \rho_{CO_2} - 1655.1 CO\% \quad (6.17)$$

$$H_2O, \quad \rho_{H_2O} = \rho_{CO_2} + 1505.9 H_2O\% \quad (6.18)$$

$$H_2, \quad \rho_{H_2} = \rho_{CO_2} - 2917.8 H_2\% \quad (6.19)$$

$$NH_3, \quad \rho_{NH_3} = \rho_{CO_2} + 218.86 NH_3\% \quad (6.20)$$

The density of a CO₂ fluid may be approximated with the following equation if the density for pure CO₂ fluid is known at the same pressure and temperature.

$$\begin{aligned} \rho_{mix} = & \rho_{CO_2} - 1705.5 N_2\% - 1402.5 CH_4\% + 270.72 H_2S\% + 1131 SO_2\% \\ & - 1152.7 Ar\% - 1248 O_2\% - 1655.1 CO\% - 2917.8 H_2\% \\ & + 218.86 NH_3\% + 1505.9 H_2O\% \end{aligned} \quad (6.21)$$

Pure CO₂ density values were simulated with Aspen HYSYS and impure CO₂ densities calculated with Equation 6.21. Table 6.5 presents the densities of impure CO₂ from Aspen HYSYS and Equation 6.21. The maximum and minimum percentage difference between the density value from Aspen HYSYS and that calculated with Equation 6.21 for the binary fluids occurs with H₂ (5.30 %) and

CH₄ (0.19 %). The density of Sheep Mountain pipeline fluid has the highest percentage difference (5.43 %).

Table 6.5: Density values from Aspen HYSYS and Equation 6.21.

Fluid	Aspen HYSYS	Equation 6.21	% difference
CO ₂ /N ₂	729.2	719.8	1.29
CO ₂ /CH ₄	733.6	735.0	0.19
CO ₂ /H ₂ S	796.1	810.5	1.80
CO ₂ /O ₂	746.1	742.7	0.46
CO ₂ /SO ₂	848.3	861.6	1.57
CO ₂ /CO	728.5	722.3	0.85
CO ₂ /H ₂	696.1	659.2	5.30
CO ₂ /Ar	759.1	747.5	1.53
CO ₂ /NH ₃	806.0	816.0	1.24
Sheep Mountain pipeline	596.3	628.6	5.43
Canyon Reef pipeline	766.9	745.6	2.78
Cortez pipeline	733.9	727.4	0.88

6.4 Viscosity of CO₂ pipeline fluids

The viscosity of CO₂ is non – linear at temperatures slightly above the critical point. At high densities, viscosity reduces with increase in temperature but at low densities, it increases with increase in temperature ([Zabaloy et al. 2005](#)). There are several equations for calculating the viscosity of gas mixtures. The [Ouyang \(2011\)](#) correlation (Equation 3.43), and the [Heidaryan et al. \(2011\)](#) correlation (Equation 2.29) are used to calculate the viscosity of pure components and the Arrhenius equation ([Yener et al. 1998](#)), Graham’s model (Equation 6.23), and Wilke’s equation (Equation 6.24) ([Davidson 1993](#)) are used to compute the viscosity of the binary CO₂ gas mixtures. Individual viscosities may be computed, and Equations 3.43, 6.22 and 6.23 used to calculate the mixture viscosity.

$$\mu_m = \mu_1^{x_1} \mu_2^{x_2} \quad (3.43)$$

$$\mu_1 = \sum_i \mu_i x_i \quad (6.22)$$

$$\mu_{mix} = \frac{\sum(\mu_i x_i \sqrt{M_i})}{\sum(x_i \sqrt{M_i})} \quad (6.23)$$

At reduced temperature and pressure, the viscosity for any two component gases is the same ([Chapoy et al. 2013](#)). The equation to calculate the viscosity of the impurity is given in Equations 6.24.

$$\mu_{imp} = \frac{\left(\frac{P_{c,imp}}{P_{c,CO_2}}\right)^{2/3} \left(\frac{M_{imp}}{M_{CO_2}}\right)^{1/2}}{\left(\frac{T_{c,imp}}{T_{CO_2}}\right)^{1/6}} \mu_{CO_2} \quad (6.24)$$

Table 6.6 shows viscosity values for CO₂/CH₄ and CO₂/Ar binary mixtures. Practical data is taken from ([Al-Siyabi 2013](#)). The viscosity of pure CO₂ was computed as the bench scale and Equation 6.24 used to calculate the viscosity of the impurity and both values combined with Equations 3.44, 6.22 and 6.23. Though the McCollum equation gave the lowest percentage deviations, it fails at various pressure and temperature combinations. This may be due to the positive and negative parameters used in the equation. Both the ([Heidaryan et al. 2011](#)) and ([Ouyang 2011](#)) equations predicted the viscosity slightly higher than the practical values. The ([Heidaryan et al. 2011](#)) correlation performed slightly better than the ([Ouyang 2011](#)) correlation and is selected. Equation 3.44 gave the lowest values which is closest to the practical data.

The values obtained from these equations vary widely from those obtained from Aspen HYSYS simulations (see Table 6.7). This means that Aspen HYSYS under-predicts the viscosity of CO₂ rich mixtures. From the gPROMS simulations, H₂ reduced the viscosity by about 11 % and H₂S, SO₂, and H₂O increased the viscosity by about 0.9 %. The lighter gases reduced the viscosity, but the heavier

gases increased the viscosity. The molecular weight of impurities has the same effect on both density and viscosity since lighter gases also reduce the density of gas mixtures.

Table 6.6: Percentage deviation of viscosity values calculated with various equations.

Imp.	Temp. and Press.	Eqn. used	Pract. data (cP)	McCollum et al.		Hei et al.		Ouyang	
				μ (cP)	% Dev.	μ (cP)	% Dev.	μ (cP)	% Dev.
CH ₄	27 °C 13.89 MPa	3.44		0.0743	4.6	0.0709	-0.14	0.072	1.5
		6.24	0.071	0.0750	5.6	0.0728	2.5	0.073	2.6
		6.25		0.0758	6.7	0.0736	3.7	0.074	3.7
	27 °C 18.93 MPa	3.44		0.074	-9.8	0.091	11.0	0.090	9.76
		6.24	0.082	0.075	-8.5	0.091	11.0	0.091	11.0
		6.25		0.075	-8.5	0.092	12.2	0.092	12.2
Ar	27 °C 13.89 MPa	3.44		0.077	5.4	0.078	6.8	0.079	8.2
		6.24	0.073	0.077	5.4	0.079	8.2	0.080	9.5
		6.25		0.077	5.4	0.079	8.2	0.080	9.5
Ar	21.1 °C 11.7 MPa	3.44		-	-	0.083	-8.8	0.118	29.6
		6.24	0.091	-	-	0.117	28.5	0.119	30.7
		6.25		-	-	0.117	28.5	0.119	30.7

Figure 6.3 shows a plot of CO₂ viscosity at various temperature and pressure values. The plot shows that CO₂ viscosity is a function of both pressure and temperature. It reduces with increase in temperature but increases with increase in pressure. Since CO₂ exist as a liquid below the critical temperature if the pressure is above the critical value, it means that liquid CO₂ has higher viscosity than supercritical CO₂, though pipeline transportation of liquid CO₂ result in lower pressure losses than supercritical CO₂; see Section 5.3.3.

Table 6.7: Viscosity of binary fluids at 15 MPa and 33 °C.

	Aspen			gPROMS	
	SRK	PR	PRSV	Ouyang	Hei et al.
Pure CO ₂	0.0491	0.0526	0.0526	0.0748	0.0736
N ₂	0.0462	0.0494	0.0494	0.0726	0.0714
CH ₄	0.0461	0.0492	0.0492	0.0721	0.0709
H ₂ S	0.0606	0.0647	0.0612	0.0754	0.0742
SO ₂	0.0624	0.0657	0.0644	0.0754	0.0742
Ar	0.0432	0.0462	0.0462	0.0740	0.0728
O ₂	0.0469	0.0500	0.0501	0.0737	0.0725
CO	0.0460	0.0495	0.0492	0.0726	0.0715
H ₂ O	0.0631	0.0678	0.0477	0.0754	0.0742
H ₂	0.0624	0.0480	0.0559	0.0666	0.0655
NH ₃	0.0515	0.0548	0.0523	0.0739	0.0727

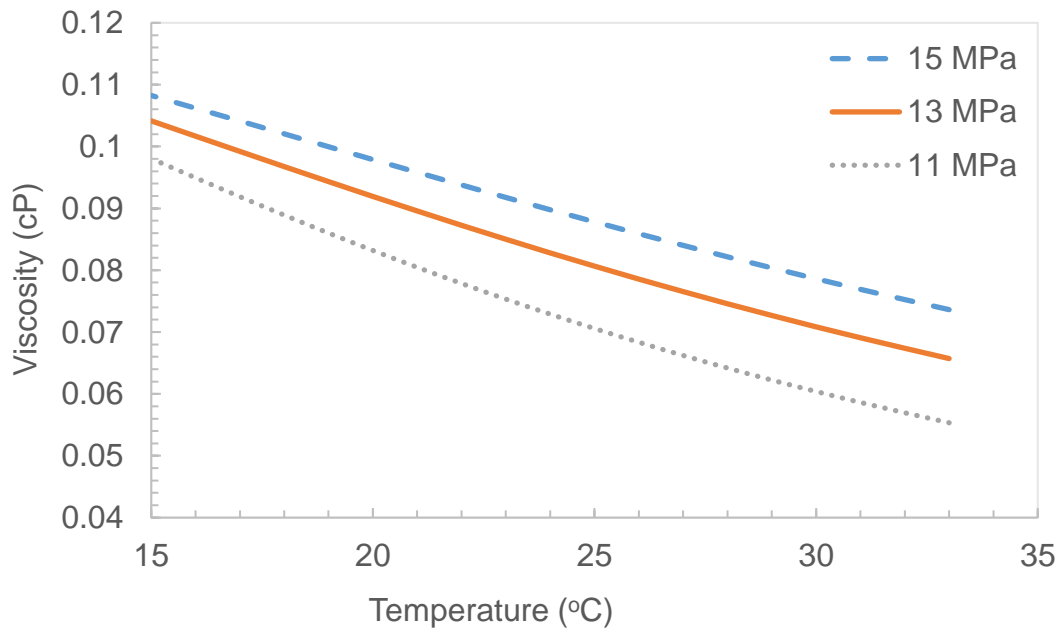


Figure 6.3: Pure CO₂ viscosity at different pressures and temperatures.

6.5 Temperature of CO₂ pipelines

Fluid temperature declines along the pipeline in the direction of flow if the surrounding temperature is lower than the fluid temperature. In situations where

the surrounding soil temperature is higher than the flowing fluid temperature, the heat transfer will be from the surrounding soil to the pipeline fluid. The temperature profile of fluids flowing in CO₂ pipelines is not fully understood. The fluid temperature of a buried pipeline does not reach the surrounding temperature. The temperature difference between the pipeline and the soil (ΔT) continually decreases, and over time, the fluid temperature does not change significantly from the pipeline inlet temperature. The total heat transferred out of the fluid is a function of the convective heat transfer from the fluid to the pipeline inner wall, the heat conducted from the inner pipeline wall to the outer wall, the heat conducted by the surrounding soil from the outer pipeline wall to the surface and finally the heat transferred away by the air currents from the soil surface. The slowest heat transfer medium is the soil. See Table 6.8 for the thermal resistance values for each medium. This slowest heat transfer component determines how fast heat is transferred away from the pipeline and is therefore the heat transfer rate determining step. The resistances to heat transfer is calculated for each step; fluid to pipeline (convection), pipeline to soil (conduction), soil to surface (conduction), and surface into the surrounding air (convection).

Table 6.8: Thermal resistance values for fluid, pipeline and soil.

Medium	Thermal resistance (K.m/W)	% of total
Fluid	0.07955	31.60
Pipeline	0.00035	0.14
Soil	0.17184	68.26
Total	0.25174	100.00

Figure 6.4 show the temperature profile of the first elemental fluid as it flows in the pipeline from the inlet to the outlet. At the start of fluid flow, the temperature of the soil surrounding the pipeline is assumed to be 7 °C. Here, only the heat

transfer from the pipeline to the soil is considered. Equations 6.26 to 6.28 (Kreith et al. 2012) are used to calculate the fluid and pipe thermal resistances and heat transfer rate. Equations 3.52 to 3.58 are used to calculate the overall heat transfer from the pipeline to the surface.

$$R_{fluid} = \frac{1}{2 \pi r_p h_{fluid}} \quad (6.26)$$

$$R_{pipe} = \frac{\ln(r_o/r_i)}{2 \pi k_{pipe}} \quad (6.27)$$

$$H_{rate} = \frac{\Delta T * L}{R_{fluid} + R_{pipe}} \quad (6.28)$$

where R_{fluid} is heat resistance of fluid (m K/W), R_{pipe} is the heat resistance of pipe (m K/W), h_{fluid} is fluid convection heat transfer coefficient (W/m² K), k_{pipe} is the thermal conductivity of pipe (W/m K), and ΔT is the difference between the fluid temperature and the soil temperature around the pipeline (K).

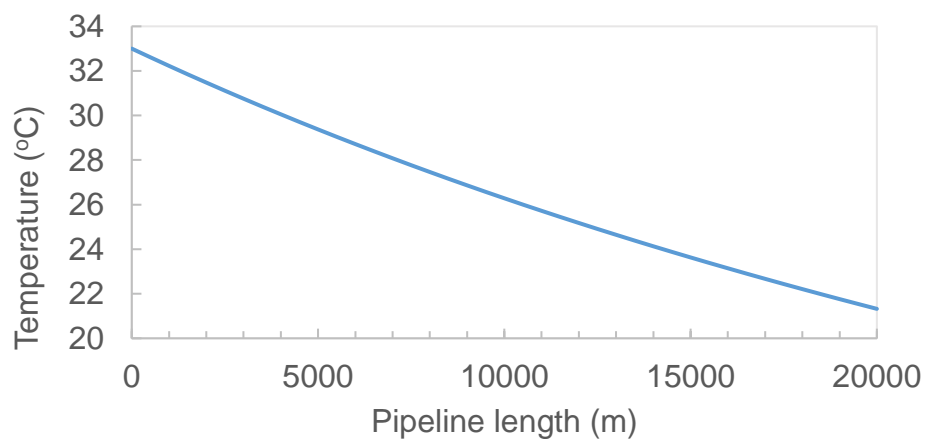


Figure 6.4: Pipeline temperature profile after first elemental flow.

The temperature outside the pipeline rises as the fluid flows in the pipeline. This means that the driving force for the heat transfer, i.e. the temperature difference, reduces. At extended time, the pipeline temperature will remain steady. Figure 6.5 shows the steady temperature profile of the pipeline. Table 6.9 shows the

outlet temperature for the various binary fluids. The effect of impurities on the temperature of the pipeline over extended time is negligible. This is because the fluid composition only affects the heat transfer from the fluid to the inner pipeline wall. The rest of the heat transfer process from the pipeline to the surface is independent of the fluid composition.

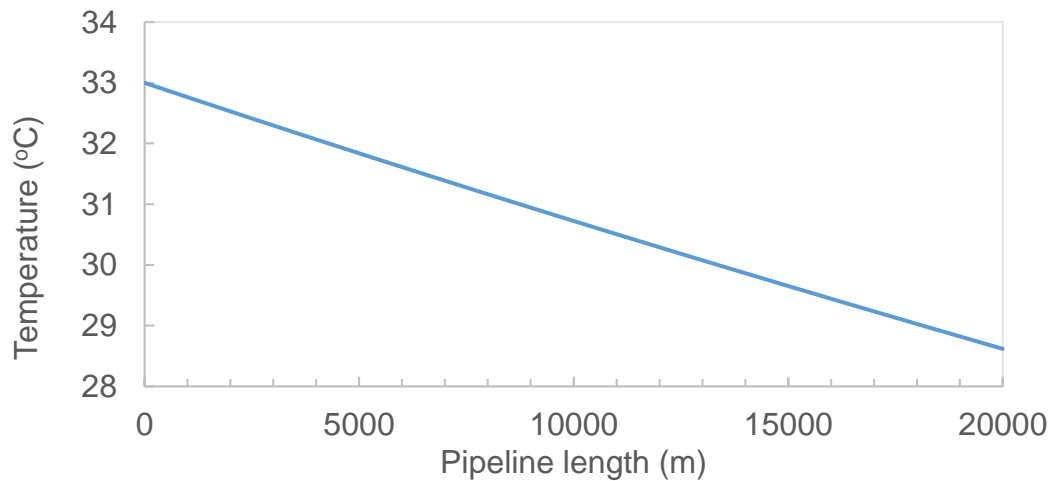


Figure 6.5: Steady temperature profile of pipeline.

Table 6.9: Pipeline final temperature of binary fluids.

Binary fluid	Final temperature (°C)
Pure CO ₂	28.62
H ₂ O	28.8
SO ₂	28.8
NH ₃	28.8
H ₂ S	28.62
Ar	28.58
CH ₄	28.59
O ₂	28.58
N ₂	28.56
CO	28.56
H ₂	28.54

6.6 Pressure of CO₂ pipelines

The most important parameter of pipeline fluid flow is pressure. Pressure is the driving force of the fluid, but it declines due to frictional, elevation and acceleration effects. For long distance pipelines, a high pressure-drop increases both the capital cost (installation of pressure boosting stations) and operational costs (running of the pressure boosting stations). Equation 6.29 gives the total pressure drop for a straight pipeline with constant cross-sectional area ([Fang et al. 2012](#)).

$$\Delta P = \Delta P_{fr} + \Delta P_{gr} + \Delta P_{ac} \quad (6.29)$$

$$\Delta P_{fr} = \frac{G^2 L f}{2 \rho D} \quad (6.31)$$

$$\Delta P_{gr} = g \left(\frac{\rho_1 + \rho_2}{2} \right) L \sin\theta \quad (6.30)$$

$$\Delta P_{ac} = G^2 \left(\frac{1}{\rho_1} - \frac{1}{\rho_2} \right) \quad (6.31)$$

where ΔP is total pressure drop (MPa), ΔP_{fr} is pressure drop due to friction (MPa), ΔP_{gr} is pressure drop due to elevation change, and ΔP_{ac} is pressure drop due to change in fluid velocity (MPa).

The pressure loss due to each component of the pressure drop equation is calculated using Equations 6.29 to 6.31 and shown on Table 6.10. The angle of elevation is assumed to be + 0.3°. H₂ caused the highest frictional pressure drop but the lowest gravitational pressure loss. SO₂ caused the lowest frictional pressure loss and highest gravitational pressure drop. Overall, H₂ caused the highest pressure loss because the gravitational pressure loss component is small compared the frictional component. Table 6.11 shows the various percentages due to acceleration, friction, and elevation pressure losses. Table 6.11 is divided into horizontal and elevation sections, to show the contributions of each

component for horizontal and elevated pipelines. It should be noted that the percentage due to elevation is a function of the angle of elevation and therefore

Table 6.10: Pressure drop of binary mixtures due to acceleration, friction and elevation.

Fluid	ΔP_{ac}	ΔP_{fr}	Total ΔP_{hor}	ΔP_{gr}	ΔP_{Total} .
Pure CO ₂	0.0042	4.8208	4.825	0.7352	5.5602
CO ₂ /N ₂	0.0044	4.9939	4.9983	0.7196	5.7179
CO ₂ /CH ₄	0.0046	4.9876	4.9922	0.7079	5.7001
CO ₂ /H ₂ S	0.0041	4.7841	4.7882	0.7307	5.5189
CO ₂ /H ₂	0.0048	5.5648	5.5696	0.7011	6.2707
CO ₂ /SO ₂	0.004	4.6978	4.7018	0.7547	5.4565
CO ₂ /Ar	0.0043	4.8462	4.8505	0.7313	5.5818
CO ₂ /CO	0.0044	4.9638	4.9682	0.7196	5.6878
CO ₂ /H ₂ O	0.0046	4.7012	4.7058	0.7099	5.4157
CO ₂ /O ₂	0.0045	4.9551	4.9596	0.7081	5.6677
CO ₂ /NH ₃	0.0046	4.9471	4.9517	0.7089	5.6606

Table 6.11: Percentage of pressure drop components.

	Percentage of pressure drop in the horizontal pipeline		Percentage of pressure drop in the inclined pipeline		
	Acceleration	Friction	Acceleration	Friction	Elevation
Pure CO ₂	0.088	99.912	0.076	86.701	13.223
CO ₂ /N ₂	0.090	99.910	0.079	87.181	12.741
CO ₂ /CH ₄	0.092	99.908	0.080	87.535	12.384
CO ₂ /H ₂ S	0.087	99.913	0.076	86.621	13.303
CO ₂ /H ₂	0.086	99.914	0.076	88.744	11.180
CO ₂ /SO ₂	0.086	99.914	0.074	86.095	13.831
CO ₂ /Ar	0.088	99.912	0.077	86.821	13.102
CO ₂ /CO	0.090	99.910	0.079	87.180	12.741
CO ₂ /H ₂ O	0.091	99.909	0.080	87.477	12.443
CO ₂ /O ₂	0.092	99.908	0.080	87.427	12.493
CO ₂ /NH ₃	0.091	99.909	0.080	87.506	12.414

changes according to the value of the angle of elevation. If the angle of elevation is increased, at a point the pressure loss due to elevation will become higher than the pressure loss due to friction. At this point, the pressure loss due to SO₂ will be higher than that due to H₂. Heavier impurities will cause higher pressure losses than lighter impurities. Overall, H₂S has the smallest pressure effect on CO₂ fluids flowing in pipelines.

6.7 Chapter conclusion

In this chapter, the effects of impurities on the properties of CO₂ fluids flowing in pipelines was simulated. Equations to convert values of pure CO₂ parameters to binary fluids parameters were formulated. These equations can be used to calculate the mixture properties if the value for pure CO₂ is known. The temperature drops for the first elemental flow and the steady prolonged flow is different. More heat is initially lost from the fluid because heat is more quickly transferred from the pipeline to the surrounding soil when the surrounding soil temperature is at ambient. The surrounding soil temperature increases as it is heated by the pipeline. Therefore, the difference in temperature (ΔT) reduces and consequently reduces the rate of heat transfer. The total heat lost from the pipeline depends on the rate of heat transferred by the soil to the surface. Since this rate becomes steady over time, the temperature of the pipeline does not change with time under continuous flow.

Most CO₂ pressure drop studies did not differentiate the acceleration and frictional pressure losses or just ignored the frictional component. From this study, it can be shown that ignoring the frictional component is justified as it contributes only a negligible percentage of the total pressure loss, a maximum of about 0.10 % of the total pressure loss in horizontal pipelines. If non horizontal pipelines with

positive elevation angles are considered, the frictional component reduces even further, to a maximum of about 0.08 % in this study. If non horizontal pipelines with negative elevation angles are considered, the percentage of total pressure drop due to acceleration will increase slightly but still negligible. This slight increase in pressure loss due to acceleration is because the elevation component no longer contributes to pressure loss but to pressure gain, thereby reducing the pressure loss. The grading of the effect of the impurities on the fluid flow parameters is presented in Table 6.12. On this Table the magnitude of the effect increases for 1 to 10.

Table 6.12: Grading of impurity impact on each parameter.

Parameter	1	2	3	4	5	6	7	8	9	10
Z – factor	H ₂	N ₂	CO	Ar	O ₂	CH ₄	H ₂ S	NH ₃	SO ₂	H ₂ O
Density	H ₂ O	SO ₂	H ₂ S	NH ₃	Ar	O ₂	CH ₄	CO	N ₂	H ₂
Viscosity	H ₂	CH ₄	N ₂	CO	O ₂	NH ₃	Ar	H ₂ S	SO ₂	H ₂ O
Temperature	H ₂	N ₂	CO	O ₂	Ar	CH ₄	H ₂ S	NH ₃	SO ₂	H ₂ O
Pressure (friction)	SO ₂	H ₂ O	H ₂ S	Ar	NH ₃	O ₂	CO	CH ₄	N ₂	H ₂

The impurities are arranged from positive or lowest effect (left) to highest negative effect (right). An impurity is considered to have a positive effect if its change on any property will result to lower pressure loss. The effect of impurities on pressure loss in Table 6.10 is that of horizontal pipeline. For non – horizontal pipelines, the effect would be different because of the contribution of the elevation component to total pressure drop.

Chapter 7: Conclusion, recommendation, and future work

7.1 Conclusion

This research work modelled and simulated the effects of impurities on CO₂ pipelines using Aspen HYSYS, gPROMS and HydraFlash software. Effects on pressure, temperature, density, viscosity, phase envelope, critical pressure and temperature were studied. All CO₂ fluid impurities reduced the volume of CO₂ transported in the pipeline and negatively impacted on one or more of the flow parameters. Previous research has not fully considered the effects of each impurity on all parameters considered in this study. The novelty of this thesis include.

- Analysis of the effect of all common impurities in CO₂ pipeline transportation. This has not been done before.
- Thermodynamic analysis of supercritical and subcritical CO₂ transportation in pipelines. The results show that specifying supercritical flow in CO₂ pipeline transportation is not justified.
- Soil heat conductivity rather than ambient temperature has appreciable impact on CO₂ pipeline transportation. This finding supports previous reports that there is negligible impact of ambient temperature on CO₂ pipelines.

The findings in this thesis has significant implications and applications in CO₂ pipeline transportation and the following conclusions can be drawn.

- Impurities have varying impacts on the parameters of CO₂ transportation in pipelines. These impurities may have varying degrees of impact according to the concentrations, which are usually different for each fluid.

At equal concentration, H₂, had the greatest impact on pressure loss (in horizontal pipelines), critical pressure, temperature change, and density and SO₂ had the greatest effect on critical temperature. At the specified maximum concentrations, N₂ having the highest concentration, had the most impact on pressure loss (in horizontal pipelines), density, critical pressure, critical temperature, phase envelope, and temperature. The degree of the impact of impurities at equal concentrations and at permitted concentrations is a useful guide during design to analyse the necessary parameters for optimisation.

- The question of the better fluid state, supercritical or subcritical, for transporting CO₂ in pipelines was answered in chapter 5. More volume of fluid is transported and for longer distances under subcritical flow than supercritical flow. Transporting fluid in subcritical conditions may require fewer boosting stations than under supercritical conditions in long distance pipelines, thus saving both capital and operational costs. It, therefore, shows that transporting CO₂ in subcritical state is more economical than transporting it in supercritical state. The evidence presented in this thesis can be used to review the specification for transporting CO₂ fluids in pipelines. The possibility of transporting CO₂ in pipelines at lower than critical pressures can be seen from the phase envelopes of the fluids and may be investigated in the future.
- Equations that convert pure CO₂ fluid parameters to impure CO₂ fluid parameters in CCTS operations have been presented. These equations performed well when compared to Aspen HYSYS, an industry standard software and practical data. Designing CO₂ fluid transportation in pipelines

can be optimised by using these equations to convert pure CO₂ fluid parameters to impure CO₂ parameters.

- The effects of each impurity have been graded in this thesis. H₂ has the worst impact on CO₂ pressure. However, in inclined pipelines, if the angle of inclination is high, H₂ could have a lower pressure loss compared to heavier impurities. At the specified maximum concentrations, N₂ with the highest concentration resulted in the highest pressure decline in horizontal pipelines. Lighter impurities have lower pressure losses than heavier impurities in inclined pipelines.
- Heat loss in the pipeline increases the density of the fluid thereby reducing the velocity of flow. Slower velocities result to lower pressure losses. However, heat loss in buried CO₂ pipelines are small and the fluid temperature changes only slightly due to the low heat conduction of the soil from the pipeline to the surface. Therefore, soil conductivity has a greater effect than ambient temperature on buried CO₂ pipelines. The effect of impurities on the temperature of a buried CO₂ pipeline is negligible.

The findings in this research can be used to adjust the allowable concentrations of the impurities. However, storage requirements and purification costs are also considered before maximum concentrations are specified. Parameters designed assuming pure CO₂ may be over-designed for CO₂ fluids with impurities having positive effects and under-designed for impurities having negative effects. To optimise the design of CO₂ pipelines, the actual fluid with the impurities should be analysed.

7.2 Recommendations

This research concentrated on the impact of single impurities on the performance of CO₂ pipelines. Steady state simulations were carried out to determine the effects all common impurities have on the flow of CO₂ fluids in pipelines. Impact of CO₂ impurities may be different in combination of other impurities. In the case of actual pipelines, the impact of all the impurities was studied. It is therefore recommended that the impact of impurities in the presence of other impurities be investigated. Lack of practical data was a hindrance in carrying out this work. It is therefore recommended that parameters for CO₂ fluids with impurities (N₂, CH₄, H₂S, SO₂, Ar, H₂, CO, H₂O, NH₃, O₂) within the pressure and temperature range of CO₂ pipelines be carried out in the laboratory. These data would be helpful in the validation of simulation results.

7.3 Further work

From the phase envelopes of CO₂ fluids with impurities, the possibility to transport rich CO₂ fluids in the dense phase, at pressures below the critical value can be seen. This possibility needs to be investigated as it has the potential of cutting down on operational (compression) cost and capital (pipes and boosting stations) costs.

This research has considered steady state flow of CO₂ fluids in pipelines because inert gases are used to pressurise the pipeline before introducing the CO₂ fluid. However, during start up, shutdown, ramp up or ramp down, the fluid flow rate changes. To accurately model the effect of impurities in these phases entails the use of dynamic models. Computational fluid dynamics (CFD) is increasingly used to model CO₂ capture processes ([Zhou et al. 2011](#)) and fluid flow in pipes ([Rzehak and Kriebitzsch 2015](#)). CFD could also be used to model the

transportation of CO₂ fluids in the pipelines. Future work could also consider the economic analysis of a large trunk pipeline transporting CO₂ fluids from several capture sources to a storage site with changing composition in the pipeline from different sources. Pipeline corrosion is also an important aspect of fluid transportation. The effect of impurities on the internal pipeline wall corrosion should be studied to understand if impurities other than H₂O have significant effect.

References

- Aaron, D. and Tsouris, C. (2005) Separation of CO₂ from flue gas: A Review. *Separation Science and Technology* 40 (1-3), 321-348.
- Adisasmito, S., Frank III, R. J. and Sloan Jr, E. D. (1991) Hydrates of carbon dioxide and methane mixtures. *Journal of Chemical and Engineering Data* 36 (1), 68-71.
- Agut, D. N., Hübner, M. and Reniers, M. (2010) Specification and Validation of gPROMS Semantics.
- Ahmad, M., Gernert, J. and Wilbers, E. (2014) Effect of impurities in captured CO₂ on liquid–vapor equilibrium. *Fluid Phase Equilibria* 363, 149 - 155.
- Al-Siyabi, I. (2013) *Effect of impurities on CO₂ stream properties*. Heriot-Watt University.
- Al-Syabi, Z., Danesh, A., Tohidi, B., Todd, A. and Tehrani, D. (2001) A residual viscosity correlation for predicting the viscosity of petroleum reservoir fluids over wide ranges of pressure and temperature. *Chemical engineering science* 56 (24), 6997-7006.
- Al Ghafri, S. Z. S., Czubinski, F. F. and May, E. F. (2018) Viscosity measurements of (CH₄ + C₃H₈ + CO₂) mixtures at temperatures between (203 and 420) K and pressures between (3 and 31) MPa. *Fuel* 231, 187-196.
- Alhajaj, A., Mac Dowell, N. and Shah, N. (2013) Multiscale design and analysis of CO₂ capture, transport and storage networks. *Energy Procedia* 37, 2552-2561.
- Allen, M. R., O.P. Dube, W. Solecki, F. Aragón-Durand, W. Cramer, S. Humphreys, M. Kainuma, J. Kala, N. Mahowald, Y. Mulugetta, R. Perez, M. Wairiu and K. Zickfeld (2018) *Framing and Context. In: Global Warming of 1.5°C. An IPCC Special Report on the impacts of global warming of 1.5°C above pre-industrial levels and related global greenhouse gas emission pathways, in the context of strengthening the global response to the threat of climate change, sustainable development, and efforts to eradicate poverty.* <https://www.ipcc.ch/>
- Antonie Oosterkamp, J. R. (2008) *State-of-the-Art Overview of CO₂ Pipeline Transport with relevance to offshore pipelines*. POL-O-2007-138-A.
- API (1991) American Petroleum Institute, Recommended practice for design and installation of offshore production platform piping systems. *API Recommended Practice* 14E (RP 14E), 5th ed.
- Arai, A. A., Morita, T. and Nishikawa, K. (2005) Analysis to obtain precise density fluctuation of supercritical fluids by small-angle X-ray scattering. *Chemical Physics* 310 (1–3), 123-128.
- Aursand, P., Hammer, M., Munkejord, S. T. and Wilhelmsen, Ø. (2013) Pipeline transport of CO₂ mixtures: Models for transient simulation. *International Journal of Greenhouse Gas Control* 15, 174-185.
- Bai, Y. and Bai, Q. (2005) *Subsea pipelines and risers*. Elsevier.
- Barton, N. A. (2003) *Erosion in elbows in hydrocarbon production systems: Review document*.
- Bauer, W. E. (2011a) Chapter 3 - Pipeline Regulatory and Environmental Permits A2 - Menon, E. Shashi. In Menon, E. S. (editor) *Pipeline Planning and Construction Field Manual*. Boston: Gulf Professional Publishing. 57-65.

- Bauer, W. E. (2011b) Chapter 4: Right-of-Way. In Menon, E. S. (editor) *Pipeline Planning and Construction Field Manual*. Boston: Gulf Professional Publishing. 67-79.
- Benson, H. Y. and Ogden, J. M. (2003) Mathematical Programming Techniques for Designing Minimum Cost Pipeline Networks for CO₂ Sequestration A2 - Gale, J. In Kaya, Y. (editor) *Greenhouse Gas Control Technologies - 6th International Conference*. Oxford: Pergamon. 627-632.
- Bentham, M., Mallows, T., Lowndes, J. and Green, A. (2014) CO₂ STORage Evaluation Database (CO₂ Stored). The UK's online storage atlas. *Energy Procedia* 63, 5103-5113.
- Besong, M. T., Maroto-Valer, M. M. and Finn, A. J. (2013) Study of design parameters affecting the performance of CO₂ purification units in oxy-fuel combustion. *International Journal of Greenhouse Gas Control* 12, 441-449.
- Böttcher, N., Taron, J., Kolditz, O., Park, C.-H. and Liedl, R. (2012) Evaluation of thermal equations of state for CO₂ in numerical simulations. *Environmental Earth Sciences* 67 (2), 481-495.
- Brown, S., Mahgereteh, H., Martynov, S., Sundara, V. and Dowell, N. M. (2015) A multi-source flow model for CCS pipeline transportation networks. *International Journal of Greenhouse Gas Control* 43, 108-114.
- Brownsort, P. A., Scott, V. and Haszeldine, R. S. (2016) Reducing costs of carbon capture and storage by shared reuse of existing pipeline-Case study of a CO₂ capture cluster for industry and power in Scotland. *International Journal of Greenhouse Gas Control* 52, 130-138.
- Caravaggio, N., Caravella, S., Ishizaka, A. and Resce, G. (2019) Beyond CO₂: A multi-criteria analysis of air pollution in Europe. *Journal of Cleaner Production* 219, 576-586.
- Chandel, M. K., Pratson, L. F. and Williams, E. (2010) Potential economies of scale in CO₂ transport through use of a trunk pipeline. *Energy Conversion and Management* 51 (12), 2825-2834.
- Chapoy, A., Burgass, R., Tohidi, B. and Alsiyabi, I. (2014) Hydrate and phase behavior modeling in CO₂-rich pipelines. *Journal of Chemical & Engineering Data* 60 (2), 447-453.
- Chapoy, A., Nazeri, M., Kapateh, M., Burgass, R., Coquelet, C. and Tohidi, B. (2013) Effect of impurities on thermophysical properties and phase behaviour of a CO₂-rich system in CCS. *International Journal of Greenhouse Gas Control* 19, 92-100.
- Chen, X., Hou, Y., Wu, W., Ren, S., Zhang, J. and Fan, J. (2009) High pressure phase behavior and density of the carbon dioxide + 1-methylimidazole binary system. *The Journal of Supercritical Fluids* 49 (3), 310-314.
- Cieutat, D., Sanchez-Moliner, I., Tsiava, R., Recourt, P., Aimard, N. and Prébendé, C. (2009) The Oxy-combustion burner development for the CO₂ pilot at Lacq. *Energy Procedia* 1 (1), 519-526.
- Cole, I. S., Paterson, D. A., Corrigan, P., Sim, S. and Birbilis, N. (2012) State of the aqueous phase in liquid and supercritical CO₂ as relevant to CCS pipelines. *International Journal of Greenhouse Gas Control* 7, 82-88.
- Cooper, R. and Barnett, J. (2014) Pipelines for transporting CO₂ in the UK. *Energy Procedia* 63, 2412-2431.
- Coquelet, C., Stringari, P., Hajiw, M., Gonzalez, A., Pereira, L., Nazeri, M., Burgass, R. and Chapoy, A. (2017) Transport of CO₂: Presentation of New

- Thermophysical Property Measurements and Phase Diagrams. *Energy Procedia* 114, 6844-6859.
- Coquelet, C., Valtz, A. and Arpentinier, P. (2014) Thermodynamic study of binary and ternary systems containing CO₂+impurities in the context of CO₂ transportation. *Fluid Phase Equilibria* 382, 205-211.
- Dashti, H., Zhehao Yew, L. and Lou, X. (2015) Recent advances in gas hydrate-based CO₂ capture. *Journal of Natural Gas Science and Engineering* 23, 195-207.
- Davidson, T. A. (1993) Simple and accurate method for calculating viscosity of gaseous mixtures.
- de Almeida, J. C., Velásquez, J. A. and Barbieri, R. (2014) A methodology for calculating the natural gas compressibility factor for a distribution network. *Petroleum Science and Technology* 32 (21), 2616-2624.
- de Koeijer, G., Henrik Borch, J., Drescher, M., Li, H., Wilhelmsen, Ø. and Jakobsen, J. (2011) CO₂ transport–Depressurization, heat transfer and impurities. *Energy Procedia* 4, 3008-3015.
- De Visser, E., Hendriks, C., Barrio, M., Mølnvik, M. J., de Koeijer, G., Liljemark, S. and Le Gallo, Y. (2008) Dynamis CO₂ quality recommendations. *International journal of greenhouse gas control* 2 (4), 478-484.
- Dooley, J. J., Dahowski, R. T. and Davidson, C. L. (2009) Comparing Existing Pipeline Networks with the Potential Scale of Future U.S. CO₂ Pipeline Networks. *Energy Procedia* 1 (1), 1595-1602.
- Duckett, A. (2016) *Cameron challenged on UK energy policy*. February 2016 edition. UK.
- Elahi, N., Shah, N., Korre, A. and Durucan, S. (2014) Multi-period Least Cost Optimisation Model of an Integrated Carbon Dioxide Capture Transportation and Storage Infrastructure in the UK. *Energy Procedia* 63, 2655-2662.
- Ely, J. F., Haynes, W. M. and Magee, J. (1987) *Thermophysical properties for special high CO₂ content mixtures*. Gas Processors Association.
- Esper, G. J., Bailey, D. M., Holste, J. C. and Hall, K. R. (1989) Volumetric behavior of near-equimolar mixtures for CO₂+CH₄ and CO₂+N₂. *Fluid Phase Equilibria* 49, 35-47.
- Fang, X., Xu, Y., Su, X. and Shi, R. (2012) Pressure drop and friction factor correlations of supercritical flow. *Nuclear Engineering and Design* 242, 323-330.
- Farris, C. (1983) Unusual design factors for supercritical CO₂/sub 2/pipelines. *Energy Prog.:(United States)* 3 (3).
- Forbes, S. M., Verma, P., Curry, T. E., Bradley, M. J., Friedmann, S. J. and Livermore, L. (2008) *CCS Guidelines: Guidelines for Carbon Dioxide Capture, Transport, and Storage*. Washington, DC: WRI.
- Forgács, P. and Horánszky, B. (2013) CO₂ Pipeline Cost Calculations, Based on Different Cost Models. *Theory, Methodology, Practice* 9 (1), 43.
- Gao, L., Fang, M., Li, H. and Hetland, J. (2011) Cost analysis of CO₂ transportation: Case study in China. *Energy Procedia* 4, 5974-5981.
- Ghanbari, M., Ahmadi, M. and Lashanizadegan, A. (2017) A comparison between Peng-Robinson and Soave-Redlich-Kwong cubic equations of state from modification perspective. *Cryogenics* 84, 13-19.
- Global_CCS_Institute (2012) *CARBON DIOXIDE (CO₂) DISTRIBUTION INFRASTRUCTURE*.

- Goos, E., Riedel, U., Zhao, L. and Blum, L. (2011) Phase diagrams of CO₂ and CO₂-N₂ gas mixtures and their application in compression processes. *Energy Procedia* 4, 3778–3785.
- Gough, C., Shackley, S., Holloway, S., Bentham, M., Bulatov, I., McLachlan, C., Klemes, J., Purdy, R. and Cockerill, T. (2006) An integrated assessment of carbon dioxide capture and storage in the UK. *In: 8th International Conference on greenhouse gas control technologies [proceedings]/[edited by Greenhouse Gas Control Technologies. Trondheim, Norway: GHGT8. Vol. 6. Greenhouse Gas Control Technologies.*
- Han, C., Zahid, U., An, J., Kim, K. and Kim, C. (2015) CO₂ transport: design considerations and project outlook. *Current Opinion in Chemical Engineering* 10, 42-48.
- Heidaryan, E., Hatami, T., Rahimi, M. and Moghadasi, J. (2011) Viscosity of pure carbon dioxide at supercritical region: Measurement and correlation approach. *The Journal of Supercritical Fluids* 56 (2), 144-151.
- Hoegh-Guldberg, O., Jacob, D., Taylor, M., Bindi, M., Brown, S., Camilloni, I., Diedhiou, A., Djalante, R., Ebi, K. L., Engelbrecht, F., Guiot, J., Hijioka, Y., Mehrotra, S., Payne, A., Seneviratne, S. I., Thomas, A., Warren, R. and Zhou, G. (2018) *Impacts of 1.5°C Global Warming on Natural and Human Systems. In: Global Warming of 1.5°C. An IPCC Special Report on the impacts of global warming of 1.5°C above pre-industrial levels and related global greenhouse gas emission pathways, in the context of strengthening the global response to the threat of climate change, sustainable development, and efforts to eradicate poverty.*
- Hwang, C.-A., Iglesias-Silva, G. A., Holste, J. C., Hall, K. R., Gammon, B. E. and Marsh, K. N. (1997) Densities of carbon dioxide+ methane mixtures from 225 K to 350 K at pressures up to 35 MPa. *Journal of Chemical & Engineering Data* 42 (5), 897-899.
- IEA GHG (2002) Transmission of CO₂ and Energy. *Transmission Study Report* (PH4/6), 140.
- IEA GHG (2005) Building the cost curves for CO₂ storage: European sector. *International Energy Agency Greenhouse Gas R&D Programme Report* Number 2005/2.
- IEA GHG (2010) *IEA_Pipeline_final_report.pdf_CO2 pipeline Infrastructure: An analysis of global challenges and opportunities.* [Report].
- IEA GHG (2014) *CO₂ Pipeline infrastructure.* [Report]. 2013/18, December, 2013.:
- Ilinova, A., Cherepovitsyn, A. and Evseeva, O. (2018) Stakeholder Management: An Approach in CCS Projects. *Resources* 7 (4), 83.
- IPCC (2007) *Climate change 2007 - Impacts, Adaptation and Vulnerability.* Cambridge University Press:
- IPCC (2011) *IPCC special report on renewable energy sources and climate change mitigation.* Cambridge University Press, Cambridge, United Kingdom and New York, NY, USA.:
- Jakobsen, J., Roussanaly, S. and Anantharaman, R. (2017) A techno-economic case study of CO₂ capture, transport and storage chain from a cement plant in Norway. *Journal of Cleaner Production* 144, 523-539.
- Jiang, S., Wang, Y. and Shi, J. (1990) Determination of compressibility factors and virial coefficients for the systems containing N₂, CO₂ and CHCl₃ by the modified Burnett method. *Fluid Phase Equilibria* 57 (1), 105-117.

- Joana, S., Joris, M. and Evangelos., T. (2011) Technical and economic characteristics of a CO₂ transmission pipeline infrastructure. *Joint Research Centre Institute for Energy, Petten*.
- Joel, A. S., Wang, M. and Ramshaw, C. (2015) Modelling and simulation of intensified absorber for post-combustion CO₂ capture using different mass transfer correlations. *Applied thermal engineering* 74, 47-53.
- Jossi, J. A., Stiel, L. I. and Thodos, G. (1962) The viscosity of pure substances in the dense gaseous and liquid phases. *AIChE Journal* 8 (1), 59-63.
- Kang, K., Huh, C., Kang, S.-G., Baek, J.-H. and Noh, H. J. (2014) Estimation of CO₂ Pipeline Transport Cost in South Korea Based on the Scenarios. *Energy Procedia* 63, 2475-2480.
- Kanniche, M., Gros-Bonnivard, R., Jaud, P., Valle-Marcos, J., Amann, J.-M. and Bouallou, C. (2010) Pre-combustion, post-combustion and oxy-combustion in thermal power plant for CO₂ capture. *Applied Thermal Engineering* 30 (1), 53-62.
- Kanti, M., Zhou, H., Ye, S., Boned, C., Lagourette, B., Saint-Guirons, H., Xans, P. and Montel, F. (1989) Viscosity of liquid hydrocarbons, mixtures and petroleum cuts, as a function of pressure and temperature. *The Journal of Physical Chemistry* 93 (9), 3860-3864.
- Kaufmann, K.-D. (2011) Carbon Dioxide Transport in Pipelines-Under Special Consideration of Safety-Related Aspects. *3rd Pipeline Technology Conference 2008*. EITEP Institute.
- Ke, J., Suleiman, N., Sanchez-Vicente, Y., Murphy, T. S., Rodriguez, J., Ramos, A., Poliakoff, M. and George, M. W. (2017) The phase equilibrium and density studies of the ternary mixtures of CO₂ + Ar + N₂ and CO₂ + Ar + H₂, systems relevance to CCS technology. *International Journal of Greenhouse Gas Control* 56, 55-66.
- Keeling, R. (2013) Recording 400 ppm CO₂ Emissions. *TheGuardian*, <https://www.theguardian.com/environment/2013/may/14/record-400ppm-co2-carbon-emissions> Accessed 02 February 2019
- Kemp, A. G. and Sola Kasim, A. (2010) A futuristic least-cost optimisation model of CO₂ transportation and storage in the UK/UK Continental Shelf. *Energy Policy* 38 (7), 3652-3667.
- Kianpour, M., Sobati, M. A. and Shahhosseini, S. (2012) Experimental and modeling of CO₂ capture by dry sodium hydroxide carbonation. *Chemical Engineering Research and Design* 90 (11), 2041-2050.
- Kijjarvi, J. (2011) Darcy friction factor formulae in turbulent pipe flow. *Lunowa Fluid Mechanics Paper* 110727.
- Kikkinides, E. S., Yang, R. and Cho, S. (1993) Concentration and recovery of carbon dioxide from flue gas by pressure swing adsorption. *Industrial & Engineering Chemistry Research* 32 (11), 2714-2720.
- Knoope, M. (2015) *Costs, safety and uncertainties of CO₂ infrastructure development*. Utrecht University.
- Knoope, M. M. J., Guijt, W., Ramírez, A. and Faaij, A. P. C. (2014) Improved cost models for optimizing CO₂ pipeline configuration for point-to-point pipelines and simple networks. *International Journal of Greenhouse Gas Control* 22, 25-46.
- Knoope, M. M. J., Ramírez, A. and Faaij, A. P. C. (2013a) Economic Optimization of CO₂ Pipeline Configurations. *Energy Procedia* 37, 3105-3112.

- Knoope, M. M. J., Ramírez, A. and Faaij, A. P. C. (2015) Investing in CO₂ transport infrastructure under uncertainty: A comparison between ships and pipelines. *International Journal of Greenhouse Gas Control* 41, 174-193.
- Knoope, M. M. J., Ramirez, C. A. and Faaij, A. P. C. (2013b) A state-of-the-art review of techno-economic models predicting the costs of CO₂ pipeline transport. *International journal of greenhouse gas control* 16, 241-270.
- Koga, T., Akashige, E., Reinstein, A., Bronner, M., Seo, Y. S., Shin, K., Rafailovich, M. H., Sokolov, J. C., Chu, B. and Satija, S. K. (2005) The effect of density fluctuations in supercritical fluids: new science and technology for polymer thin films. *Physica B: Condensed Matter* 357 (1–2), 73-79.
- Kreith, F., Manglik, R. M. and Bohn, M. S. (2012) *Principles of heat transfer*. Cengage learning.
- Kuby, M. J., Middleton, R. S. and Bielicki, J. M. (2011) Analysis of cost savings from networking pipelines in CCS infrastructure systems. *Energy Procedia* 4, 2808-2815.
- Kwak, T. and Mansoori, G. (1986) Van der Waals mixing rules for cubic equations of state. Applications for supercritical fluid extraction modelling. *Chemical engineering science* 41 (5), 1303-1309.
- Lake, J. A., Johnson, I. and Cameron, D. D. (2016) Carbon Capture and Storage (CCS) pipeline operating temperature effects on UK soils: The first empirical data. *International Journal of Greenhouse Gas Control* 53, 11-17.
- Lazic, T., Oko, E. and Wang, M. (2014) Case study on CO₂ transport pipeline network design for Humber region in the UK. *Proceedings of the Institution of Mechanical Engineers, Part E: Journal of Process Mechanical Engineering* 228 (3), 210-225.
- Lemontzoglou, A., Pantoleontos, G., Asimakopoulou, A. G., Tsongidis, N. I. and Konstandopoulos, A. G. (2017) Analysis of CO₂ transport including impurities for the optimization of point-to-point pipeline networks for integration into future solar fuel plants. *International Journal of Greenhouse Gas Control* 66, 10-24.
- Leung, D. Y., Caramanna, G. and Maroto-Valer, M. M. (2014) An overview of current status of carbon dioxide capture and storage technologies. *Renewable and Sustainable Energy Reviews* 39, 426-443.
- Li, H., Jakobsen, J. P., Wilhelmsen, Ø. and Yan, J. (2011a) PVT_{xy} properties of CO₂ mixtures relevant for CO₂ capture, transport and storage: Review of available experimental data and theoretical models. *Applied Energy* 88 (11), 3567-3579.
- Li, H., Wilhelmsen, Ø., Lv, Y., Wang, W. and Yan, J. (2011b) Viscosities, thermal conductivities and diffusion coefficients of CO₂ mixtures: Review of experimental data and theoretical models. *International Journal of Greenhouse Gas Control* 5 (5), 1119-1139.
- Li, H. and Yan, J. (2009) Impacts of equations of state (EOS) and impurities on the volume calculation of CO₂ mixtures in the applications of CO₂ capture and storage (CCS) processes. *Applied Energy* 86 (12), 2760-2770.
- Lipponen, J., McCulloch, S., Keeling, S., Stanley, T., Berghout, N. and Berly, T. (2017) The politics of large-scale CCS deployment. *Energy Procedia* 114, 7581-7595.

- Liu, S., Zhang, Y., Chi, Y., Song, Y., Yang, M., Liu, Y. and Lv, P. (2017) Density characteristics of CO₂-CH₄ binary mixtures at temperatures from (300 to 308.15) K and pressures from (2 to 18) MPa. *The Journal of Chemical Thermodynamics* 106, 1-9.
- Loáiciga, H. A. (2013) CO₂ Capture and Geologic Storage: The Possibilities. *Groundwater* 51 (6), 816-821.
- Lopez-Echeverry, J. S., Reif-Acherman, S. and Araujo-Lopez, E. (2017) Peng-Robinson equation of state: 40 years through cubics. *Fluid Phase Equilibria* 447, 39-71.
- Luo, X., Mistry, K., Okezue, C., Wang, M., Cooper, R., Oko, E. and Field, J. (2014a) Process simulation and analysis for CO₂ transport pipeline design and operation—case study for the Humber region in the UK. *Computer aided chemical engineering*. Vol. 33. Elsevier. 1633-1638.
- Luo, X., Wang, M., Oko, E. and Okezue, C. (2014b) Simulation-based techno-economic evaluation for optimal design of CO₂ transport pipeline network. *Applied Energy* 132, 610-620.
- Mahabadian, M. A., Chapoy, A., Burgass, R. and Tohidi, B. (2016) Development of a multiphase flash in presence of hydrates: Experimental measurements and validation with the CPA equation of state. *Fluid Phase Equilibria* 414, 117 - 132.
- Mahgerfteh, H., Zhang, P. and Brown, S. (2016) Modelling brittle fracture propagation in gas and dense-phase CO₂ transportation pipelines. *International Journal of Greenhouse Gas Control* 46, 39-47.
- Mangold, F., Pilz, S., Bjelic, S. and Vogel, F. (2019) Equation of State and Thermodynamic Properties for Mixtures of H₂O, O₂, N₂, and CO₂ from Ambient up to 1000 K and 280 MPa. *The Journal of Supercritical Fluids*.
- Martynov, S., Brown, S., Mahgerfteh, H. and Sundara, V. (2013) Modelling choked flow for CO₂ from the dense phase to below the triple point. *International Journal of Greenhouse Gas Control* 19, 552-558.
- Masson-Delmotte, V., Zhai, P., Pörtner, H.-O., Roberts, D., Skea, J., Shukla, P. R., Pirani, A., Moufouma-Okia, W., Péan, C. and Pidcock, R. (2018) Global warming of 1.5 C. *An IPCC Special Report on the impacts of global warming of 1.5*.
- Mazzocolia, M., Guidob, G. D., Bosioa, B., Elisabetta Aratoa and Pellegrini, L. A. (2013) CO₂-mixture Properties for Pipeline Transportation in the CCS Process. *Chemical Engineering Transactions* 32, 1861 - 1866.
- Mazzoldi, A., Hill, T. and Colls, J. (2008) CO₂ transportation for carbon capture and storage: Sublimation of carbon dioxide from a dry ice bank. *International Journal of Greenhouse Gas Control* 2 (2), 210-218.
- McCollum, D. L. and Ogden, J. M. (2006) Techno-economic models for carbon dioxide compression, transport, and storage & correlations for estimating carbon dioxide density and viscosity.
- McCoy, S. and Rubin, E. (2008) An engineering-economic model of pipeline transport of CO₂ with application to carbon capture and storage. *International Journal of Greenhouse Gas Control* 2 (2), 219-229.
- Middleton, R. S. and Bielicki, J. M. (2009) A scalable infrastructure model for carbon capture and storage: SimCCS. *Energy Policy* 37 (3), 1052-1060.
- Middleton, R. S., Kuby, M. J. and Bielicki, J. M. (2012) Generating candidate networks for optimization: The CO₂ capture and storage optimization problem. *Computers, Environment and Urban Systems* 36 (1), 18-29.

- Mohitpour, M., Golshan, H. and Murray, A. (2003a) *Pipeline Design & Construction*. ASME. Vol. first ed. ASME Press, New York, NY.
- Mohitpour, M., Golshan, H. and Murray, A. (2003b) *Pipeline Design & Construction*. first ed. edition. ASME Press. New York, NY.:
- Mollersten, K., Luleå University of, T., Department of Engineering, S., Mathematics, Energy, E. and Energy, S. (2004) Efficient energy systems with CO₂ capture and storage from renewable biomass in pulp and paper mills. *Renewable Energy* 29 (9), 1583-1598.
- Monsalvo, M. A., Baylaucq, A., Reghem, P., Quiñones-Cisneros, S. and Boned, C. (2005) Viscosity measurements and correlations of binary mixtures: 1, 1, 1, 2-tetrafluoroethane (HFC-134a)+ tetraethylene glycol dimethylether (TEGDME). *Fluid phase equilibria* 233 (1), 1-8.
- Morbee, J., Serpa, J. and Tzimas, E. (2012) Optimised deployment of a European CO₂ transport network. *International Journal of Greenhouse Gas Control* 7, 48-61.
- Munkejord, S. T., Hammer, M. and Løvseth, S. W. (2016) CO₂ transport: Data and models – A review. *Applied Energy* 169, 499-523.
- Na, T., Baodong, C., Limin, H., Qisheng, C. and Qi, W. (2012) Research on the Overall Heat Transfer Coefficients of Crude Oil Pipeline and Product Pipeline Laid in One Ditch. *Petroleum Science and Technology* 30 (3), 247-255.
- Nair, P. K. and Rahmanian, N. (2017) Impact of impurities on formation of carbon-dioxide hydrates. In *6th International Conference on Petroleum Engineering*. Madrid, Spain: June 29 - 30, 2017.
- Neele, F., Koenen, M., van Deurzen, J., Seebregts, A., Groenenberg, H. and Thielemann, T. (2011) Large-scale CCS transport and storage networks in North-west and Central Europe. *Energy Procedia* 4, 2740-2747.
- Nimtz, M., Klatt, M., Wiese, B., Kühn, M. and Joachim Krautz, H. (2010) Modelling of the CO₂ process- and transport chain in CCS systems—Examination of transport and storage processes. *Chemie der Erde - Geochemistry* 70, 185-192.
- Noothout, P., Wiersma, F., Hurtado, O., Macdonald, D., Kemper, J. and van Alphen, K. (2014) CO₂ Pipeline Infrastructure – Lessons Learnt. *Energy Procedia* 63, 2481-2492.
- Oei, P.-Y., Herold, J. and Mendelevitch, R. (2014) Modeling a Carbon Capture, Transport, and Storage Infrastructure for Europe. *Environmental Modeling & Assessment* 19 (6), 515-531.
- Ogden, J. M., Yang, C., Johnson, N., Ni, J. and Johnson, J. (2004) *Conceptual design of optimized fossil energy systems with capture and sequestration of carbon dioxide*. DE-FC26-02NT41623.
- Oke, A., Mahgereteh, H., Economou, I. and Rykov, Y. (2003) A transient outflow model for pipeline puncture. *Chemical engineering science* 58 (20), 4591-4604.
- Olajire, A. A. (2010) CO₂ capture and separation technologies for end-of-pipe applications – A review. *Energy* 35 (6), 2610-2628.
- Ouyang, L.-B. (2011) New correlations for predicting the density and viscosity of supercritical carbon dioxide under conditions expected in carbon capture and sequestration operations. *The Open Petroleum Engineering Journal* 4 (1).

- Ozanne, H. S. (2011) Chapter 2 - Route Selection A2 - Menon, E. Shashi. In Menon, E. S. (editor) *Pipeline Planning and Construction Field Manual*. Boston: Gulf Professional Publishing. 43-56.
- Parfomak, P. W. and Folger, P. (2007) *Carbon Dioxide (CO₂) Pipelines for Carbon Sequestration_Emerging Policy Issues.pdf*.
- Patchigolla, K. and Oakey, J. E. (2013) Design Overview of High Pressure Dense Phase CO₂ Pipeline Transport in Flow Mode. *Energy Procedia* 37, 3123-3130.
- Pensado, A. S., Pádua, A. A. H., Comuñas, M. J. P. and Fernández, J. (2008) High-pressure viscosity and density of carbon dioxide + pentaerythritol ester mixtures: Measurements and modeling. *AIChE Journal* 54 (6), 1625-1636.
- Piippo, S., Lauronen, M. and Postila, H. (2018) Greenhouse gas emissions from different sewage sludge treatment methods in north. *Journal of Cleaner Production* 177, 483-492.
- Porter, R. T., Mahgerefteh, H., Brown, S., Martynov, S., Collard, A., Woolley, R. M., Fairweather, M., Falle, S. A., Wareing, C. J. and Nikolaidis, I. K. (2016) Techno-economic assessment of CO₂ quality effect on its storage and transport: CO₂QUEST: An overview of aims, objectives and main findings. *International Journal of Greenhouse Gas Control* 54, 662-681.
- PowerPlantCCS (2010) *Pipeline Based Transportation*. http://www.powerplantccs.com/ccs/tra/tra_pipe.html Accessed 19 May.
- Proust, P. and Vera, J. (1989) PRSV: The stryjek-vera modification of the peng-robinson equation of state. Parameters for other pure compounds of industrial interest. *The Canadian Journal of Chemical Engineering* 67 (1), 170-173.
- Race, J. M., Wetenhall, B., Seevam, P. N. and Downie, M. J. (2012) Towards a CO₂ pipeline specification: defining tolerance limits for impurities. *Journal of Pipeline Engineering* 11 (3).
- Raimondi, L. (2014) CO₂ Transportation with Pipelines-Model Analysis for Steady, Dynamic and Relief Simulation. *Chem. Eng. Trans* 36, 619-624.
- Rainbolt, J. E., Koech, P. K., Yonker, C. R., Zheng, F., Main, D., Weaver, M. L., Linehan, J. C. and Heldebrant, D. J. (2011) Anhydrous tertiary alkanolamines as hybrid chemical and physical CO₂ capture reagents with pressure-swing regeneration. *Energy & Environmental Science* 4 (2), 480.
- Ramdharee, S., Muzenda, E. and Belaid, M. (2013) A review of the equations of state and their applicability in phase equilibrium modeling. International Conference on Chemical and Environmental Engineering.
- Rehan, M., Rahmanian, N., Hyatt, X., Peletiri, S. P. and Nizami, A.-S. (2017) Energy Savings in CO₂ Capture System through Intercooling Mechanism. *Energy Procedia* 142, 3683-3688.
- Rehm, B., Haghshenas, A., Paknejad, A. S. and Schubert, J. (2008) Situational problems in MPD. *Managed Pressure Drilling*. Elsevier. 39-80.
- Rzehak, R. and Kriebitzsch, S. (2015) Multiphase CFD-simulation of bubbly pipe flow: A code comparison. *International Journal of Multiphase Flow* 68, 135-152.
- Salam, K., Arinkoola, A., Araromi, D. and Ayansola, Y. (2013) Prediction of Hydrate formation conditions in Gas pipelines. *International Journal of Engineering* 2 (8), 327-331.

- Sanchez-Vicente, Y., Drage, T. C., Poliakoff, M., Ke, J. and George, M. W. (2013) Densities of the carbon dioxide+ hydrogen, a system of relevance to carbon capture and storage. *International Journal of Greenhouse Gas Control* 13, 78-86.
- Sani, F. M., Huizinga, S., Esaklul, K. and Nestic, S. (2019) Review of the API RP 14E erosional velocity equation: Origin, applications, misuses, limitations and alternatives. *Wear* 426, 620-636.
- Seevam, P. N., Race, J. M., Downie, M. J. and Hopkins, P. (2008) Transporting the next generation of CO₂ for carbon, capture and storage: the impact of impurities on supercritical CO₂ pipelines. *2008 7th International Pipeline Conference*. American Society of Mechanical Engineers Digital Collection.
- Selma, L., Seigo, O., Dohle, S. and Siegrist, M. (2014) Public perception of carbon capture and storage (CCS): A review. *Renewable and Sustainable Energy Reviews* 38, 848-863.
- Sloan, E. D. (2003) Fundamental principles and applications of natural gas hydrates. *Nature* 426 (6964), 353-363.
- Stryjek, R. and Vera, J. (1986) PRSV: An improved Peng—Robinson equation of state for pure compounds and mixtures. *The canadian journal of chemical engineering* 64 (2), 323-333.
- Svedeman, S. (1995) Experimental Study of the Erosional/Corrosional Velocity Criterion for Sizing Multiphase Flow Lines, Phase II-Experimental Results, Final Report. *SwRI Project* (04-6461).
- Tan, Y., Nookuea, W., Li, H., Thorin, E., Zhao, L., Yan, J., Mälardalens, h., Framtidens, e. and Akademin för ekonomi, s. o. t. (2015) Property Impacts on Performance of CO₂ Pipeline Transport. *Energy Procedia* 75, 2261-2267.
- Tarafder, A. and Guiochon, G. (2011) Use of isopycnic plots in designing operations of supercritical fluid chromatography: I. The critical role of density in determining the characteristics of the mobile phase in supercritical fluid chromatography. *Journal of Chromatography A* 1218 (28), 4569-4575.
- Teh, C., Barifcani, A., Pack, D. and Tade, M. O. (2015) The importance of ground temperature to a liquid carbon dioxide pipeline. *International Journal of Greenhouse Gas Control* 39, 463-469.
- Towler, B. F., Agarwal, D. and Mokhatab, S. (2007) Modeling Wyoming's Carbon Dioxide Pipeline Network. *Energy Sources, Part A: Recovery, Utilization, and Environmental Effects* 30 (3), 259-270.
- Twu, C. H., Sim, W. D. and Tassone, V. (2002) Getting a handle on advanced cubic equations of state. *Chemical engineering progress* 98 (11), 58-65.
- Valderrama, J. O. and Silva, A. (2003) The state of the cubic equations of state. *Industrial & engineering chemistry research* 42 (8), 1603-1618.
- Van der Stelt, T., Nannan, N. and Colonna, P. (2012) The iPRSV equation of state. *Fluid Phase Equilibria* 330, 24-35.
- Vandeginste, V. and Piessens, K. (2008) Pipeline design for a least-cost router application for CO₂ transport in the CO₂ sequestration cycle. *International Journal of Greenhouse Gas Control* 2 (4), 571-581.
- Wang, M. and Lawal, A. (2013) *Special issue on process and mechanical engineering for carbon capture and transport*. SAGE Publications Sage UK: London, England.

- Wang, Z., Cardenas, G. I., Fimbres Weihs, G. A. and Wiley, D. E. (2013) Optimal Pipeline Design with Increasing CO₂ Flow Rates. *Energy Procedia* 37, 3089-3096.
- Wang, Z., Fimbres Weihs, G. A., Cardenas, G. I. and Wiley, D. E. (2014) Optimal pipeline design for CCS projects with anticipated increasing CO₂ flow rates. *International Journal of Greenhouse Gas Control* 31, 165-174.
- Waters, C. N., Zalasiewicz, J., Summerhayes, C., Barnosky, A. D., Poirier, C., Galuszka, A., Cearreta, A., Edgeworth, M., Ellis, E. C. and Ellis, M. (2016) The Anthropocene is functionally and stratigraphically distinct from the Holocene. *Science* 351 (6269), aad2622.
- Wei, Y. S. and Sadus, R. J. (2000) Equations of state for the calculation of fluid-phase equilibria. *AIChE Journal* 46 (1), 169-196.
- Weihs, G. A. F., Wiley, D. E. and Ho, M. (2011a) Steady-state optimisation of CCS pipeline networks for cases with multiple emission sources and injection sites: south-east Queensland case study. *Energy Procedia* 4, 2748 - 2755.
- Weihs, G. F., Wiley, D. and Ho, M. (2011b) Steady-state optimisation of CCS pipeline networks for cases with multiple emission sources and injection sites: South-east Queensland case study. *Energy Procedia* 4, 2748-2755.
- Wetenhall, B., Aghajani, H., Chalmers, H., Benson, S. D., Ferrari, M. C., Li, J., Race, J. M., Singh, P. and Davison, J. (2014a) Impact of CO₂ impurity on CO₂ compression, liquefaction and transportation. *Energy Procedia* 63, 2764-2778.
- Wetenhall, B., Race, J., Aghajani, H. and Barnett, J. (2017) The main factors affecting heat transfer along dense phase CO₂ pipelines. *International Journal of Greenhouse Gas Control* 63, 86-94.
- Wetenhall, B., Race, J. M. and Downie, M. J. (2014b) The Effect of CO₂ Purity on the Development of Pipeline Networks for Carbon Capture and Storage Schemes. *International Journal of Greenhouse Gas Control* 30, 197-211.
- White, F. M. (2011) *Fluid Mechanics*. 7th edition. McGraw-Hill.
- Whittaker, S. and Worth, K. (2011) Aquistore: A fully integrated demonstration of the capture, transportation and geologic storage of CO₂. *Energy Procedia* 4, 5607-5614.
- Wilhelmsen, Ø., Skaugen, G., Jørstad, O. and Li, H. (2012) Evaluation of SPUNG* and Other Equations of State for Use in Carbon Capture and Storage Modelling. *Energy Procedia* 23, 236-245.
- Witkowski, A., Majkut, M. and Rulik, S. (2014a) Analysis of pipeline transportation systems for carbon dioxide sequestration. *Archives of Thermodynamics* 35 (1), 117-140.
- Witkowski, A., Rusin, A., Majkut, M., Rulik, S. and Stolecka, K. (2013) Comprehensive analysis of pipeline transportation systems for CO₂ sequestration. Thermodynamics and safety problems. *Energy Conversion and Management* 76, 665-673.
- Witkowski, A., Rusin, A., Majkut, M. and Stolecka, K. (2014b) The Analysis of Pipeline Transportation Process for CO₂ Captured from Reference Coal-Fired 900 Mw Power Plant to Sequestration Region. *Chemical and Process Engineering-Inzynieria Chemiczna I Procesowa* 35 (4), 497-514.
- Wolfram, S. (2002) *A new kind of science*. Vol. 5 (page 996). Wolfram media Champaign, IL.

- Woolley, R. M., Fairweather, M., Wareing, C. J., Falle, S. A., Proust, C., Hebrard, J. and Jamois, D. (2014) Measurement and modelling of the near-field structure of large-scale sonic CO₂ releases from pipelines. *Computer Aided Chemical Engineering*. Vol. 33. Elsevier. 919-924.
- Worth, K., White, D., Chalaturnyk, R., Sorensen, J., Hawkes, C., Rostron, B., Johnson, J. and Young, A. (2014) Aquistore Project Measurement, Monitoring, and Verification: From Concept to CO₂ Injection. *Energy Procedia* 63, 3202-3208.
- Yang, M., Song, Y., Jiang, L., Zhao, Y., Ruan, X., Zhang, Y. and Wang, S. (2014) Hydrate-based technology for CO₂ capture from fossil fuel power plants. *Applied Energy* 116, 26-40.
- Yener, M. E., Kashulines, P., Rizvi, S. S. and Harriott, P. (1998) Viscosity measurement and modeling of lipid-supercritical carbon dioxide mixtures. *The Journal of Supercritical Fluids* 11 (3), 151-162.
- Zabaloy, M. S., Vasquez, V. R. and Macedo, E. A. (2005) Viscosity of pure supercritical fluids. *The Journal of Supercritical Fluids* 36 (2), 106-117.
- Zahid, U., Lee, U., An, J., Lim, Y. and Han, C. (2014) Economic analysis for the transport and storage of captured carbon dioxide in South Korea. *Environmental Progress & Sustainable Energy* 33 (3), 978-992.
- Zargarzadeh, P., Chahardehi, A. and Brennan, F. (2013) Development of a failure assessment diagram based method for engineering criticality assessment of CO₂ transportation pipelines. *Proceedings of the Institution of Mechanical Engineers, Part E: Journal of Process Mechanical Engineering* 227 (2), 140-145.
- Zhang, Z. X., Wang, G. X., Massarotto, P. and Rudolph, V. (2006) Optimization of pipeline transport for CO₂ sequestration. *Energy Conversion and Management* 47 (6), 702-715.
- Zhou, W., Zhao, C., Duan, L., Liu, D. and Chen, X. (2011) CFD modeling of oxy-coal combustion in circulating fluidized bed. *International Journal of Greenhouse Gas Control* 5 (6), 1489-1497.

Appendix A

Table A 1: Regression values for density equation ([McCollum and Ogden 2006](#))

Temp (°C)	$a (x^6)$	$b (x^5)$	$c (x^4)$	$d (x^3)$	$e (x^2)$	$f (x)$	g
10.0	-6.99274E-07	8.56082E-05	-4.41249E-03	1.25510E-01	-2.19938E+00	2.81960E+01	7.68647E+02
15.6	-2.92964E-07	6.57269E-05	-4.75451E-03	1.67603E-01	-3.31969E+00	4.21135E+01	6.70554E+02
21.1	-7.86428E-06	8.72837E-04	-4.02787E-02	9.97669E-01	-1.42859E+01	1.21788E+02	3.84188E+02
26.7	-4.14913E-05	4.43672E-03	-1.95389E-01	4.55038E+00	-5.96084E+01	4.30173E+02	-5.36390E+02
32.2	-1.10256E-03	1.13457E-01	-4.76665E+00	1.04530E+02	-1.26111E+03	7.94772E+03	-1.97102E+04
37.8	-5.42882E-04	5.98138E-02	-2.70792E+00	6.44535E+01	-8.50922E+02	5.92597E+03	-1.63183E+04
43.3	9.60943E-04	-9.44447E-02	3.73493E+00	-7.54076E+01	8.07616E+02	-4.21227E+03	8.42194E+03

Table A 2: Regression coefficients for μ Equation 2.15 ([McCollum and Ogden 2006](#))

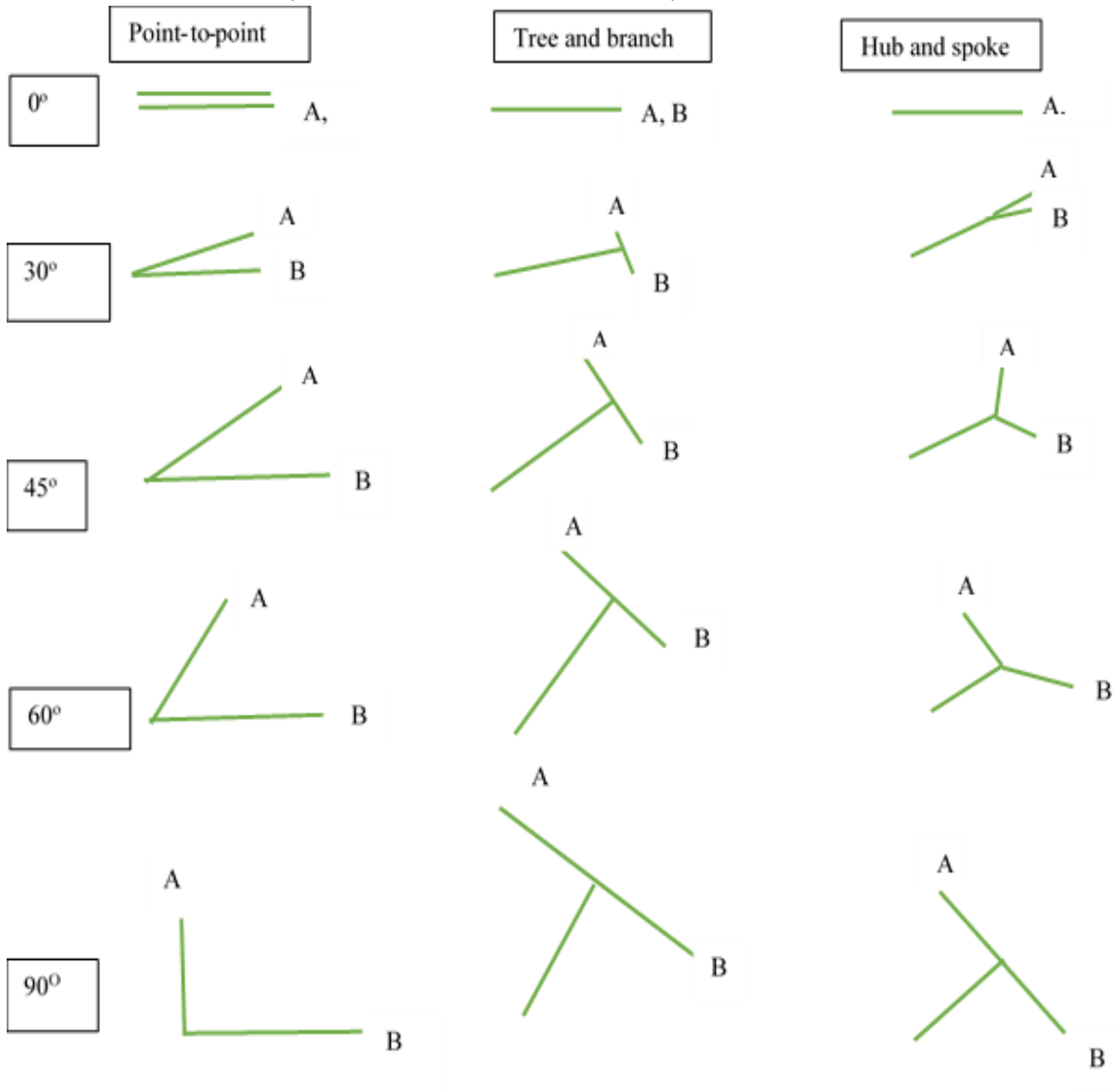
Temp (°C)	$a (x^6)$	$b (x^5)$	$c (x^4)$	$d (x^3)$	$e (x^2)$	$f (x)$	g
10.0	-1.80098E-13	1.96869E-11	-9.09904E-10	2.33381E-08	-3.70759E-07	5.35319E-06	7.07073E-05
15.6	-3.83675E-13	4.25032E-11	-1.97443E-09	4.99914E-08	-7.54380E-07	8.42586E-06	5.17798E-05
21.1	-9.83505E-13	1.08507E-10	-4.97927E-09	1.22724E-07	-1.75059E-06	1.58647E-05	2.01512E-05
26.7	-4.04273E-12	4.32435E-10	-1.90732E-08	4.45698E-07	-5.87710E-06	4.39583E-05	-6.75597E-05
32.2	2.27771E-10	-2.27111E-08	9.15360E-07	-1.89857E-05	2.12163E-04	-1.19673E-03	2.68350E-03
37.8	9.44539E-11	-9.37386E-09	3.75251E-07	-7.70019E-06	8.44425E-05	-4.57587E-04	9.69405E-04
43.3	4.61459E-11	-4.64533E-09	1.89478E-07	-3.98321E-06	4.49854E-05	-2.50385E-04	5.50761E-04

Table A 3: PVT values for CO₂ + CH₄ binary mixtures ([Hwang et al. 1997](#))

Pressure (MPa)	Temperature (°C)	CO ₂ mol %	CH ₄ mol %	Density (kg/m ³)	z- factor
14.3	15.56	9.8	90.2	147	0.7623
19.37	26.85	9.8	90.2	183.3	0.7958
10.37	26.85	29.8	70.2	101.26	0.7716
13.94	26.85	29.8	70.2	144.82	0.7250
17.30	26.85	29.8	70.2	183.33	0.7108
20.73	26.85	29.8	70.2	216.23	0.7226
83.64	26.85	66.82	33.18	177.95	0.6544
10.08	26.85	66.82	33.18	242.24	0.5792
11.78	26.85	66.82	33.18	315.62	0.5198
13.90	26.85	66.82	33.18	397.06	0.4875
16.60	26.85	66.82	33.18	469.72	0.4921
19.33	26.85	66.82	33.18	518.82	0.5188
7.79	26.85	90.10	9.90	279.20	0.4613
8.20	26.85	90.10	9.90	344.28	0.3838
8.67	26.85	90.10	9.90	439.43	0.3261
10.92	26.85	90.10	9.90	635.20	0.2842
13.71	26.85	90.10	9.90	706.83	0.3217
17.91	26.85	90.10	9.90	763.50	0.3879
15.42	76.85	90.10	9.90	375.05	0.5826
18.03	76.85	90.10	9.90	456.33	0.5600

Appendix B

Point-to-point, tree - branch and hub - spoke scenarios. ([IEA GHG 2010](#))



Appendix C

Table C 1: Dependence of density regression equation coefficient on temperature ([McCollum and Ogden 2006](#))

Temp (°C)	a(X ⁶)	b(X ⁵)	c(X ⁴)	d(X ³)	e(X ²)	f(X)	g
4.4	-9.54845E-08	1.97920E-05	-1.41421E-03	5.06981E-02	-1.07669E+00	1.77109E+01	8.42753E+02
10.0	-6.99274E-07	8.56082E-05	-4.41249E-03	1.25510E-01	-2.19938E+00	2.81960E+01	7.68647E+02
15.6	-2.92964E-07	6.57269E-05	-4.75451E-03	1.67603E-01	-3.31969E+00	4.21135E+01	6.70554E+02
21.1	-7.86428E-06	8.72837E-04	-4.02787E-02	9.97669E-01	-1.42859E+01	1.21788E+02	3.84188E+02
26.7	-4.14913E-05	4.43672E-03	-1.95389E-01	4.55038E+00	-5.96084E+01	4.30173E+02	-5.36390E+02
32.2	-1.10256E-03	1.13457E-01	-4.76665E+00	1.04530E+02	-1.26111E+03	7.94772E+03	-1.97102E+04
37.8	-5.42882E-04	5.98138E-02	-2.70792E+00	6.44535E+01	-8.50922E+02	5.92597E+03	-1.63183E+04
43.3	9.60943E-04	-9.44447E-02	3.73493E+00	-7.54076E+01	8.07616E+02	-4.21227E+03	8.42194E+03
48.9	1.02964E-03	-1.05231E-01	4.36150E+00	-9.33059E+01	1.07660E+03	-6.23329E+03	1.42664E+04

Table C 2: Dependence of viscosity regression equation coefficient on temperature ([McCollum and Ogden 2006](#))

Temp (°C)	a(X ⁶)	b(X ⁵)	c(X ⁴)	d(X ³)	e(X ²)	f(X)	g
4.4	-4.13198E-14	5.05771E-12	-2.67210E-10	8.10161E-09	-1.59689E-07	3.68596E-06	8.53395E-05
10.0	-1.80098E-13	1.96869E-11	-9.09904E-10	2.33381E-08	-3.70759E-07	5.35319E-06	7.07073E-05
15.6	-3.83675E-13	4.25032E-11	-1.97443E-09	4.99914E-08	-7.54380E-07	8.42586E-06	5.17798E-05
21.1	-9.83505E-13	1.08507E-10	-4.97927E-09	1.22724E-07	-1.75059E-06	1.58647E-05	2.01512E-05
26.7	-4.04273E-12	4.32435E-10	-1.90732E-08	4.45698E-07	-5.87710E-06	4.39583E-05	-6.75597E-05
32.2	2.27771E-10	-2.27111E-08	9.15360E-07	-1.89857E-05	2.12163E-04	-1.19673E-03	2.68350E-03
37.8	9.44539E-11	-9.37386E-09	3.75251E-07	-7.70019E-06	8.44425E-05	-4.57587E-04	9.69405E-04
43.3	4.61459E-11	-4.64533E-09	1.89478E-07	-3.98321E-06	4.49854E-05	-2.50385E-04	5.50761E-04
48.9	2.17356E-11	-2.27268E-09	9.72054E-08	-2.16667E-06	2.62433E-05	-1.57279E-04	3.81014E-04

